

**Non-Equilibrium Molecular Dynamics Simulations of Gas Phase Separations  
and Transport in Porous Membranes**

Aydin Ozcan

This thesis is presented to UCL in partial fulfilment of the requirements  
for the Degree of Doctor of Philosophy

Supervisors

Professor Ozgur Yazaydin

Dr Matteo Salvalaglio

Department of Chemical Engineering

2019



## **DECLARATION**

I, Aydin Ozcan confirm that the work presented in this thesis is my own. Where information has been derived from other sources, I confirm that this has been indicated in the thesis.

Aydin Ozcan

## ABSTRACT

Industrial membranes have huge importance for various application areas such pharmaceutical, petro-chemical, materials purification and biomedical industries. As a concrete example, the market share of dialysis applications of membranes alone exceeds one billion dollars annually. Therefore, designing target-specific membranes have a great significance and using computer simulations opens a wide window for this purpose. Thus, various research groups around the world try to understand transport mechanism inside the membranes in atomistic level as we summarized in literature review. In this study, we introduced a new non-equilibrium molecular dynamics simulation method to perform realistic permeation simulations for molecules across a membrane. The methodology is based on controlling concentration of species at the inlet and outlet of the membrane with self-adaptive biasing forces. We demonstrate the new method for various gas separations through a flexible ZIF-8 membrane, PIM-1/ZIF-8 Mixed Matrix Membrane and assembled ZIF-8 nanoparticles models. The results show that the new method successfully maintains a concentration gradient between the inlet and outlet of the membrane facilitating the diffusion of molecules. The main novelty of the methodology introduced in this study is that it allows continuous steady state simulations of mixture permeation through a membrane while maintaining the concentration of the species at the inlet and outlet of membrane. We demonstrated that by performing comparatively long simulations (range of  $\mu\text{s}$ ) and maintain concentration gradient along these long trajectories.

## IMPACT STATEMENT

Membrane separation of mixtures has paramount importance due to propose an alternative to intensive energy traditional separation methods. For this reason, an extensive amount of research was dedicated to develop novel membranes for target applications. Generally, polymeric membranes are widely used materials used to separate gas mixtures. However, polymer materials suffer from permeability-selectivity trade-off which imposes an upper bound to separation performance of polymeric membranes known as Robeson upper bound. MOFs are a recent class of hybrid inorganic/organic porous crystalline materials and have received a great deal of attention for innovative separation technologies due to their exceptional chemical and thermal stability. Therefore, a vibrant research activity was developed on manufacturing MOF membranes in recent years. In this thesis, to elucidate the gas transport mechanism through ultrathin MOF membranes, we introduced a method to perform membrane separation simulation in atomistic level resolution. We called this method as Concentration Gradient Driven Molecular Dynamics (CGD-MD) and separation gas mixtures were studied for the first time under non-equilibrium conditions for ultrathin MOF membranes. Due to the great interest in experimental membrane community on Polymer/MOF Mixed Matrix Membranes (MMMs), we performed gas separation simulations for MMMs which was also first nonequilibrium molecular dynamics (NEMD) study for gas separation with a MMM. One of the biggest challenges for MMMs is to understand polymer/filler interface interactions (also known as “surface compatibility”). We proposed a free energy calculation perspective for this long-standing surface compatibility problem.

## ACKNOWLEDGEMENTS

I am finalising my thesis writing in my room with full of books and luggage around. N6 5AX was my-sweet-home for last three years with immense amount of wonderful memories. On my glass table next to a Victorian bay window, I read many books, many research papers and now, I am tapping onto my keyboard for the last lines of my thesis. My personal library is backing me behind and probably; the dominating question of remaining life is spiralling in my worried mind: How I will carry all of my books to next stop of my nomadic academic life?

First of all, I would like to express my gratitude towards Prof. Ozgur Yazaydin, for his support and guidance throughout my PhD. I also would like to thank to my second supervisor Dr. Matteo Salvalaglio for teaching me on various subject. I would like to thank Scientific and Technological Research Council of Turkey (TUBITAK) for financially supporting initial phase of my doctoral research. I would to thank to UCL engineering faculty's prize committee for awarding me prestigious Dean's Prize.

I have been very fortunate to have chance of meeting amazing scientists in many different events in many different countries. First, I would like to thank to Dr. Rocio Semino and Prof. Guillaume Maurin for considering me to an opening in their prolific research team. This was a real honour to me and I will definitely try my best to deserve your support and encouragement. I would also thank to Prof. Thijs Vlugt and Dr. Remco Hartkamp for showing me as candidate to a prestigious Marie Curie fellowship. I definitely appreciated your detailed feedback and help to improve my initial proposal, Thijs. You thought me a lot on writing a good research proposal. I would like to thank Prof. Yannis Kevrekidis for making the best

presentation I have ever attend and giving me some very useful advice at follow-up meeting. I am also thankful to Prof. Mark Tuckerman for suggesting me a paper of Kolmogorov on complexity when we had a chance for conversation in Lausanne last September. It was eye-opening for me to see how some (g)oldies can precede some very current research hype and trend.

Today's science is a team game, that's why my special thanks towards my dear group friends, Dr. Isil Akpinar, Dr. Benjamin Tam, Dr. Sada Namsani, Dr. Naghme Saeidi Bidokthi, Kai Bin Yu and Turan Selman Erkal.

Isil was (by far) best experimentalist I have ever known; Ben was the best cook (even far better than my mum:). Sada was very helpful in any respect with a solid spirit of being senior to poor PhD students like us and listened many comments of me. Kai was Nero-coffee mate and I really enjoyed his company of me to cheap Indian and Malay food. Selman was my usual roommate in conference occasions with his astonishing, heavy sleep.

Furthermore, my sincere thanks to office folks, Maria, Sakiru, Abeer, Anh, Zeynep, Tran, Ilaria, Vaselina, Nicholas, Loukas and Olivera. In particular, I would like to thank to super-staff of our departmental office, Katy Le Lion, for solving problems with the speed of light, and Lee for welcoming us every day at the gate of Engineering Building's entrance. Don't worry Lee, Chelsea will be great again and please, take care of your health.

June, 19

## PUBLICATIONS

List of publications associated with this thesis:

1. **Ozcan, A.**, Perego, C., Salvalaglio, M., Parrinello, M. and Yazaydin, O., 2017. Concentration gradient driven molecular dynamics: a new method for simulations of membrane permeation and separation. *Chemical science*, 8(5), pp.3858-3865
2. Chen, C., **Ozcan, A.**, Yazaydin, A.O. and Ladewig, B.P., 2019. Gas permeation through single-crystal ZIF-8 membranes. *Journal of Membrane Science*, 575, pp.209-216.
3. Namsani, S., **Ozcan, A.**, Yazaydin, A.O, 2019. Direct simulation of ternary mixture separation in a ZIF-8 membrane at molecular scale. *Advanced Theory and Simulations*, DOI:10.1002/adts.201900120.
4. **Ozcan, A.**, Semino, R., Guillaume, M., Yazaydin A.O., Modelling of Gas Transport through Polymer/MOF Interfaces: A Microsecond-Scale Concentration Gradient-Driven Molecular Dynamics Study. *Chemistry of Materials*, 2020, 32, 1288-1296.
5. **Ozcan, A.**, Yazaydin A.O., Atomistic Modelling of CO<sub>2</sub> permeation trough Assembled MOF membranes, (to be submitted)

## CONTENTS

<b>ABSTRACT</b> .....	<b>3</b>
<b>IMPACT STATEMENT</b> .....	<b>4</b>
<b>ACKNOWLEDGEMENTS</b> .....	<b>5</b>
<b>PUBLICATIONS</b> .....	<b>7</b>
<b>LIST OF FIGURES</b> .....	<b>11</b>
<b>LIST OF TABLES</b> .....	<b>13</b>
<b>LIST OF ABBREVIATIONS</b> .....	Error! Bookmark not defined.
<b>Chapter 1: INTRODUCTION</b> .....	<b>16</b>
1.1: INTRODUCTION.....	16
1.2: Equations and Terminology .....	18
1.2.1: Permeability: .....	18
1.2.2: Selectivity:.....	20
1.3: Some Industrial Gas Separation Applications.....	21
1.3.1: Hydrogen recovery: .....	21
1.3.2: Air separation: .....	23
1.3.3: Natural gas purification: .....	25
1.4: Materials for Gas Separation membranes: .....	26
1.4.1: Polymeric membranes .....	26
1.4.2: Carbon Molecular Sieve Membranes .....	26
1.4.3: Carbon Nanotube Membranes.....	27
1.4.4: Zeolite Membranes.....	27
1.4.5: MOF membranes .....	28
1.4.5.1: ZIF-8: .....	28
1.4.5.2: HKUST-1: .....	29

1.4.5.3: MIL-53: .....	30
1.4.6: Mixed Matrix Membranes.....	33
1.4.6.1: Matrimid:.....	34
1.4.6.2: Ultem:.....	34
1.4.6.3: Polysulfone:.....	34
1.5: References: .....	40
<b>Chapter 2: LITERATURE REVIEW .....</b>	<b>50</b>
2.1: BACKGROUND THEORY .....	55
2.1.1: Molecular Simulations: .....	55
2.1.2: Molecular Interactions: .....	59
2.1.3: Molecular Simulation Methods:.....	60
2.1.3.1: Monte Carlo (MC) Simulations: .....	61
2.1.3.2: Molecular Dynamics (MD) Simulation: .....	62
2.1.4: Short-Cuts.....	63
2.2: THESIS AIM AND OUTLINE.....	64
2.3: References .....	66
<b>Chapter 3: CONCENTRATION GRADIENT DRIVEN MOLECULAR DYNAMICS: A NEW METHOD FOR SIMULATIONS OF MEMBRANE PERMEATION AND SEPARATION.....</b>	<b>71</b>
3.1: Introduction .....	71
3.2: Models & Computational Details .....	73
3.2.1: Concentration Gradient Driven Molecular Dynamics .....	73
3.2.2: Simulation Details .....	77
3.3: Results and Discussion.....	83
3.3.1: Permeation of Pure Methane, Ethylene and Ethane .....	83
3.3.2: Equimolar ethylene/ethane mixture separation .....	89
3.4: Conclusions .....	91

3.5: References .....	93
<b>Chapter 4: MODELLING GAS TRANSPORT THROUGH POLYMER/MOF INTERFACES: A MICROSECOND SCALE CONCENTRATION GRADIENT DRIVEN MOLECULAR DYNAMICS STUDY .....</b>	<b>97</b>
4.1: Introduction .....	97
4.2: Models & computational details .....	100
4.2.1: Construction of the bare PIM-1 and ZIF-8 models, and PIM-1/ZIF-8 mixed matrix membrane model.....	100
4.2.2: Modelling of the gas transport .....	102
4.3: Results and Discussion.....	105
4.4: Conclusions .....	115
4.5 References: .....	116
<b>Chapter 5: ATOMISTIC SIMULATIONS OF CO<sub>2</sub> PERMEATION THROUGH ASSEMBLED MOF STRUCTURES: A NON-EQUILIRIUM MOLECULAR DYNAMICS (NEMD) STUDY .....</b>	<b>126</b>
5.1: Introduction .....	126
5.2: Models and Methods .....	129
5.3: Results and Discussion.....	131
5.3.1: CO <sub>2</sub> permeation through ZIF-8 Membrane.....	131
5.3.2: Interfacing two thin ZIF-8 slabs.....	133
5.3.3: CGD-MD simulations for Interfaced ZIF-8 Slabs: .....	136
5.4: Conclusions .....	138
5.5: References .....	139
<b>Chapter 6: GENERAL CONCLUSIONS AND DISCUSSIONS .....</b>	<b>143</b>
6.1: References .....	149
<b>Chapter 7: APPENDICES.....</b>	<b>152</b>

## LIST OF FIGURES

Figure 1-1 Crystal structures of ZIF-8, HKUST-1 and MIL-53 (from left to right) .....	30
Figure 2-1. Some example simulation boxes for membrane transport simulations: a) Simulation box of Murad et al. (Murad and Gupta, 2000), b) Simulation box of Kalra et al. (Kalra et al., 2003), c) Simulation box of Gupta et al. (Gupta et al., 2015), d) Simulation box of Gupta et al. for pervaporation membrane study (Gupta et al., 2016), e) Steered MD simulation box of Zhu et al. (Fangqiang Zhu, 2002), f) Boundary driven MD simulation box of Frentrup et al. (Frentrup et al., 2012)....	51
Figure 3-1 Conceptual representation of the concentration gradient driven MD method. Red line demonstrates an arbitrary concentration profile. Dashed line shows the boundaries of the simulation box. Fluid molecules return to feed side from the permeate side through the periodic boundary .....	75
Figure 3-2 The variation of flux with respect to inlet force constant. The outlet force constant, was kept fixed at 500,000 kJ.nm <sup>3</sup> /mol. The flux remains same within the margin of statistical error. Black squares 10 bar feed pressure, red circles 5 bar feed pressure and blue triangles 4bar feed pressure. ....	77
Figure 3-3 Starting (top) and after 10ns (bottom) configurations for pure (a) methane, (b) ethylene and (c) ethane.....	82
Figure 3-4 The variation of inlet (black lines) and outlet (red lines) concentrations for (a) methane, (b) ethylene and (c) ethane as a function of simulation time in production runs. The instantaneous values are represented with faded colour, while the full colour curves are moving averages obtained with a characteristic smoothing time of 0.5 ns. ....	84
Figure 3-5 The variation of outlet concentrations for (a) methane, (b) ethylene and (c) ethane as a function of simulation time in production runs. The instantaneous values are represented with faded colour, while the full-colour curves are moving averages obtained with a characteristic smoothing time of 0.5 ns. ....	85

Figure 3-6 Concentration profiles of (a) methane, (b) ethylene and (c) ethane molecules along the z coordinate of the simulation box. ....	86
Figure 3-7 The variation of methane flux ( $J_z$ ) with concentration gradient .....	87
Figure 3-8 Variation of inlet (black lines) and outlet (red lines) concentrations for a) ethylene and b) ethane for the equimolar mixture as a function of simulation time in the production run. The instantaneous values are represented with faded colour, while the full-colour curves are moving averages obtained with a characteristic smoothing time of 0.5 ns. ....	90
Figure 3-9 Concentration histograms of ethylene (left) and ethane (right) in ICR during the equimolar mixture simulation. ....	91
Figure 4-1. Illustration of a) ZIF-8 membrane, b) PIM-1 membrane and c) composite PIM-1/ZIF-8 - membrane structural models used in the CGD-MD simulations. Color code is as follows: C (grey), H (white) N (blue), O (red) and Zn (steel blue). ....	102
Figure 4-2. Density profiles of pure H <sub>2</sub> and CH <sub>4</sub> along the a) PIM-1 and b) ZIF-8 membranes.....	108
Figure 4-3. Mean residence times of H <sub>2</sub> and CH <sub>4</sub> along the z direction of the a) PIM-1 and b) ZIF-8 membranes.....	109
Figure 4-4. Density profiles of H <sub>2</sub> and CH <sub>4</sub> in a) pure component and b) mixture simulations along the z direction of the composite PIM-1/ZIF-8 membrane. ....	111
Figure 4-5. Mean residence times of H <sub>2</sub> and CH <sub>4</sub> along the composite PIM-1/ZIF-8 membrane in pure component and mixture simulations. ....	114
Figure 5-1. Parallel and series configurations with two ZIF-8 slabs with Figure a) and b), respectively. Transparent regions stand for high permeability component of the composite structure. Color code is as follows: C (cyan), H (white) N (blue), O (red) and Zn (steel blue). ....	132
Figure 5-2. FES for assembling two ZIF-8 slab models .....	134
Figure 5-3 RTD for assembled low and high permeability ZIF-8 slabs. ....	137

## LIST OF TABLES

Table 1-1 The membrane gas separation applications .....	20
Table 1-2 Some prominent thin-film MOF membranes for gas separation and the corresponding metal ions, ligands and the apertures of MOFs .....	31
Table 1-3 MOF-MMM polymer membranes for gas separation applications and their selectivity .....	35
Table 3-1 The deviation of ICR concentration from the target value as a function of inlet force constant. Obtained over 40ns production run after 10ns initial run. The outlet force constant, was kept fixed at 500,000 kJ.nm <sup>3</sup> /mol.....	76
Table 3-2 Parameters used in Eq. 1 and 2 and the width of the control regions, $V^{CR}/(L_x \times L_y)$ .....	79
Table 3-3 The average concentrations in ICR and OCR for methane, ethylene and ethane.....	84
Table 3-4 Permeabilities ( $10^{-13}$ mol.m/m <sup>2</sup> .s.Pa) for methane, ethylene and ethane. ....	88
Table 3-5 The average concentrations in ICR and OCR for ethylene and ethane in the equimolar mixture simulation.....	91
Table 4-1. Comparison of experimental and simulated ideal H <sub>2</sub> /CH <sub>4</sub> permselectivities in PIM-1 and ZIF-8 membranes.....	106
Table 4-2. Comparison of H <sub>2</sub> /CH <sub>4</sub> permselectivities in the composite PIM-1/ZIF-8 membrane obtained from the pure and mixture CGD-MD simulations and that of obtained based on the serial model.....	113
Table 5-1 Comparison of direct atomistic simulation results with three different macroscopic MMM permeability prediction models. ....	136

## LIST OF ABBREVIATIONS

AMBER	Assisted Model Building with Energy Refinement
BTC	Benzene tricarboxylic acid
BDC	Benzene dicarboxylate
CGD-MD	Concentration Gradient Driven Molecular Dynamic
CMS	Carbon Molecular Sieve
CNT	Carbon Nanotube
COM	Center of Mass
GCMC	Grand Canonical Monte Carlo
EMD	Equilibrium Molecular Dynamics
FES	Free Energy Surface
HKUST	Hong Kong University of Science and Technology
LJ	Lennard Jones
MIL	Matériau Institut Lavoisier
MMM	Mixed Matrix Membrane
MOFs	Metal-Organic Frameworks
NEMD	Non-equilibrium Molecular Dynamics
DCV-GCMD	Dual Control Volume Grand Canonical Molecular Dynamics

PEM	Particle Mesh Ewald
UFF	Universal Force Field
ZIF	Zeolitic Imidazole Framework
VdW	Van der Waals
WT-MetaD	Well-Tempered Metadynamics
IFR	Inlet Force Region
ICR	Inlet Control Region
ITR	Inlet Transition Region
OFR	Outlet Force Region
OCR	Outlet Control Region
OTR	Outlet Transition Region

## **Chapter 1: INTRODUCTION**

---

### **1.1: INTRODUCTION**

Jean Antoine (Abbé) Nollet reported that a pig bladder (i.e., a natural membrane) was more permeable to water than to ethanol in 1748 (Böddeker 1995, Nollet 1995). This was the first recorded semi-permeable membrane. After the first spark from liquid separation, researchers paid their attention to gas permeation (and separation) and in 1831, John Kearsley Mitchell made an observation regarding gas transport through balloons prepared from natural rubber (Baker 2012, Sanders, Smith et al. 2013). The observation was found to be simple but intriguing: After filling a series of rubber balloons with hydrogen and leaving them to be soared up the ceiling of the lecture room, the balloons have descended from the ceiling over time. Mitchell (Mitchell 1995) hypothesised that the hydrogen was passing through the inflated surface of these rubber balloons in a way. Further experiments proved that many different gases passed through the same material with different rates and this critical concept have preceded later the commercial development of polymeric gas separation membranes (Koros and Fleming 1993).

Today's membrane gas separation industry has heavily initiated by developments of membrane technology for water treatment applications (Baker and Lokhandwala 2008). In 1960, Sidney Loeb and Sirivasan Sourirajan have achieved to produce first asymmetric reverse osmosis membrane for water desalination at University of California. Los Angeles (UCLA) (Loeb 1960, Sidney and Srinivasa 1964). The idea of "asymmetric membrane" is to combine thin and selective

polymer layer on top of a much thicker and non-selective (or less selective) support layer. This microporous support part provides mechanical robustness to membrane, while the dense skin layer executes the separation of salt from water. These membranes showed an unprecedented performance for water desalination at that time, they exhibited 20 times the permeance of any membrane then known and good water/salt selectivity. This breakthrough made membrane based separation economically desirable for desalination (Galizia, Chi et al. 2017). It took another decade to fabricate the membranes on an industrial scale and embedding them into large membrane area modules. Reverse osmosis membranes for water treatment process of ultrafiltration were established their place in market by the late 1970s. These initial efforts for water desalination membranes have paved the way for developing technology for high performance gas separation membranes.

In 1980, first gas separating membranes were launched by a company called Permea for hydrogen-separation (MacLean, Bollinger et al. 1986, Baker 2012). This was the first large industrial application of gas separation membranes. Permea adapted the asymmetric membrane technology to gas separation and their polysulfone membrane was an immediate success, particularly for the separation and recovery of hydrogen from the purge gas streams of ammonia plants. Within a few years, Permea systems were installed in many such plants (Henis 1994). This rapid success encouraged other companies to develop their own technologies. By the mid-1980s, Cynara and Separex developed their cellulose acetate membranes to remove carbon dioxide from natural gas (Spillman 1989). Simultaneously, Generon introduced a membrane system to separate nitrogen from air. This first air separation systems were based on poly(4-methyl-1-pentene) (TPX) membranes

with an oxygen/nitrogen but there were not competitive enough for commercial purposes. By 1990, Generon, Praxair, and Medal had all achieved to produce better technologies with custom polymer membranes for air separation applications. These membranes could produce better than 99% nitrogen and suggested a cost-competitive option to delivered nitrogen for many small users. This applications has expanded to about one-third of new nitrogen production capacity present; 5000-10 000 nitrogen systems have been installed worldwide to date (Baker 2002).

Before introducing significant industrial gas separation in current market, it could be illustrative to present some significant equations and terminology related to gas separation membranes.

## **1.2: Equations and Terminology**

Here, it is aimed to summarise briefly the basic equations and terminology which is being used to describe gas transport in membranes and evaluate membrane material performance. Membrane performance is often characterized by total gas mass transfer and separation efficiency factor and these properties are generally calculated by permeability and membrane selectivity.

### **1.2.1: Permeability:**

Pure gas permeation through a membrane is defined as steady-state gas flux of molecule A normalized with the trans-membrane pressure difference,  $P_2-P_1$  and multiplied with membrane thickness (Mulder 2012):

$$P_A = \frac{J_A l}{P_1 - P_2} \quad (1.1)$$

In the equation 1.1,  $P_1$  and  $P_2$  stand for feed side pressure and permeate side pressure respectively,  $l$  is membrane thickness,  $J_A$  is mass flux of molecule A through membrane and  $P_A$  corresponds to permeability of molecule A. Typically permeability coefficients are expressed in  $\text{mol.m/m}^2.\text{s.Pa}$  unit. Barrer is also another common unit for measuring permeability named after famous British zeolite scientist Richard Barrer which equals  $3.348 \times 10^{-16} \text{ mol.m/m}^2.\text{s.Pa}$ . Permeability values can vary significantly between different membranes. For example, oxygen permeability in poly(acrylonitrile) (PAN) membranes are spectacularly low (around  $2 \times 10^{-4}$  Barrer) (Allen, Fujii et al. 1977), whereas some poly(diphenylacetylene) membranes have an oxygen permeability of 20 000 Barrer (Hu, Shiotsuki et al. 2008). This enormous range of gas permeabilities in different membranes exemplifies the strong relation between of gas permeability and membrane material structure. “Solution-Diffusion model” is the most well-known model in order to this relation between gas permeability and membrane structure. The solution-diffusion model separates gas permeability coefficient into two part as a gas solubility coefficient,  $S_A$ , and diffusion coefficient,  $D_A$  (Equation 1.2) (Baker 2012, Mulder 2012):

$$P_A = S_A D_A \quad (1.2)$$

The diffusion coefficient is commonly expressed in  $\text{cm}^2/\text{s}$ , and solubility coefficient is defined as ratio between concentration of gas in membrane and pressure of gas contiguous to membrane. The adsorbed amount of gas molecules and their diffusion inside the membrane structure play the major role for different magnitudes permeability values according different membrane material (Baker 2002).

Another parameter related to permeability and very frequently used in membrane industry is gas permeance which is defined as  $\text{permeance} = (\text{permeability}) / (\text{membrane thickness})$ . If a membrane has high permeance, membrane unit can be smaller and this leads to reduction of total cost of membrane unit (Sanders, Smith et al. 2013).

### 1.2.2: Selectivity:

To characterise the ability of membrane to separate two gases (namely, A and B), selectivity factor is defined according to gas permeabilities (Equation 1.3):

$$\alpha_{A/B} = \frac{P_A}{P_B} \quad (1.3)$$

By combining Eq. 1.2 with Eq. 1.3, we can infer that membrane selectivity could be written as combination of two parts, which is attributed to diffusion selectivity and adsorption selectivity.

**Table 1-1** The membrane gas separation applications

Application	Separation	Market Size
Hydrogen recovery	H <sub>2</sub> /N <sub>2</sub> , H <sub>2</sub> /CH <sub>4</sub> , H <sub>2</sub> /CO	~ 200 million dollars/year
Air separation	O <sub>2</sub> /N <sub>2</sub>	~ 800 million dollars/year
Natural gas purification	CO <sub>2</sub> /CH <sub>4</sub> , HS <sub>2</sub> /CH <sub>4</sub>	~ 300 million dollars/year

After a summary of some necessary terminology to evaluate membrane performance, we may return to discussion of industrially relevant gas separation applications. The “big four” membrane gas separation applications which have

80–90% of the current gas separation membrane market share are listed in Table 1-1. Whole market has expanded very significantly over the past 25 years, and current sales are in the range of \$1.0–1.5 billion/year (Galizia, Chi et al. 2017).

Currently, separation processes lead to nearly 4500 trillion kcal of energy per year in the United States, which corresponds to nearly 22% of total chemical plants energy consumption (Ren, Patel et al. 2006, Sholl and Lively 2016). Big portion of this energy consumption is due to distillation process. Over 40,000 distillation columns are used for over 200 different separations in the United States, which corresponds to huge portion of industrial separation energy consumption (Figuroa, Fout et al. 2008, Sanders, Smith et al. 2013). Membranes do not require thermal driving force to separate mixtures and this make them very desirable to reduce this huge energy cost for separation (Sholl and Lively 2016). Some of industrially important gas separation would be summarised briefly in the following section:

### **1.3: Some Industrial Gas Separation Applications**

#### **1.3.1: Hydrogen recovery:**

Hydrogen has smaller kinetic diameter with respect to other gases such as nitrogen, methane and carbon dioxide. This makes hydrogen highly permeable in membranes typically and leading to high selectivity for hydrogen to other gases (Sanders, Smith et al. 2013). Ammonia purge gas was the first largescale commercial gas separation membrane application for hydrogen recovery (Baker 2012). Today, ammonia purge gas recovery, oxo-chemical synthesis and refinery off-gas purification are the main industrial applications which membranes have

been heavily used for hydrogen separation (Stookey, Patton et al. 1986, Baker 2002, Baker 2012). Monsanto was the first company in this market, offering a polysulfone membrane for H<sub>2</sub> separation in 1979 (Lonsdale 1982) and these membranes can achieve 95% recovery of H<sub>2</sub> from ammonia purge gas recovery (Galizia, Chi et al. 2017). Other important hydrogen separations are adjusting molar ratios of syngas (H<sub>2</sub>/CO) and hydrogen recovery in refinery hydrotreaters (H<sub>2</sub>/CH<sub>4</sub>). Syngas is a mixture of H<sub>2</sub> and CO produced from steam reforming of natural gas, oxidation of heavy oils, or gasification of coal (Scott 1995). Depending on the method used to produce syngas, H<sub>2</sub>:CO ratios in the mixture could vary between 50% and 18% (Liu, Song et al. 2010). Membranes were used to adjust this variable composition. Refinery-exhausted gas purification is another hydrogen-based commercial membrane application. Petroleum crude feedstocks contain many different molecular weight products that must be separated before use. The heavier fraction of these products is often cracked, i.e., broken into smaller components, through a catalytic process known as hydrocracking. This process relies on injecting hydrogen into the cracker to improve several aspects of the reaction chemistry. For example, hydrogen helps eliminate unsaturated hydrocarbons and reduces the formation of coke (Posey Jr 1983). Increasing the purity of hydrogen used in a hydrocracker can increase the life of the cracker catalyst and increase the production of higher paraffinic compounds (Posey Jr 1983). It is highly desirable to recycle H<sub>2</sub> from the hydrocracker products to the hydrocracker feed. Polymer membranes are used in the recycle loop to achieve this separation.

### **1.3.2: Air separation:**

Air separation is accomplished by several industrial processes in today market (Gottschlich and Roberts 1990, Sircar 2002). Nitrogen enrichment is the largest market for membrane-based air separation is for air separation (Baker 2002, Baker 2012, Sanders, Smith et al. 2013, Galizia, Chi et al. 2017). Several N<sub>2</sub> enrichment applications for membranes include refrigeration, inerting to increase the nitrogen purity. Other than these already well-established application for membrane use, there are some more potential application areas such as metallurgical processes and gas feeds for the electronics industry. But membranes are not very desirable for these markets because of the high gas purity requirements for N<sub>2</sub> streams in these applications (Yampolskii and Freeman 2010). Therefore, current focus for N<sub>2</sub> separation membranes focused on improving membrane selectivity. Some of the earliest air separation membranes were produced by Generon and Permea companies in the mid-1980s (Baker 2012). Generon was used poly(4-methyl-1-pentene) (TPX) as polymer, and had selectivities of approximately 4, which limits in widespread industrial use (Baker 2012). New research for better performing membrane materials quickly improved the technology for air separation, and by the early 1990s, several new membranes were enter to market, including tetrahalogenated bisphenol based polycarbonates by Generon (Sanders Jr, Clark et al. 1988, Beck and Sanders Jr 1990), polyimides by Praxair (Baker 2002), and polyimide and polyaramide membranes by Medal (Baker 2012). During this time, the push for nitrogen enrichment applications brought about significant advances in the design and fabrication of many asymmetric membrane systems. For example, commercial membranes have also been developed for water/nitrogen

separation (Coan and Jensvold 2007, Bernardo, Drioli et al. 2009). In the US, China and the European Union, compressing air requires approximately 8% of all electricity used by industry (Saidur, Rahim et al. 2010), and membrane dehydrators are vital component of today's technology to dry compressed air due to its simplicity and robustness of relative to the competing technologies which is based on condensation or solid desiccants (Baker 2012). The first of these type air dehydration membranes were marketed in 1987 by Permea and was used to replace desiccants in refrigeration dehydrators. Producing dry air for military applications such as fire control, electronics and communication systems is significant market and membranes were a promising technology also for these market (Theis and Titus 1996). Today, Air Products is a strong player of military air-drying market and sells dehydration membranes under the trade name CACTUS for high pressure dehydration applications. Another important air separation membrane application is On-Board Inert Gas Generation Systems (OBIGGS), which targets generation of nitrogen-rich air for fuel tank to reduce explosion potential of flammable fuel/air mixtures in the inlet space of fuel tanks (Sanders, Smith et al. 2013). Following the unfortunate aviation accident of TWA Flight 800 in 1996, which was blamed on a flame attenuation and explosion in the fuel tank, the US Federal Aviation Administration (FAA) began exploring the possible technologies for nitrogen enrichment of circulating air in fuel tanks of commercial aircraft. Today, systems have been installed on many commercial aircraft to reduce the potential for sparks from rotating components in fuel tank systems causing explosion (Jones 2004, Schwalm 2007).

### **1.3.3: Natural gas purification:**

Natural gas is an exciting “playground” for a membrane scientist which includes a complex mixture of methane, carbon dioxide, ethane, higher hydrocarbons, hydrogen sulphide and trace components of many other compounds such as benzene, toluene, ethylbenzene, and xylenes (Baker and Lokhandwala 2008). The actual composition of natural gas highly depends on the well and delivery of natural gas to national pipeline grid requires treatment. This treatment is needed to prevent pipeline corrosion and adjust the heating value fuel up to a standard level. U.S. pipeline regulations require that natural gas should contain less than 2% CO<sub>2</sub>, up to 4 ppm H<sub>2</sub>S, 120 ppm water (Kohl and Nielsen 1997). The main technology for natural gas adjustment is amine absorption, which has been used since the early 1930s. Some long-standing problems of amine absorption such as high capital and maintenance cost, low regenerability and high environmental footprint have encouraged the development of alternative technologies. Membrane systems and membrane/absorption hybrid systems for natural gas purification emerged as promising alternative for bare amine absorption (Cooley and Coady 1978). The first membranes for natural gas purification were developed in the early to mid-1980s. W.R. Grace, Separex and Cynara developed membranes based on cellulose acetate for natural gas purification (Baker 2012). These cellulose acetate membranes are still widely used today, but polyimides and other materials have gained some attraction in this field over the past 20 years (Baker 2012).

## **1.4: Materials for Gas Separation membranes:**

### **1.4.1: Polymeric membranes**

The numbers of polymers used in commercial systems are limited, even though large number of polymeric materials were investigated for gas separation applications. Within a polymer membrane, pores and pore channels have a wide range of sizes instead of being uniform. In industrial application, generally polymer membranes with controllable pore structures are preferred for robust separation performance. Therefore, almost all industrial membrane gas separation processes exploit glassy polymers. Some industrially important polymers for membrane production can be listed as Polyimide, PTMSP, Amorphous Teflon and PIMs (Sanders, Smith et al. 2013).

### **1.4.2: Carbon Molecular Sieve Membranes**

Carbon molecular sieve (CMS) membranes have long back history after first development by Richard Barrer in mid-50s. Many of the CMS membranes have been produced from polymeric precursors by pyrolysis. Polyimides are most common precursors but they are very costly for large production. Polyacrylonitrile proposed as a promising material for replacement. One of the main problems of CMS membranes is their high level of brittleness (Ash, Barrer et al. 1963, Ash, Barrer et al. 1973, Ash, Barrer et al. 1976). That hinders their commercialisation even though great effort devoted to their development. Today, there is no industrial producer of commercial CMS membrane modules.

### **1.4.3: Carbon Nanotube Membranes**

Using Carbon nanotubes (CNTs) as a membrane material for separation applications were initially proposed by computational studies (Skoulidas, Ackerman et al. 2002, Sokhan, Nicholson et al. 2002, Sokhan, Nicholson et al. 2004, Chen and Sholl 2006). CNTs have many different properties from conventional membrane materials such as smoothness of inner surface, very high rigidity, nonpolar nature of the  $sp^2$  carbon network. Some of the initial theoretical predictions were verified experimentally in later studies. Gas flow in CNT membranes is 1-2 order of magnitude higher than commercial polycarbonate nanoporous membranes. Even though, fast mass transport is an advantage for CNT membranes to enhance selectivity between different gas molecules remains as big challenge. This selectivity problem hampers the industrial applications of CNT membranes.

### **1.4.4: Zeolite Membranes**

In the last three decades, zeolite membrane studies were performed very extensively in terms of their bulk synthesis, membrane preparation technique and different gas separation applications (Lovallo, Gouzinis et al. 1998, Yang, Crittenden et al. 1999, Caro, Noack et al. 2000). Zeolites membranes have higher thermal and chemical resistance compared with polymer membranes and this makes them preferable for industrial applications (Krishna and Baur 2003). The first commercial application of zeolite membranes was solvent dehydration by pervaporation. Some other plants were started to install worldwide since 2001, on the other hand there have not been an industrial application data for gas separation

yet. Two main reasons for lack of industrial application in gas separation field for zeolite membranes are cost infeasibility and poor reproducibility of performance (Lee, Funke et al. 2008).

#### **1.4.5: MOF membranes**

Metal Organic Framework (MOF) membranes were emerging class of membrane within last two decades as an alternative to more traditional materials such as zeolites. Due their vast variations in geometry, cell size and functionality of its components led more than 70000 different MOF structures reported with in last decade. MOF have typically high surface areas, permanent porosity, wide variety of pores sizes and reasonable chemical-thermal resistance (Furukawa, Cordova et al. 2013). Porosity and surface area of MOFs are generally higher than more traditional materials such as activated carbon and zeolites. Their interesting physical and chemical properties made MOF desirable very wide spectrum of different applications such as gas storage, gas separation, catalysis, sensory applications, drug delivery and microelectronics. An experimental thin-film MOF membrane data is given in **Table 1-2**. Even though many different MOF materials (Galizia, Chi et al. 2017) are examined for membrane studies, here we will summarise three most commonly used MOF structures: ZIF-8, HKUST-1 and MIL-53.

##### **1.4.5.1: ZIF-8:**

Zeolitic imidazolate frameworks (ZIFs) are by tetrahedrally coordinated imidazolate linkers with metal ions (usually zinc and cobalt). They have structural and bond angle similarities with zeolites that's why called as "zeolitic" (Park, Ni et

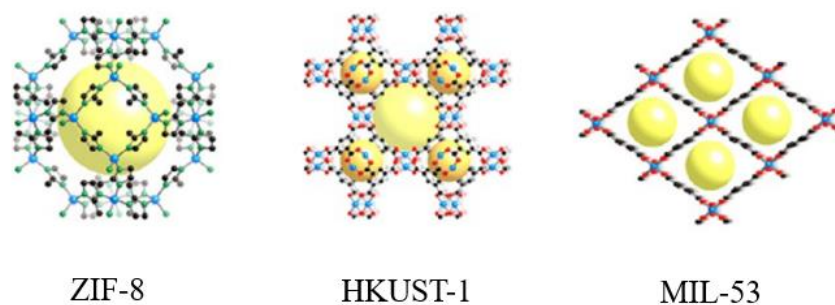
al. 2006). ZIF-8 is the most extensively used ZIFs for gas separation membranes due its small pore aperture 3.4 Angstroms. This small pore aperture makes ZIF-8 very desirable for gas separation by considering kinetic diameters of simple gas molecules such H<sub>2</sub>, CH<sub>4</sub>, CO<sub>2</sub> etc. Additional to that, ZIF-8 shows an interesting phenomenon called “gate opening” mechanics. Methyl group of imidazolate linker which extend into pore aperture, can rotate and generate a flexible pore-opening mechanism which permits large molecules such as (propane and propylene) to permeate through ZIF-8 membrane (Fairen-Jimenez, Moggach et al. 2011, Peralta, Chaplais et al. 2012, Casco, Cheng et al. 2016). This gate “gate-opening” mechanism makes ZIF-8 rather interesting for some specific applications such as olefin-paraffin separation.

#### **1.4.5.2: HKUST-1:**

HKUST-1 was named after Hong Kong University of Science and Technology where place they synthesised first. It has cubic unit cell with 9 Angstroms pore channel surround by 5 Angstroms diameter tetrahedral windows (Chui, Lo et al. 1999). Despite of the fact that it has slightly big pore network for gas separation, it exhibits an exceptional mechanism called “open-metal” sites. By applying solvent exchange and/or heating, weakly bound solvent or water molecules can be removed from metal sites and that metal sites become under-coordinated (Lin, Kim et al. 2013, Bae, Choi et al. 2017). These coordinatively unsaturated metal sites contribute additional gas capacity and show some promising results especially separation of polar/nonpolar mixtures such CO<sub>2</sub>/CH<sub>4</sub>.

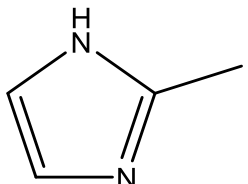
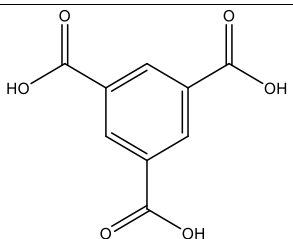
### 1.4.5.3: MIL-53:

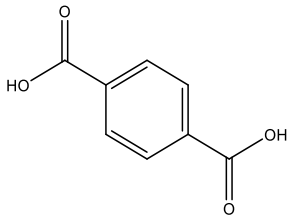
MIL-53 named after Materials Institute Lavoisier are embodied by trivalent metal cations (typically Al, but also Cr, Fe and Ga) (Llewellyn, Horcajada et al. 2009, Volklinger, Loiseau et al. 2009, Bourrelly, Moulin et al. 2010, Boutin, Coudert et al. 2010) and terephthalic acid ligands. MIL-53 has wine-rack-like structure with large pore sizes around 8.5 Angstroms. Crystal structure of MIL-53 is well-known as being very flexible and show solid-solid phase transition due to various external stimuli such as adsorption-desorption of specific gases (such as CO<sub>2</sub>), temperature-pressure changes, applied electric field etc. This interesting phenomena is called as “breathing effect” (Serre, Millange et al. 2002, Loiseau, Serre et al. 2004, Springuel-Huet, Nossov et al. 2010) in the literature and pores of MIL-53 opens and closes analogous to an accordion expanding and compressing due to external effects. What makes these phenomena more interesting is that, it is fully reversible. Structure returns to its initial position when the external stimuli turned off.



**Figure 1-1** Crystal structures of ZIF-8, HKUST-1 and MIL-53 (from left to right)

**Table 1-2** Some prominent thin-film MOF membranes for gas separation and the corresponding metal ions, ligands and the apertures of MOFs

MOFs	Metal ions	Ligand	Pore Aperture (Angstroms (Å))	Gas Separation	Mixture Selectivity	Ref.
<b>ZIF-8</b>	Zinc	 2-methylimidazole	3,4	H <sub>2</sub> /CO <sub>2</sub> :50/50	5.5	(Liu, Wang et al. 2014)
				H <sub>2</sub> /N <sub>2</sub> :50/50	9.5	
				H <sub>2</sub> /CH <sub>4</sub> :50/50	6.5	(Brown, Brunelli et al. 2014)
				H <sub>2</sub> /CH <sub>4</sub> :50/50	11.2	
				H <sub>2</sub> /C <sub>3</sub> H <sub>8</sub> :50/50	318	
				C <sub>3</sub> H <sub>6</sub> /C <sub>3</sub> H <sub>8</sub> :50/50	14.5	
				H <sub>2</sub> /C <sub>3</sub> H <sub>8</sub> :50/50	545	
C <sub>2</sub> H <sub>6</sub> /C <sub>3</sub> H <sub>8</sub> :50/50	80	(Pan and Lai 2011)				
C <sub>2</sub> H <sub>4</sub> /C <sub>3</sub> H <sub>8</sub> :50/50	167					
<b>HKUST-1</b>	Copper	 1,3,5 benzenetricarboxylic acid	9	H <sub>2</sub> /N <sub>2</sub> :50/50	8.9	(Ben, Lu et al. 2012)
				H <sub>2</sub> /CO <sub>2</sub> :50/50	9.24	(Guo, Zhu et al. 2009)
				H <sub>2</sub> /N <sub>2</sub> :50/50	7.0	
				H <sub>2</sub> /CO <sub>2</sub> :50/50	6.84	

<b>MIL-53</b>	Aluminium		8.5	H <sub>2</sub> /CH <sub>4</sub> :50/50	20.7	(Zhang, Zou et al. 2012)
				H <sub>2</sub> /N <sub>2</sub> :50/50	23.9	
				H <sub>2</sub> /CO <sub>2</sub> :50/50	30.9	
		1,4 benzenedicarboxylic acid				

#### **1.4.6: Mixed Matrix Membranes**

Polymeric membranes have a trade-off between gas selectivity and gas permeability, on the other hand inorganic membranes have scale up problems. Mixed matrix membranes (MMMs) are proposed as a solution of these problems. By combining polymers and inorganic filler as composited membrane, it was assumed that superior properties of polymeric (high permeability) and MOFs (high selectivity) can match and gas separation performance of the composite membrane can surpass the performance of its individual parts. Many different MMMs have been studied in the literature with various different inorganic fillers such as carbon molecular sieves, zeolites, silica gels, carbon nanotubes. Unfortunately, most of these composite structures exhibit poor polymer-inorganic filler compatibility and filler segregation in polymer matrix. These problems hamper the industrial scale application of MMMs with more traditional inorganic fillers. On the other hand, various MOF based MMMs showed good results in lab scale and MOF based MMMs is and rapidly growing research area. Chemical diversity of MOF structures lead more possibility for better polymer-filler compatibility. Well dispersion of fillers with good polymer-filler interfacial contact improves overall performance of the composite MMMs and there are some promising data available in literature for polymer-MOF structures. Some of these polymer-MOF MMM results are summarised in Table 1-3. The polymers given in Table 1-3 is described very briefly below to complete the discussion.

#### **1.4.6.1: Matrimid:**

Matrimid was originally developed for use in micro electronic industry but later find applications in gas separation membrane market. Its mechanical strength makes it suitable for harsh working environments. Additionally, its good solubility in common solvents allows easy processibility which is very important for membrane fabrication. Matrimid membranes show best combination CO<sub>2</sub>/CH<sub>4</sub> selectivity and CO<sub>2</sub> permeability trade-off in commercially available polymer membranes.

#### **1.4.6.2: Ultem:**

Ultem is a polyetherimide polymer material which was developed in early 80s. They exhibit excellent mechanical strength, outstanding heat resistance and stress reliability 19. Ultem is an attractive material for gas separation because of it has good selectivity for different gas pairs. Additionally, it has plasticisation due gas permeation and it is less costly compared to Matrimid. However, the low permeability puts limit to its applications. To enhance its gas permeation performance, mixed-matrix membranes (MMMs) concept has been explored recently in literature.

#### **1.4.6.3: Polysulfone:**

Polysulfone polymers consists diphenylene sulfone repeat units which creates immense backbone rigidity. This property provides molecular immobility, high strength, good creep resistance and stability. First, large scale membrane separation application with polysulfone membrane was developed by Monsanto in

late 1970s and polysulfone membranes were used widely for gas separation from that date.

**Table 1-3** MOF-MMM polymer membranes for gas separation applications and their selectivity

<b>MOF</b>	<b>Polymer</b>	<b>MOF Percentage</b>	<b>Gas separation</b>	<b>Mixture Selectivity</b>	<b>Ref.</b>
<b>ZIF-8</b>	Matrimid	20	H <sub>2</sub> /CO <sub>2</sub> :50/50	7	(Ordonez, Balkus Jr et al. 2010)
	Ultem	17	CO <sub>2</sub> /N <sub>2</sub> :20/80	21	(Dai, Johnson et al. 2012)
<b>HKUST-1</b>	Matrimid	10	CO <sub>2</sub> /CH <sub>4</sub> :35/65	18	(Basu, Cano-Odena et al. 2011)
			CO <sub>2</sub> /N <sub>2</sub> :35/65	8	
<b>MIL-53</b>	Polysulfone	30	CO <sub>2</sub> /CH <sub>4</sub> :50/50 CO <sub>2</sub> /N <sub>2</sub> :50/50	14.7 18	(Basu, Cano-Odena et al. 2010)
	Matrimid	15	CO <sub>2</sub> /CH <sub>4</sub> :50/50	8.5	(Chen, Vinh-Thang et al. 2015)
	Ultem	15	CO <sub>2</sub> /CH <sub>4</sub> :50/50	42.8	

## 1.5: Models for Predicting Permeation of Mixed Matrix Membranes (MMMs):

### 1.5.1: Predictive Models

Predictive models for MMMs have been developed for estimating effective permeability of a penetrant molecule through MMM as function of continuous phase (matrix) and dispersed phase (filler) permeabilities and fractional ratio between volumes of phases. The simplest examples of these predictive models are series and parallel two layer models (Vinh-Thang and Kaliaguine 2013). The equations for series and parallel two-layer models can be written as following respectively:

$$P_{eff}^{series} = \frac{P_m P_f}{\phi_m P_m + \phi_f P_m} \quad (1.4)$$

$$P_{eff}^{parallel} = \phi_m P_m + \phi_f P_f \quad (1.5)$$

In these equations,  $P_m$  is permeability of polymer matrix,  $P_f$  is permeability of porous filler structure,  $\phi_m$  is volume fraction of polymer component of whole composite membrane whereas  $\phi_f$  belongs to volume fraction of filler.

### 1.5.2: Maxwell Model and Te Hennepe Models

Other than these two-simple models, Maxwell was developed later by using an analogy between previously developed models for electric field permittivity through composite structures:

$$P_{eff}^{Maxwell} = P_m \left[ \frac{P_f + 2P_m - 2\phi_f(P_m - P_f)}{P_f + 2P_m + \phi_f(P_m - P_f)} \right] \quad (1.6)$$

In Maxwell Model,  $P_m$  is permeability of polymer matrix,  $P_f$  is permeability of porous filler structure,  $\phi_f$  is volume fraction of porous filler material. Series and Parallel assume that high aspect ratio fillers distribute in polymer matrix with a certain configuration but Maxwell model introduces randomly distributed spherical fillers. Maxwell model is most widely used MMM permeability prediction model by far due to its simplicity, good predictive performance for low filler loading which was demonstrated by many different studies. But, it also well-know that predictive performance of Maxwell diminishes excessively when volume ratio of filler exceeds 0.25-0.3. To fix this issue, Te Hennepe model (Hennepe, Smolders et al. 1991) was introduced by assuming cubic shaped filler geometry:

$$P_{eff}^{Te\ Hennepe} = P_m \left[ \left( 1 - \phi_f^{\frac{1}{3}} \right) + \frac{\frac{3}{2} \phi_f^{\frac{1}{3}} P_m}{P_m \phi_m + \frac{3}{2} \phi_f P_f} \right]^{-1} \quad (1.7)$$

In Te Hanepe Model,  $P_m$  is permeability of polymer matrix,  $P_f$  is permeability of porous filler structure,  $\phi_f$  is volume fraction of porous filler material. The basic assumption of Te Hanepe model is to replace spherical filler assumption of Maxwell Model with cubic filler particles.

### 1.5.3: Cussler Model

Another model which including filler geometry is known as Cussler model (Cussler 1990). In Cussler model was developed for flake shaped particles an assigned an aspect ratio  $\lambda$  (which ratio between to width and thickness of the flake) to each particle:

$$P_{eff}^{Cussler} = P_m \left[ (1 - \phi_f) + \left( \frac{P_f}{\phi_f P_c} + \frac{4(1-\phi_f)}{\lambda_f^2 \phi_f} \right)^{-1} \right]^{-1} \quad (1.8)$$

In Cussler Model,  $P_m$  is permeability of polymer matrix,  $P_f$  is permeability of porous filler structure,  $\phi_f$  is volume fraction of porous filler material and  $\lambda_f$  is the aspect ratio of filler particles. In this model, filler particles are defined with shape parameter  $\lambda_f$  instead of taking them spherical or cubic.

#### 1.5.4: KJN model

More recently, Kang, Jones and Nair proposed a model that not only includes the shape of filler but also orientation of it. This method assumes cylindrical filler particle and two dimensional MMM structure. The method is called as KJN model (Kang, Jones et al. 2011) and its formula is as following:

$$P_{eff}^{KJN} = P_m \left[ \left( 1 - \frac{\cos\theta}{\cos\theta + \lambda_f \sin\theta} \phi_f \right) + \frac{P_f}{P_c} \left( 1 - \frac{\cos\theta}{\cos\theta + \lambda_f \sin\theta} \right) \phi_f \right]^{-1} \quad (1.9)$$

Where  $P_m$  is permeability of polymer matrix,  $P_f$  is permeability of porous filler structure,  $\phi_f$  is volume fraction of porous filler material and  $\lambda_f$  is the aspect ratio of filler particles and  $\theta$  is angle between filler orientation and flux direction. For random distribution of particles this value should averaged between 0 and  $\pi/2$ .

This list of predictive effective permeability models for MMMs is far from being complete, there are many other methods available in literature. For further investigation, following reference could be consulted (Vinh-Thang and Kaliaguine 2013).

There has been an increasing trend in the number of publications relating with novel membranes over the past decade (Galizia, 2017). Thousands of different porous materials have been synthesized recent years (Groom, 2016) and considerable portion of them used as membrane material. All these newly categorized materials have been proposing new opportunities to develop better

performing membrane materials but understanding molecular transport through these various kind of different materials is still a challenging problem. This makes computational approach inevitable to tackle this highly complex problem.

Even though there have been significant efforts to model membrane materials in both realistic and detailed way, currently available methods and strategies is far from being complete. Most of membrane modelling effort remains in continuum level phenomenological models (Cussler, 1990, Hennepe, 1991) and atomistic level methods have their own limitations (Chen, 2006). Other than well-known time and length scale problem of current atomistic simulations, capturing non-equilibrium nature of membrane separation with an atomistic simulation remains as a challenge. To propose a remedy these long-standing problems, we proposed a non-equilibrium methodology to perform membrane separation for long simulation times (in principle, infinitely long). The work presented in this thesis gives an opportunity perform mixture membrane separation under constant inlet composition as a contribution to currently available methods. The methodology was tested for Metal Organic Framework (MOF) membranes and Mixed Matrix Membranes (MMMs) and it performed well both single and mixture gas permeations for variety of different molecules. This new method provides new opportunities to shed light to highly complex problem of molecular transport through nanoporous materials.

## 1.6: References:

1. Allen, S., et al. (1977). "The barrier properties of polyacrylonitrile." Journal of Membrane Science **2**: 153-163.
2. Ash, R., et al. (1973). "Isothermal and thermo-osmotic transport of sorbable gases in microporous carbon membranes." Philosophical Transactions of the Royal Society of London. Series A, Mathematical and Physical Sciences **275**(1249): 255-307.
3. Ash, R., et al. (1963). "Flow of adsorbable gases and vapours in a microporous medium, II. Binary Mixtures." Proceedings of the Royal Society of London. Series A. Mathematical and Physical Sciences **271**(1344): 19-33.
4. Ash, R., et al. (1976). "Sorption and flow of carbon dioxide and some hydrocarbons in a microporous carbon membrane." Journal of Membrane Science **1**: 17-32.
5. Bae, J., et al. (2017). "Multiple coordination exchanges for room-temperature activation of open-metal sites in metal–organic frameworks." ACS applied materials & interfaces **9**(29): 24743-24752.
6. Baker, R. W. (2002). "Future directions of membrane gas separation technology." Industrial & engineering chemistry research **41**(6): 1393-1411.
7. Baker, R. W. (2012). Membrane technology and applications, John Wiley & Sons.

8. Baker, R. W. and K. Lokhandwala (2008). "Natural gas processing with membranes: an overview." Industrial & engineering chemistry research **47**(7): 2109-2121.
9. Basu, S., et al. (2010). "Asymmetric Matrimid@[Cu<sub>3</sub> (BTC) <sub>2</sub>] mixed-matrix membranes for gas separations." Journal of Membrane Science **362**(1-2): 478-487.
10. Basu, S., et al. (2011). "MOF-containing mixed-matrix membranes for CO<sub>2</sub>/CH<sub>4</sub> and CO<sub>2</sub>/N<sub>2</sub> binary gas mixture separations." Separation and Purification Technology **81**(1): 31-40.
11. Beck, H. N. and E. S. Sanders Jr (1990). Composition useful in process for preparing powder membranes from tetrahalobisphenol a polycarbonates, Google Patents.
12. Ben, T., et al. (2012). "Polymer-Supported and Free-Standing Metal–Organic Framework Membrane." Chemistry–A European Journal **18**(33): 10250-10253.
13. Bernardo, P., et al. (2009). "Membrane gas separation: a review/state of the art." Industrial & engineering chemistry research **48**(10): 4638-4663.
14. Bøddeker, K. W. (1995). "Commentary: Tracing membrane science." Journal of Membrane Science **100**(1): 65-68.
15. Bourrelly, S., et al. (2010). "Explanation of the adsorption of polar vapors in the highly flexible metal organic framework MIL-53 (Cr)." Journal of the American Chemical Society **132**(27): 9488-9498.

16. Boutin, A., et al. (2010). "The behavior of flexible MIL-53 (Al) upon CH<sub>4</sub> and CO<sub>2</sub> adsorption." The Journal of Physical Chemistry C **114**(50): 22237-22244.
17. Brown, A. J., et al. (2014). "Interfacial microfluidic processing of metal-organic framework hollow fiber membranes." Science **345**(6192): 72-75.
18. Caro, J., et al. (2000). "Zeolite membranes—state of their development and perspective." Microporous and Mesoporous Materials **38**(1): 3-24.
19. Casco, M. E., et al. (2016). "Gate-opening effect in ZIF-8: the first experimental proof using inelastic neutron scattering." Chemical Communications **52**(18): 3639-3642.
20. Chen, H. and D. S. Sholl (2006). "Predictions of selectivity and flux for CH<sub>4</sub>/H<sub>2</sub> separations using single walled carbon nanotubes as membranes." Journal of Membrane Science **269**(1-2): 152-160.
21. Chen, X. Y., et al. (2015). "Membrane gas separation technologies for biogas upgrading." Rsc Advances **5**(31): 24399-24448.
22. Chui, S. S.-Y., et al. (1999). "A chemically functionalizable nanoporous material [Cu<sub>3</sub> (TMA)<sub>2</sub> (H<sub>2</sub>O)<sub>3</sub>]<sub>n</sub>." Science **283**(5405): 1148-1150.
23. Coan, F. L. and J. A. Jenvold (2007). Air dehydration membrane, Google Patents.
24. Cooley, T. and A. Coady (1978). Removal of H<sub>2</sub> S and/or CO<sub>2</sub> from a light hydrocarbon stream by use of gas permeable membrane, Google Patents.

25. Cussler, E. (1990). "Membranes containing selective flakes." Journal of Membrane Science **52**(3): 275-288.
26. Dai, Y., et al. (2012). "Ultem®/ZIF-8 mixed matrix hollow fiber membranes for CO<sub>2</sub>/N<sub>2</sub> separations." Journal of Membrane Science **401**: 76-82.
27. Fairen-Jimenez, D., et al. (2011). "Opening the gate: framework flexibility in ZIF-8 explored by experiments and simulations." Journal of the American Chemical Society **133**(23): 8900-8902.
28. Figueroa, J. D., et al. (2008). "Advances in CO<sub>2</sub> capture technology—the US Department of Energy's Carbon Sequestration Program." International journal of greenhouse gas control **2**(1): 9-20.
29. Furukawa, H., et al. (2013). "The chemistry and applications of metal-organic frameworks." Science **341**(6149): 1230444.
30. Galizia, M., et al. (2017). "50th anniversary perspective: Polymers and mixed matrix membranes for gas and vapor separation: A review and prospective opportunities." Macromolecules **50**(20): 7809-7843.
31. Gottschlich, D. E. and D. L. Roberts (1990). Energy minimization of separation processes using conventional/membrane hybrid systems, EG and G Idaho, Inc., Idaho Falls, ID (USA).
32. Guo, H., et al. (2009). "'Twin copper source' growth of metal-organic framework membrane: Cu<sub>3</sub>(BTC)<sub>2</sub> with high permeability and selectivity for recycling H<sub>2</sub>." Journal of the American Chemical Society **131**(5): 1646-1647.

33. Henis, J. M. (1994). Commercial and practical aspects of gas separation membranes, CRC Press: Boca Raton, FL.
34. Hennepe, H. t., et al. (1991). "Exclusion and tortuosity effects for alcohol/water separation by zeolite-filled PDMS membranes." Separation science and technology **26**(4): 585-596.
35. Hu, Y., et al. (2008). "Synthesis and properties of indan-based polyacetylenes that feature the highest gas permeability among all the existing polymers." Macromolecules **41**(22): 8525-8532.
36. Jones, P. E. (2004). Modular on-board inert gas generating system, Google Patents.
37. Kang, D.-Y., et al. (2011). "Modeling molecular transport in composite membranes with tubular fillers." Journal of Membrane Science **381**(1-2): 50-63.
38. Kohl, A. L. and R. Nielsen (1997). Gas purification, Elsevier.
39. Koros, W. J. and G. Fleming (1993). "Membrane-based gas separation." Journal of Membrane Science **83**(1): 1-80.
40. Krishna, R. and R. Baur (2003). "Modelling issues in zeolite based separation processes." Separation and Purification Technology **33**(3): 213-254.
41. Lee, J. B., et al. (2008). "High selectivities in defective MFI membranes." Journal of Membrane Science **321**(2): 309-315.

42. Lin, L. C., et al. (2013). "Understanding CO<sub>2</sub> dynamics in metal–organic frameworks with open metal sites." Angewandte Chemie International Edition **52**(16): 4410-4413.
43. Liu, K., et al. (2010). Hydrogen and syngas production and purification technologies, John Wiley & Sons.
44. Liu, Y., et al. (2014). "MOF membrane synthesis in the confined space of a vertically aligned LDH network." Chemical Communications **50**(32): 4225-4227.
45. Llewellyn, P., et al. (2009). "Complex adsorption of short linear alkanes in the flexible metal-organic-framework MIL-53 (Fe)." Journal of the American Chemical Society **131**(36): 13002-13008.
46. Loeb, S. (1960). "Sourirajan,“." Sea Water Demineralization By Means of a Semipermeable Membrane,” UCLA Department of Engineering Report: 60-60.
47. Loiseau, T., et al. (2004). "A rationale for the large breathing of the porous aluminum terephthalate (MIL-53) upon hydration." Chemistry–A European Journal **10**(6): 1373-1382.
48. Lonsdale, H. (1982). "The growth of membrane technology." Journal of Membrane Science **10**(2-3): 81-181.
49. Lovallo, M. C., et al. (1998). "Synthesis and characterization of oriented MFI membranes prepared by secondary growth." AICHE journal **44**(8): 1903-1913.

50. MacLean, D., et al. (1986). Gas separations using composite hollow fiber membranes, CRC Press: Boca Raton, FL.
51. Mitchell, J. K. (1995). "On the penetrativeness of fluids." Journal of Membrane Science **100**(1): 11-16.
52. Mulder, J. (2012). Basic principles of membrane technology, Springer Science & Business Media.
53. Nollet, J. A. A. (1995). "Investigations on the causes for the ebullition of liquids." Journal of Membrane Science **100**(1): 1-3.
54. Ordonez, M. J. C., et al. (2010). "Molecular sieving realized with ZIF-8/Matrimid® mixed-matrix membranes." Journal of Membrane Science **361**(1-2): 28-37.
55. Pan, Y. and Z. Lai (2011). "Sharp separation of C2/C3 hydrocarbon mixtures by zeolitic imidazolate framework-8 (ZIF-8) membranes synthesized in aqueous solutions." Chemical Communications **47**(37): 10275-10277.
56. Park, K. S., et al. (2006). "Exceptional chemical and thermal stability of zeolitic imidazolate frameworks." Proceedings of the National Academy of Sciences **103**(27): 10186-10191.
57. Peralta, D., et al. (2012). "Comparison of the behavior of metal–organic frameworks and zeolites for hydrocarbon separations." Journal of the American Chemical Society **134**(19): 8115-8126.
58. Posey Jr, L. G. (1983). Processes, Google Patents.

59. Ren, T., et al. (2006). "Olefins from conventional and heavy feedstocks: Energy use in steam cracking and alternative processes." Energy **31**(4): 425-451.
60. Saidur, R., et al. (2010). "A review on compressed-air energy use and energy savings." Renewable and Sustainable Energy Reviews **14**(4): 1135-1153.
61. Sanders, D. F., et al. (2013). "Energy-efficient polymeric gas separation membranes for a sustainable future: A review." Polymer **54**(18): 4729-4761.
62. Sanders Jr, E. S., et al. (1988). Process for preparing POWADIR membranes from tetrahalobisphenol A polycarbonates, Google Patents.
63. Schwalm, G. K. (2007). On-board inert gas generation system, Google Patents.
64. Scott, K. (1995). Handbook of industrial membranes, Elsevier.
65. Serre, C., et al. (2002). "Very Large Breathing Effect in the First Nanoporous Chromium (III)-Based Solids: MIL-53 or  $\text{CrIII}(\text{OH})\{\text{O}_2\text{C}-\text{C}_6\text{H}_4-\text{CO}_2\}\cdot x\text{H}_2\text{O}\cdot y$ ." Journal of the American Chemical Society **124**(45): 13519-13526.
66. Sholl, D. S. and R. P. Lively (2016). "Seven chemical separations to change the world." Nature News **532**(7600): 435.
67. Sidney, L. and S. Srinivasa (1964). High flow porous membranes for separating water from saline solutions, Google Patents.
68. Sircar, S. (2002). "Pressure swing adsorption." Industrial & engineering chemistry research **41**(6): 1389-1392.

69. Skoulidas, A. I., et al. (2002). "Rapid transport of gases in carbon nanotubes." Physical review letters **89**(18): 185901.
70. Sokhan, V., et al. (2004). "Transport properties of nitrogen in single walled carbon nanotubes." The Journal of chemical physics **120**(8): 3855-3863.
71. Sokhan, V. P., et al. (2002). "Fluid flow in nanopores: Accurate boundary conditions for carbon nanotubes." The Journal of chemical physics **117**(18): 8531-8539.
72. Spillman, R. W. (1989). "Economics of gas separation membranes." Chemical engineering progress **85**(1): 41-62.
73. Springuel-Huet, M.-A., et al. (2010). "129Xe NMR study of the framework flexibility of the porous hybrid MIL-53 (Al)." Journal of the American Chemical Society **132**(33): 11599-11607.
74. Stookey, D., et al. (1986). "Membranes separate gases selectively." Chemical engineering progress **82**(11): 36-40.
75. Theis, T. and S. Titus (1996). "The Development of Permeable Membrane Air Dehydrators for the US Navy." Naval engineers journal **108**(3): 243-265.
76. Vinh-Thang, H. and S. Kaliaguine (2013). "Predictive models for mixed-matrix membrane performance: a review." Chemical reviews **113**(7): 4980-5028.
77. Volkringer, C., et al. (2009). "XRD and IR structural investigations of a particular breathing effect in the MOF-type gallium terephthalate MIL-53 (Ga)." Dalton Transactions(12): 2241-2249.

78. Yampolskii, Y. and B. Freeman (2010). Membrane gas separation, John Wiley and Sons.
79. Yang, M., et al. (1999). "The hindering effect of adsorbed components on the permeation of a non-adsorbing component through a microporous silicalite membrane: the potential barrier theory." Journal of Membrane Science **156**(1): 1-9.
80. Zhang, F., et al. (2012). "Hydrogen Selective NH<sub>2</sub>-MIL-53 (Al) MOF Membranes with High Permeability." Advanced Functional Materials **22**(17): 3583-3590.

## Chapter 2: LITERATURE REVIEW

Membranes have gained a significant workplace and found many different applications in chemical processes. Nano-level design principles provide significant opportunities to design better performing membranes. Controlling permeation of molecules through membrane structure is the ultimate goal of rational membrane design. Atomistic molecular dynamics simulations give a significant toolkit to gain fundamental understanding on permeation of penetrants through a membrane material. It should be stressed that membrane separation is a non-equilibrium process and that out of equilibrium condition should be considered in membrane simulation methodology. A variety of approaches that has been used to impose non-equilibrium conditions in MD simulations for membrane separation studies are summarized in Figure 2-1 and explained in following paragraphs.

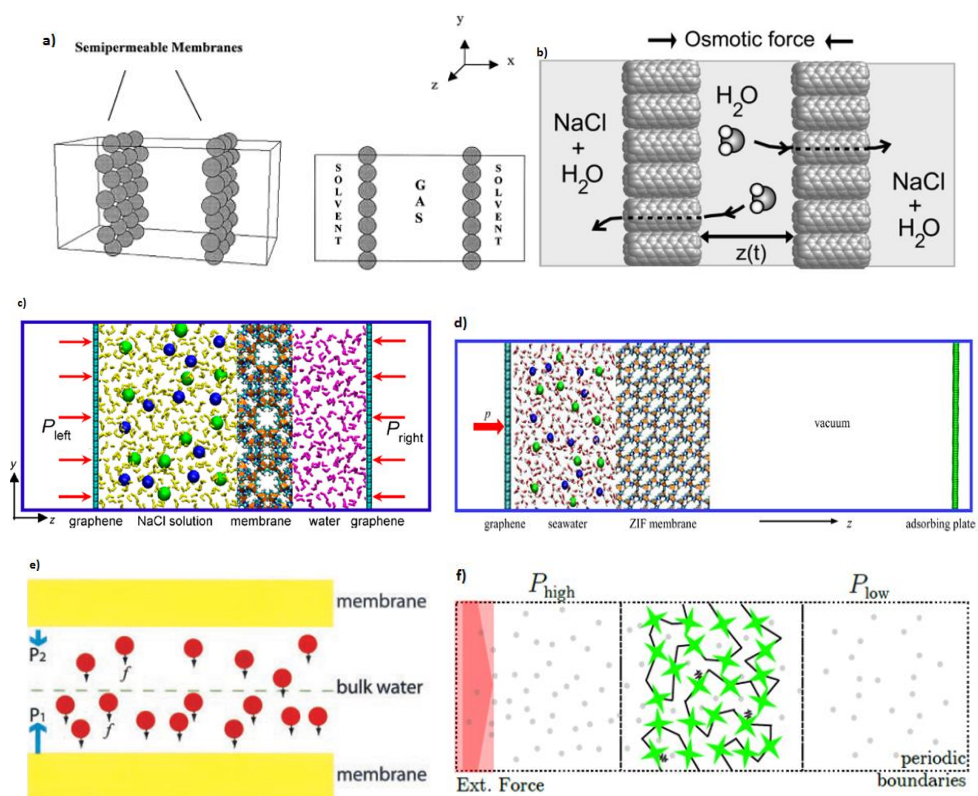


**Figure 2-1.** Some example simulation boxes for membrane transport simulations:

a) Simulation box of Murad et al. (Murad and Gupta, 2000), b) Simulation box of Kalra et al. (Kalra et al., 2003), c) Simulation box of Gupta et al. (Gupta et al., 2015), d) Simulation box of Gupta et al. for pervaporation membrane study (Gupta et al., 2016), e) Steered MD simulation box of Zhu et al. (Fangqiang Zhu, 2002), f) Boundary driven MD simulation box of Frentrup et al. (Frentrup et al., 2012)

In early membrane simulations with molecular dynamics, researchers attempted to construct their simulation boxes in a smart way to model membrane transport more realistically. The studies by Prof. Sohail Murad can be considered as a good representatives of this approach (Murad and Powles, 1993, Murad and Gupta, 2000, Lin and Murad, 2001, Murad and Nitsche, 2004). In this methodology, molecules were “sandwiched” between two parallel membranes and the transport properties of these molecules observed until the system reaches the equilibrium. Similar simulation box set up was used by Kalra et al. to model the osmotic water transport through a Carbon Nanotube (CNT) membrane (Kalra et al., 2003). This investigation became highly cited due to unveiling of fast water transport mechanism through CNT membranes. However, these approaches have transient nature and once the system reaches the equilibrium, molecular transport stops. Therefore, the simulation time is apparently limited with number molecules sandwiched between two parallel membranes.

To keep thermodynamic gradient fixed, researchers came up with another idea: A method was based upon maintaining constant chemical potential at inlet and outlet of a membrane. This idea, in principle, is the exact solution to impose non-

equilibrium conditions during an MD simulation of a membrane process and it is called as dual control volume grand canonical molecular dynamics (DCV-GCMD) technique (Heffelfinger and Swol, 1994). This is a hybrid Monte-Carlo (MC) and MD method which defines two control volumes at the feed and permeate sides of the membrane and keeps the chemical potential in these control volumes fixed by employing insertion and deletion of the fluid molecules. This simulation technique was utilised by many researchers for different membrane systems such as simple slit-shaped pores (Cracknell et al., 1995), porous silica membranes (Phillip I. Pohl, 1999) and carbon molecular sieve (CMS) membranes (Lifang Xu., 2004). However, a major problem with DCV-GCMD method appears for dense fluid systems. It does not work efficiently since the acceptance rates for the insertion/deletion moves for MC become extremely small. Moreover, according to Hato et al. (Ható et al., 2015) coupling MC moves with MD can be problematic since the ratio of insertion/deletion steps vs. MD steps should be optimised in order to perform a reliable simulation.

Placing impermeable-moving walls in a simulation box and exerting a constant force on them to create a piston effect is another common approach to maintain non-equilibrium conditions in MD simulations. For instance, Wang et al. studied water transport through CNT membranes by placing two moving walls at opposite ends of the simulation box (Wang et al., 2013). By applying a larger force on the feed side wall and a smaller force on the permeate side wall in opposite directions, they maintained a higher pressure on the feed side and lower pressure on the permeate side. This created a pressure gradient and pushed the water molecules through pores of the CNT membrane. Same authors applied a similar

approach for polyamide (PA) membranes (Wang et al., 2016) to study water transport. In another recent study, Shen et al.(Shen et al., 2016) had applied the moving wall approach to explore the potential of polymeric FT-30 membrane in reverse osmosis. Hu et al.(Hu et al., 2011) and Gupta et al.(Gupta et al., 2015) again used the moving wall approach to investigate water desalination in zeolitic imidazolate frameworks (ZIFs). In another study, Gupta et al.(Gupta et al., 2016) used a modified approach with a similar spirit to elucidate desalination in five different ZIFs in a pervaporation membrane setting. On the feed side, a force was applied on an impermeable wall to push the saline water through the membrane, but on the far end of the permeate side; a fixed wall was placed which interacted with the fluid molecules through a strong attractive force. This wall was designed to act like an adsorbing plate which attracted all molecules diffused to the permeate side on itself to create a vacuum effect near the surface of the membrane's permeate side. Non-equilibrium MD (NEMD) simulations with moving impermeable walls have a disadvantage that the simulation time is limited by the number of molecules placed on the feed side. Because, once all the fluid molecules are pushed to the permeate side by the moving wall; the feed is depleted, simulation terminates. Another shortcoming of using an impermeable wall to push fluid molecules through a membrane is that it is not possible to keep the concentration of species constant in feed side if the simulation involves a mixture separation. Because the concentration of the less diffusive species will increase on the feed side as the mixture is pushed towards the membrane by the impermeable wall. Therefore; it is not possible to run a steady state and continuous membrane simulation with impermeable walls in simulation box. In order to address the feed depletion problem in an NEMD simulation with impermeable walls, Cabrales-Navarro et

al.(Cabrales-Navarro et al., 2013) considered moving a certain number of molecules from the permeate side to the feed side at regular time intervals (every 50 ps in their work). While this approach ensured the simulation can be run continuously, it did not essentially provide a steady state simulation due to the transfer of fluid molecules from one side to another externally by hand.

Another way of imposing non-equilibrium conditions for an MD membrane simulation is to apply a continuous external force on the molecules (which is called. steered-molecular dynamics) along the direction perpendicular to the membrane and with periodic boundary conditions in all directions so that feed depletion can be avoided. Using this method, Zhu et al. (Fangqiang Zhu, 2002) investigated the transport of water through a biological membrane. This ensured the circulation of molecules in the permeate side back to the feed side through the periodic boundary. Ding et al.(Ding et al., 2015) used a similar approach to examine the water desalination performance of a polyamide polymer membrane. On the other hand, this method does not provide a way for controlling the concentration of species. Moreover, applying an external force all over the simulation box requires care because if the bias exceeds a critical level then thermostat or barostat algorithms can fail to do their job due to fictional increase of particle velocities (Ható et al. 2015). To address this concern, in their study of gas permeation through slit pores, Frentrup et al. (Frentrup et al., 2012) restricted the external force in to a considerably small region in the simulation box and they named their method as "boundary-driven NEMD" in attribution the position of the small force region placed at the boundary of the simulation box. Same authors extended their method to investigate single gas permeation of CO<sub>2</sub> and He through a PIM-1 polymer

membrane (Frentrup et al., 2015). Even though their methodology allows the circulation of fluid molecules between permeate and feed sides to ensure a continuous simulation, it does not provide control over the density of fluids at the inlet and outlet of the membrane. Hato et al.(Ható et al., 2015) proposed a methodology which to address the shortcomings of previous methods which was essentially a combination of the method of Frentrup et al.(Frentrup et al., 2012) and DCV-GCMD method of Heffelfinger et al. (Heffelfinger and Swol, 1994) recently which requires the coupling of MC and MD algorithms.

## **2.1: BACKGROUND THEORY**

### **2.1.1: Molecular Simulations:**

In his famous “Lectures on Physics”, great American physicist Richard Feynman encapsulates whole idea in single sentence: “Everything in physics can be understood in terms of the jiggings and wiggings of atoms.” (Feynman et al., 1964). The key point is to interpret the “jiggles” and “wiggles” in consistent and rigorous way.

In order to be consistent, the discussion should pursue in the chronological order. Thermodynamics had revolutionized the understanding and perspective of scientists nearly 150 years ago. Understanding the equivalence between heat and work (first law of thermodynamics) and defining a new function so called entropy (second law of thermodynamics) were first two big achievements of early thermodynamics researchers. Even though thermodynamics was a great tool to describe nature, it is intrinsically phenomenological. That means it can describe

“expansion of gas when it is heated up” but could not explain “why gases expand when they are heated up?”

Statistical mechanics is the machinery to answer this “why” question. General scheme of statistical mechanics was explained in many great physics textbooks (Callen, 2006, Landau and Lifshitz, 1980, Huang, 1963, Kardar, 2007). Starting from atoms and molecules and describing motion of them (as translation, rotation, vibration etc.) in a mathematical framework, statistical mechanics could be able to re-derive all thermodynamically relations.

Molecular Simulations, as its name suggests, describe the model system starting from atomistic details. At this scale, every atomic unit is associated with 6 different degrees of freedom: 3 for position ( $\vec{r}$ ) and three for momentum ( $\vec{p}$ ). This defines a microscopic scale definition of model system and the space of all possible microscopic states is called as phase space.

The statistical mechanics offers a systematic framework which applies the statistical tools to reduce huge dimensionality of phase space to limited number of thermodynamic variables that characterize the system at the macroscale, such as the temperature (T), volume (V) or number of molecules (N). They are called as macrostates. To map a set of microstates to a unique macrostate, statistical ensembles are needed and depending to thermodynamic quantity measured and allowed to exchange with an external bath, several statistical ensembles can be defined.

The mathematical workhorse of the statistical mechanics is partition functions. In an NVT ensemble, a system is described with fixed number of

particles (N), fixed volume (V) and fixed temperature (T). Every microstate  $i$  can be associated with an energy level  $E_i$  and partition function of an NVT system can be written as (Equation 2.1)

$$Z = \sum_i e^{-\frac{E_i}{kT}} \quad (2.1)$$

Eq.2.1 gives the partition function of a system which has discrete energy levels. This summation over all microstates can be replaced by integration over all phase space (Equation 2.2):

$$Z = \frac{1}{N! h^{3N}} \iint d^N r d^N p e^{-\frac{E(r,p)}{kT}} \quad (2.2)$$

Where  $h$  is Planck constant and normalises the integrand, which is the unit of action,  $N!$  accounts for the indistinguishability of particles and their permutations which leads to same microstate. Quantum statistical mechanics gives the justification for this Planck constant at denominator with Heisenberg's uncertainty principle. As a pictorial explanation,  $h^{3N}$  hypercubes define "pixels" of phase space to make a partition of it and count to possible quantum states.

The integration in Eq.2.2 is directly related with Helmholtz Free energy,  $F$  (Equation 2.3) :

$$F = -kT \ln(Z) \quad (2.3)$$

Finally, thermodynamic variables could be obtained from corresponding derivatives of free energy expression (Equation 2.4):

$$S = -\left(\frac{\partial A}{\partial T}\right)_{N,V} ; \quad P = -\left(\frac{\partial A}{\partial V}\right)_{N,T} ; \quad \mu = -\left(\frac{\partial A}{\partial N}\right)_{V,T} \quad (2.4)$$

Obviously, the main problem is reduced to calculate partition function which is a problem of high dimensional integration in principle. However, dimension of this integration is related to the total number of particles (N) in the system and in the thermodynamically limit (N goes to Avogadro number), calculation of these integrals becomes impossibly tedious.

Computers had come into picture in that phase. Early researchers had believed that computers could achieve the calculations of these heavy integrations (Theodorou, 2010). In advance, thanks to elegant algorithms, computers play a key role on various chemical, biological and materials science applications in today's scientific research.

Before discussing these elegant algorithms, it is needed to return the Eq.2.1. The “ $E_i$ ” is the energy of  $i^{\text{th}}$  state in Eq.2.1. Describing energy of a system is not a trivial issue, but Hamiltonian mechanics gives mathematical framework of it (Landau, 1980). According to this approach, a Hamiltonian needed to be defined which relates every state of momentum and position to its energy. The Hamiltonian could be divided into two parts (Equation 2.5): Kinetic and Potential parts. Kinetic part is related to the momentum coordinates of the state as well as, potential part is related to position coordinates.

$$H(r_1, r_2, \dots, r_N, p_1, \dots, p_N) = K(p_1, \dots, p_N) + U(r_1, \dots, r_N) \quad (2.5)$$

Definition of kinetic part is simple quadratic equation between momentum and energy and defining potential part need a serious consideration. It will be discussed in “Molecular Interactions” section.

### 2.1.2: Molecular Interactions:

How atoms and molecules interact with each other? It is difficult but inevitable question to model materials. Molecular interactions govern the molecular motion, hence designates phase-space trajectories. Molecular interactions are mainly split into two: Intermolecular and intramolecular interactions. Historically, scientists had begun to think on molecular interaction for simple ideal gases initially, therefore, modelling intermolecular interactions is a little pre-dated than intramolecular ones.

Lenard-Jones potential provides a simple representation of interaction between molecules. The interaction potential is given below (Equation 2.6):

$$V_{LJ}(r_{ij}) = 4\varepsilon \left[ \left( \frac{\sigma}{r_{ij}} \right)^{12} - \left( \frac{\sigma}{r_{ij}} \right)^6 \right] \quad (2.6)$$

In Eq.2.6  $r_{ij}$  is the distance between  $i^{\text{th}}$  and  $j^{\text{th}}$  particles. Two parameters ( $\sigma$  and  $\varepsilon$ ) define size and interaction between two particles, respectively. 6-term and 12-term correspond to attractive part of the LJ potential and repulsive part, respectively. In addition to dispersive and repulsive interaction, electrostatic interaction should also be considered for charged particles. The Coulomb potential associated with electrostatic interaction can be described by (Equation 2.7):

$$V_C(r_{ij}) = \frac{1}{4\pi\varepsilon_0} \frac{q_i q_j}{r_{ij}} \quad (2.7)$$

In Eq.2.7,  $\varepsilon_0$  is the vacuum permittivity,  $r_{ij}$  is the distance between  $i^{\text{th}}$  and  $j^{\text{th}}$  particles and  $q_i$  and  $q_j$  are

electron charge around particle  $i$  and  $j$ , respectively.

Intramolecular interactions can be described as for total energy of “bonded” system (Equation 2.8):

$$\begin{aligned}
 U = & \sum_{bonds} u_b(r) + \sum_{bends} u_\theta(\theta) + \sum_{torsion} u_\phi(\phi) + \sum_{improper} u_\chi(\chi) \\
 & + \sum_{bond-bond} u_{bb'}(r, r') + \sum_{bond-bend} u_{b\theta'}(r, \theta') \\
 & + \sum_{bend-bend} u_{\theta\theta'}(\theta, \theta') + \dots
 \end{aligned} \tag{2.8}$$

In Eq.2.8, first term is harmonic interaction between two bonded atoms, second term is harmonic bending interaction between three bonded atoms and third term is periodic interaction between 4 bonded atoms etc. In our model, we used only the first four terms to model the interaction between bonded atoms.

For Eq.2.6, Eq.2.7 and Eq.2.8, pre-defined parameters are needed. These parameter sets are called as “force fields”. AMBER (Yong Duan, 2003), OPLS (Jorgensen, 1998), CHARMM (Vanommeslaeghe et al., 2010), DREIDING (Mayo et al., 1990), UFF (Rappé et al., 1992) are some popular examples of generic force fields.

### 2.1.3: Molecular Simulation Methods:

Monte Carlo and Molecular Dynamics methods are the most common simulation methodologies for materials modelling at molecular level. Monte Carlo (MC) is a probabilistic method to determine equilibrium properties of materials whereas; Molecular Dynamics (MD) is a deterministic one to describe dynamics of the microscopic system by integration equation of motion for every particle.

### 2.1.3.1: Monte Carlo (MC) Simulations:

The definition of partition function is given in Eq.2.1. In classical statistical mechanics, the mean value of an observable A could be calculated as:

$$\langle A \rangle = \frac{\sum_i A_i e^{-\frac{E_i}{kT}}}{\sum_i e^{-\frac{E_i}{kT}}} \quad (2.9)$$

For continuous energy spectrum system, the summations in Eq.2.9 turn into integration and the energy term should be deduced as Hamiltonian. Hamiltonian is function of positions and momenta; therefore, integration should be performed over r and p coordinates of the system. The integration over momenta could be carried out analytically due to quadratic relation between kinetic part of Hamiltonian and momenta. However, integration over position coordinate is more difficult due to complex nature of dependence of Potential part Hamiltonian to position. Thus, if the observable A only depends on positions, the Eq.2.9 becomes:

$$\langle A \rangle = \frac{\int dr_1 dr_2 \dots dr_n e^{-\frac{U(r_1, \dots, r_N)}{kT}} A(r_1, \dots, r_N)}{\int dr_1 dr_2 \dots dr_n e^{-\frac{U(r_1, \dots, r_N)}{kT}}} \quad (2.10)$$

It is not possible to compute partition function for large system ( $N > 100$ ) and complex functional form of potential energy. Monte Carlo scheme proposes an elegant way to achieve this integration. The algorithm uses random movements to sample the phase space. The Monte Carlo algorithm takes an initial configuration of the system, then performs a random evolution over system configuration, calculates the energy difference ( $\Delta U$ ) between these two configurations and associated Boltzmann factor with energy difference ( $\exp(-\Delta U/kT)$ ) and lastly it decides whether the new configuration will be accepted or not according to this

Boltzmann factor. But, it should be stressed here this Metropolis spirit version of MC algorithms are only valid under assumption of symmetric proposal distribution. Sometimes a symmetric proposal distribution might not be optimal and a correction factor, the Hasting ratio, is applied to correct this bias. Hasting ratio usually speed up convergence and this version of MC algorithm is called Metropolis-Hasting MC method.

### 2.1.3.2: Molecular Dynamics (MD) Simulation:

Molecular Dynamics algorithm depends on explicit movement of all particles in a specified system. The molecules are taken as “classical” objects and MD solves classical equation of motion. Intermolecular force between molecules  $i$  and  $j$  could be calculated as follows (Equation 2.11)

$$f_{ij} = -\frac{\partial u_{ij}}{\partial r_{ij}} \quad (2.11)$$

In Eq.2.11,  $f_{ij}$  is intermolecular forces between particle  $i$  and  $j$ ,  $u_{ij}$  is intermolecular potential and  $r_{ij}$  is the distance between particle  $i$  and  $j$ . After determining forces between all particles at initial configuration, Newton’s equations could be integrated. According to Leap-Frog algorithm, Newton’s law of motions is integrated by discretising differential definition of acceleration and velocity:

$$v\left(t + \frac{1}{2}\Delta t\right) = v\left(t - \frac{1}{2}\Delta t\right) + \frac{\Delta t f(t)}{m} \quad (2.12)$$

$$r(t + \Delta t) = r(t) + \Delta t v\left(t + \frac{1}{2}\Delta t\right) \quad (2.13)$$

Leap-frog algorithm uses forces to update velocity at mid-time interval than the updated velocity to update position data as it is shown in Eq.2.12 and Eq.2.13. Leap-frog algorithm is both symplectic and time reversible which is important to generate ergodic trajectories along the simulation. The advantage of a symplectic algorithm is to possess global stability. Since the area bounded by adjacent trajectories is preserved due to Liouville's theorem (Kardar, 2007) in a symplectic algorithm, the coordinates (hence, the energy) will not increase without bound during a sufficiently long simulation.

#### **2.1.4: Short-Cuts**

Calculation of interactions among too many particles is computationally infeasible. A number of "short cuts" were invented to reduce the computational effort for molecular interactions.

Number of particles is excessively limited with respect to thermodynamic limit of particles. To overcome this limitation, Periodic Boundary Conditions (PBC) is a commonly used trick. PBC treats single cell of simulation box as a centre of periodic lattice identical cells. When PBC is applied, the number of pairwise interactions increases due to periodic "*images*" of particles inside the simulation box. To overcome the issue of increased number of *image's interactions*, minimum image convention is applied. That implies every particle could only interact with one single "image" of every other particle.

Another short cut implementation to reduce the calculation of the amount of interactions is *cut-off radius*. This trick implies that the only interactions inside

cut-off radius around a particle would include and the interaction over truncation would account implicitly.

The implicit correlation to total energy is called as tail correction and it is calculated as follows:

$$\Delta U_{tail} = \frac{\rho}{2} \int_{r_c}^{\infty} u(r) 4\pi r^2 dr \quad (2.14)$$

In Eq.2.14  $\rho$  is molecular density and  $u(r)$  is pairwise interaction between molecules and  $r_c$  is cut-off radius.

An additional approximation to calculate unlike Lenard-Jones sites is *Lorentz-Berthelot mixing rule* which proposes to carry out calculation with the following approach:

$$\sigma_{AB} = \frac{\sigma_A + \sigma_B}{2} \quad (2.15)$$

$$\varepsilon_{AB} = \sqrt{\varepsilon_A \varepsilon_B} \quad (2.16)$$

The Lenard Jones interaction between molecules type A and molecule type B could be calculated with the parameter defined in Eq.2.15 and Eq.2.16.

## 2.2: THESIS AIM AND OUTLINE

The aim of this study is to develop novel methodologies in order to carry out more realistic membrane permeation and separation simulations in atomistic level.

The main objectives of this study:

- To propose a new Non-Equilibrium Molecular Dynamics (NEMD) method to perform membrane simulations under more realistic setup and conditions.
- To test the proposed methodology for novel membrane structures and compare these full atomistic simulation results with experimental data available in literature.
- To extend the performance analysis of membranes into new gas mixtures and composite membranes.
- Particularly, we are interested in MOF-Polymer mixed matrix membranes (MMMs) and their separation performances for gas mixtures. To evaluate applicability of proposed methodology to complex MMM structures in long time and length scales with respect to current limits of atomistic MD simulations.
- To investigate multi-interface membranes' separation performances and bring some insight to surface compatibility of Mixed Matrix Membrane from atomistic free energy calculation methods.
- To model inter-particle surface resistance and propose a method to calculate surface permeation directly from NEMD simulations.

## 2.3: References

1. Cabrales-Navarro, F. A., et al. (2013). "Molecular dynamics simulations of metal-organic frameworks as membranes for gas mixtures separation." Journal of Membrane Science **428**: 241-250.
2. Callen, H. B. (2006). Thermodynamics & an Intro. to Thermostatistics, John wiley & sons.
3. Cracknell, R. F., et al. (1995). "Direct molecular dynamics simulation of flow down a chemical potential gradient in a slit-shaped micropore." Physical Review Letters **74**(13): 2463-2466.
4. Ding, M., et al. (2015). "On the structure and rejection of ions by a polyamide membrane in pressure-driven molecular dynamics simulations." Desalination **368**: 76-80.
5. Fangqiang Zhu, E. T., Klaus Schulten (2002). "Pressure-Induced Water Transport in Membrane Channels Studied by Molecular Dynamics." Biophysical Journal **83**: 154-160.
6. Feynman, R. P., et al. (1964). Feynman Lecture on Physics, vol. II, Addison-Wesley.
7. Frentrup, H., et al. (2012). "Transport diffusivities of fluids in nanopores by non-equilibrium molecular dynamics simulation." Molecular Simulation **38**(7): 540-553.

8. Frentrup, H., et al. (2015). "In Silico Determination of Gas Permeabilities by Non-Equilibrium Molecular Dynamics: CO<sub>2</sub> and He through PIM-1." Membranes (Basel) **5**(1): 99-119.
9. Gupta, K. M., et al. (2016). "Seawater Pervaporation through Zeolitic Imidazolate Framework Membranes: Atomistic Simulation Study." ACS Appl Mater Interfaces **8**(21): 13392-13399.
10. Gupta, K. M., et al. (2015). "Water Desalination through Zeolitic Imidazolate Framework Membranes: Significant Role of Functional Groups." Langmuir **31**(48): 13230-13237.
11. Ható, Z., et al. (2015). "A simple method for the simulation of steady-state diffusion through membranes: pressure-tuned, boundary-driven molecular dynamics." Molecular Simulation **42**(1): 71-80.
12. Heffelfinger, G. S. and F. v. Swol (1994). "Diffusion in Lennard-Jones fluids using dual control volume grand canonical molecular dynamics simulation (DCV-GCMD)." The Journal of Chemical Physics **100**(10): 7548.
13. Hu, Z., et al. (2011). "Zeolitic imidazolate framework-8 as a reverse osmosis membrane for water desalination: insight from molecular simulation." Journal of Chemical Physics **134**(13): 134705.
14. Huang, K. (1963). *Statistical mechanics*, Wiley, New York.
15. Jorgensen, W. L. (1998). "OPLS force fields." Encyclopedia of computational chemistry.

16. Kalra, A., et al. (2003). "Osmotic water transport through carbon nanotube membranes." Proceedings of the National Academy of Sciences **100**(18): 10175-10180.
17. Kardar, M. (2007). Statistical physics of particles, Cambridge University Press.
18. Landau, L. D. and E. Lifshitz (1980). Statistical physics, part I, pergamon, Oxford.
19. Lifang Xu, M. G. S., Muhammad Sahimi, Theodore T. Tsotsis "Nonequilibrium Molecular Dynamics Simulation of Transport of Gas Mixtures in Nanopores." Physical Review Letters **80**(16): 3511-3514.
20. Lin, J. and S. Murad (2001). "A computer simulation study of the separation of aqueous solutions using thin zeolite membranes." Molecular Physics **99**(14): 1175-1181.
21. Mayo, S. L., et al. (1990). "DREIDING: a generic force field for molecular simulations." Journal of Physical chemistry **94**(26): 8897-8909.
22. Murad, S. and S. Gupta (2000). "A simple molecular dynamics simulation for calculating Henry's constant and solubility of gases in liquids." Chemical Physics Letters **319**(1-2): 60-64.
23. Murad, S. and L. C. Nitsche (2004). "The effect of thickness, pore size and structure of a nanomembrane on the flux and selectivity in reverse osmosis separations: a molecular dynamics study." Chemical physics letters **397**(1): 211-215.

24. Murad, S. and J. Powles (1993). "A computer simulation of the classic experiment on osmosis and osmotic pressure." The Journal of chemical physics **99**(9): 7271-7272.
25. Phillip I. Pohl, G. S. H. (1999). "Massively parallel molecular dynamics simulation of gas permeation across porous silica membrane." Membrane Science **155**: 1-7.
26. Rappé, A. K., et al. (1992). "UFF, a full periodic table force field for molecular mechanics and molecular dynamics simulations." Journal of the American chemical society **114**(25): 10024-10035.
27. Shen, M., et al. (2016). "Dynamics of water and solute transport in polymeric reverse osmosis membranes via molecular dynamics simulations." Journal of Membrane Science **506**: 95-108.
28. Theodorou, D. N. (2010). "Progress and outlook in Monte Carlo simulations." Industrial & Engineering Chemistry Research **49**(7): 3047-3058.
29. Vanommeslaeghe, K., et al. (2010). "CHARMM general force field: A force field for drug-like molecules compatible with the CHARMM all-atom additive biological force fields." Journal of Computational Chemistry **31**(4): 671-690.
30. Wang, L., et al. (2013). "Nonequilibrium molecular dynamics simulation of pressure-driven water transport through modified CNT membranes." Journal of Chemical Physics **138**(12): 124701.

31. Wang, L., et al. (2016). "Molecular dynamic simulations of pressure-driven water transport through polyamide nanofiltration membranes at different membrane densities." RSC Adv. **6**(68): 63586-63596.
32. Yong Duan, C. W., Shibasish Chowdhury, Mathew C. Lee, Guoming Xiong, Wei Zhang, Rong Yang, Piotr Cieplak, Ray Luo, Taisung Lee, James Caldwell, Junmei Wang, Peter Kollman (2003). "A Point-Charge Force Field for Molecular Mechanics Simulations of Proteins Based on Condensed-Phase Quantum Mechanical Calculations." Journal of Computational Chemistry **24**(16): 1999-2012.

## **Chapter 3: CONCENTRATION GRADIENT DRIVEN MOLECULAR DYNAMICS: A NEW METHOD FOR SIMULATIONS OF MEMBRANE PERMEATION AND SEPARATION**

---

### **3.1: Introduction**

Membrane separations of mixtures are economically significant processes widely used in petrochemical, pharmaceutical, biomedical, food and water treatment industries. (Baker, 2000) Water desalination technology, for example, is one of the major application areas of industrial membranes. Worldwide water desalination plants processes nearly 70 million cubic meters per day (Sakai et al., 2016) and membrane-based processes account for more than 60% of the entire water desalination market.(Gude, 2016) Another application area for membranes is gas separation. Hydrogen recovery, air separation, CO<sub>2</sub> separation, natural gas sweetening, alkane-alkene separation are examples of important industrial processes where membrane based separation technologies are eminently utilized.(P. Bernardo, 2009, David S. Sholl, 2016) A significant example of commercial application of membranes in gas separation is an 830,000 Nm<sup>3</sup>/h system provided by Cynara-NATCO for the separation of CO<sub>2</sub> from natural gas operating on an offshore platform located in the Gulf of Thailand.(Callison and Davidson, 2007)

Polymers, carbon molecular sieves and zeolites are materials commonly used in commercial membranes (P. Bernardo, 2009, David S. Sholl, 2016). On the other hand, ongoing research in materials science and chemistry have provided new candidate materials to manufacture membranes; such as metal-organic frameworks

(MOFs) (Qiu et al., 2014), carbon nanotubes (Bruce J. Hinds, 2004) (CNTs) and graphene oxide (R. K. Joshi, 2014).

Developing novel membranes for a specific separation is a challenging task and requires a detailed understanding of the complex transport mechanisms down at the nanometer scale. Molecular dynamics (MD) is a simulation method which can be used to understand such complexities with atomic resolution. Classical MD simulations unveils the interactions between molecules at the atomistic level by exploiting empirical force fields (Allen and Tildesley, 1989).

In this study, we present a new NEMD method which allows the simulation of permeation of a mixture kept at a fixed composition through a membrane and avoids the feed depletion issue without the need for coupling an MC scheme. The proposed method builds on CuMD, a recent technique developed to model crystal growth in solutions at constant chemical potential by using a non-conservative force (Perego et al., 2015). In our new NEMD method we use self-adjusting bias forces to control the mixture composition in selected regions of the simulation box in order to continuously enforce a concentration difference between the inlet and outlet of the membrane. This method has two main advantages over the previously implemented methodologies; first, it is completely deterministic since no stochastic move like particle insertion-deletion is needed, and second, it allows us to perform simulations of mixture permeation through membranes at fixed feed composition.

We first explain the new methodology and then demonstrate it by simulating permeation of pure methane ( $\text{CH}_4$ ), ethylene ( $\text{C}_2\text{H}_4$ ) and ethane ( $\text{C}_2\text{H}_6$ ) through a zeolitic imidazolate framework-8 (ZIF-8) (Park et al., 2006) membrane, and by applying it for the separation of an equimolar ethylene/ethane mixture, again in a ZIF-8 membrane. We chose the separation of ethylene from ethane due its

paramount importance. Market data confirm the necessity of this separation; the demand of ethylene as feedstock in chemical industry for production of rubbers, plastics and other valuable chemical products is almost 25 trillion tons per annum and the biggest portion of ethylene comes as by-product of oil refineries in the form of a mixture of ethane/ethylene (Van Miltenburg et al., 2006). On the other hand, this is an extremely difficult separation due to the fact that the kinetic diameters of ethylene (4.16 Å) and ethane (4.44 Å) are very close to each other (Rungta et al., 2013).

## **3.2: Models & Computational Details**

### **3.2.1: Concentration Gradient Driven Molecular Dynamics**

The diffusive transport of fluids across membranes is a non-equilibrium process. To faithfully reproduce this fact in our modelling, we aim to carry out simulations in which a steady state concentration gradient is maintained between the two sides of the membrane surrounded by a fluid, pure or a mixture. To this aim here we introduce two separate control regions, inlet control region (ICR), located on the feed side of the membrane, and the outlet control region (OCR), on the permeate side of the membrane (Figure 3-1). The control regions and the membrane are separated by two transition regions; inlet transition region (ITR) and the outlet transition region (OTR). The concentrations in the ICR and OCR are controlled by applying on the fluid molecules two separate external forces which are localized in two regions, the inlet force region (IFR) and outlet force region (OFR), which are adjacent to ICR and OCR, respectively. The external forces are perpendicular to the membrane surface and regulate the flux of molecules across the IFR (and OFR)

in order to restrain the concentration in the ICR (and OCR) to a selected target value. This makes it possible to impose two different concentrations in the inlet and outlet control region, where the forces are defined by the following equations:

$$F_i^I = k_i^I (n_i^{T,I} - n_i^{ICR}) G^I(z - Z_F^I, w) \quad (3.1)$$

$$F_i^O = k_i^O (n_i^{T,O} - n_i^{OCR}) G^O(z - Z_F^O, w) \quad (3.2)$$

where  $i$  indicates the fluid species subject to  $F$ , the superscripts  $I$  and  $O$  refer to inlet and outlet, respectively,  $k_i^I$  and  $k_i^O$  are force constants,  $n_i^{T,I}$  and  $n_i^{T,O}$  are target concentration on the feed and permeate side of the membrane, and  $n_i^{ICR}$ ,  $n_i^{OCR}$  are the instantaneous concentrations in the ICR and OCR respectively.  $G^I$  and  $G^O$  are two bell-shaped functions of width  $w$ , centred in  $Z_F^I$  and  $Z_F^O$  respectively, these latter indicating the  $z$  coordinate of the IFR and OFR. Therefore  $G^I$  and  $G^O$  serve the purpose of localising the application of the bias force within the IFR and OFR, respectively.  $n_i^{ICR}$  and  $n_i^{OCR}$  are calculated as:

$$n_i^{CR} = \frac{1}{V^{CR}} \sum_j^{N_i} \theta(z_j) \quad (3.3)$$

where  $V^{CR}$  is the volume of control region,  $N_i$  is the total number of molecules of species  $i$  in the simulation box and  $\theta(z_j)$  is a selection function defined as:

$$\theta(z_j) = \begin{cases} 1 & \text{if } z_j \text{ inside CR} \\ 0 & \text{otherwise} \end{cases} \quad (3.4)$$

where  $z_j$  is the  $z$  coordinate of a fluid molecule. We note that the direction (sign) of the force,  $F_i$ , in Eq. 3.1 changes in such a way that if the number of molecules in a control region is larger than the target value then the force repels

molecules from the control region towards the bulk, and if it is smaller, then the force attracts the molecules from the bulk to the control region. The value of the force constant,  $k_i$ , is instrumental in achieving the target density in the control regions and needs to be tuned (see Table 3-1 and Figure 3-2). We underline that, in order to establish a steady state concentration gradient, the use of periodic boundary conditions (PBCs) along the z direction is crucial. Indeed, as the molecules permeate through the membrane, they can flow from the outlet of the membrane back to the inlet region, establishing a stationary flux.

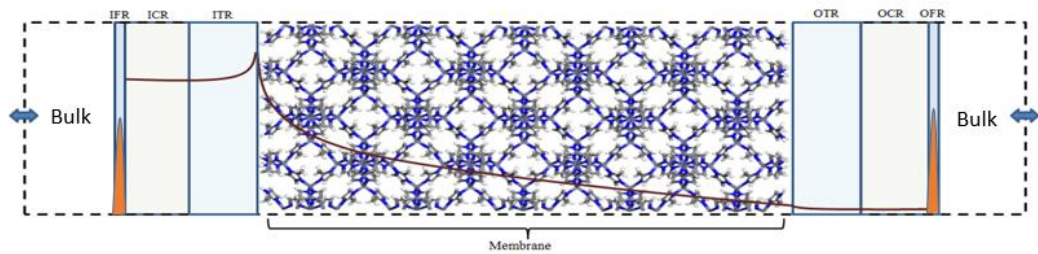


**Figure 3-1** Conceptual representation of the concentration gradient driven MD method. Red line demonstrates an arbitrary concentration profile. Bell-shaped functions are shown in orange and peak of it corresponds to centre of IFR along z-direction. Dashed line shows the boundaries of the simulation box. Fluid molecules return to feed side from the permeate side through the periodic boundary (shown with the two-way arrows).

**Table 3-1** The deviation of ICR concentration from the target value as a function of inlet force constant,  $k_i^I$ . Obtained over 40ns production run after 10ns initial run. The outlet force constant,  $k_i^O$ , was kept fixed at 500,000 kJ.nm<sup>3</sup>/mol. Other parameters were as follows;  $w = 0.25$  nm,  $Z_F^I = 4.875$ ,  $Z_F^O = 23.625$ , and width of the control regions,  $V^{CR}/(L_x \times L_y) = 2.5$ .

	$k_i^I$ (kJ.nm <sup>3</sup> /mol)	1000	3000	5000	7000	8000
Deviation from ICR target concentration (molecule/nm <sup>3</sup> )	Target ICR concentration = 0.2454 molecule/nm <sup>3</sup> , corresponding to 10 bar.	0.0581	0.0296	0.0218	0.0163	0.0144
	Target ICR concentration = 0.1217 molecule/nm <sup>3</sup> , corresponding to 5 bar.	0.0265	0.0163	0.0123	0.0116	0.0056
	Target ICR concentration = 0.0972 molecule/nm <sup>3</sup> , corresponding to 4 bar.	0.0144	0.0005	0.0020	0.0038	0.0018

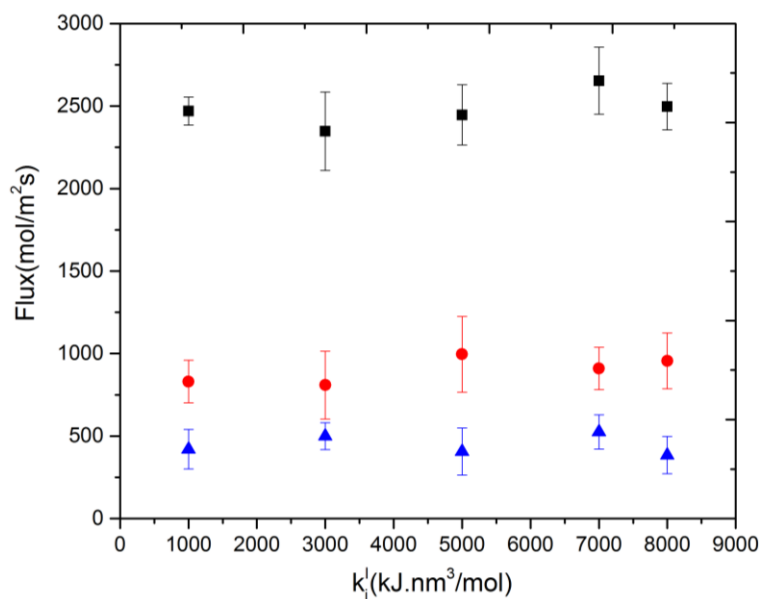


**Figure 3-2** The variation of flux with respect to inlet force constant,  $k_i^I$ . The outlet force constant,  $k_i^O$ , was kept fixed at 500,000 kJ.nm<sup>3</sup>/mol. The flux remains same within the margin of statistical error. Black squares 10 bar feed pressure, red circles 5 bar feed pressure and blue triangles 4bar feed pressure.

### 3.2.2: Simulation Details

In order to demonstrate our method ZIF-8 was chosen to construct the membrane model in our simulations. ZIF-8 is formed by the assembly of Zn metal atoms and methyl imidazole bridging ligands. It has a sodalite topology with unit cell dimensions  $a=b=c=16.991 \text{ \AA}$ , a pore diameter of  $11.6 \text{ \AA}$ , and a pore aperture of  $3.4 \text{ \AA}$ . The membrane was constructed by replicating the ZIF-8 unit cell by 2 x 2 x 5 in the x, y, and z directions, respectively. Zinc atoms at both ends of the membrane were removed and dangling nitrogen atoms were terminated by hydrogens. The dimensions of the resulting membrane were  $L_x=L_y=3.3982$  and  $L_z=8.4955 \text{ nm}$  (Figure 3-2). The membrane was placed in the centre of a simulation

box which is 28.4955 nm in the z directions and with dimensions equal to the membrane in the x and y directions.

ZIF-8 membrane was modelled as a flexible structure using the force field recently developed by Krokidas et al. (Krokidas et al., 2015). Since in their work a continuous periodic structure of ZIF-8 was studied partial atomic charges for surface atoms were not present. We calculated the charges for the dangling nitrogen atoms and the hydrogens used for terminations by DFT calculation with Gaussian 09 by using hybrid B3LYP density functional with 6-311g++(2d,2p) basis set and scaled the charges reported by Krokidas et al.(Krokidas et al., 2015) accordingly. Bond stretching, bond bending and torsional energy parameters for these surface atoms were taken from GAFF (Yong Duan, 2003) force field. In order to prevent drifting of membrane in the z direction due to the concentration gradient, membrane atoms within the first 4Å of the membrane at both ends were tethered to their initial positions.

Methane, ethylene and ethane were modelled using the TraPPE force field (Siepmann, 1998). In this force field a carbon atom and the hydrogens bonded are treated as a united atom. Hence, methane was represented as a single united atom (CH<sub>4</sub>), ethylene consisted two CH<sub>2</sub> united atoms and ethane two CH<sub>3</sub> united atoms. The bond between the united atoms in ethylene and the ethane were rigid as defined in the TraPPE force field. Lorentz-Berthelot mixing rules were applied between unlike atoms. The cut-off distance for Lenard-Jones interactions was set at 12 Å. The electrostatic interactions were computed using the particle mesh Ewald (PME) method and for the real part of the Ewald sum the cut-off distance was set to 12 Å.

The permeations of 4 different systems through the ZIF-8 membrane were simulated. These were pure methane, ethylene and ethane, and an equimolar mixture of ethylene and ethane. MD simulations were performed with GROMACS 5.1.2 software (Abraham et al., 2015) in the NVT ensemble. Temperature was kept constant at 300 K using a Nose-Hoover thermostat. The choice of Nose-Hoover thermostat was due to its being deterministic and time-reversible in all degrees of freedom. A time step of 1 fs was used and PBCs were applied in all directions. Simulations were first equilibrated for at least 10 ns followed by 40 ns production runs. Simulation data including the trajectory were saved every 500 steps (0.5 ps). Standard deviations of the ensemble averages were computed by breaking the production runs into 5 blocks.

A private version of PLUMED 2.2.2 plugin (Tribello et al., 2014) was used to apply the bias forces,  $F_i^I$  and  $F_i^O$ , in order to control concentrations in ICR and OCR. Target concentration in the ICR was set to a molecular density which corresponds to the total feed pressure (which varied between 2 to 40 bars in our simulations) based on the pressure/density data from the NIST database. (Lemmon et al., 2005) The target concentration in the OCR was set to 0 to create a vacuum effect on the permeate side in all simulations. Here we note that in MD simulations of membranes creating a vacuum effect is a challenging task. To create the vacuum effect, a larger outlet force constant,  $k_i^O$ , was used compared to the inlet force constant,  $k_i^I$ . The values of parameters used in Eqs. 3.1 & 3.2 and the locations of the force and control regions are given in Table 3-2.

**Table 3-2** Parameters used in Eq. 1 and 2 and the width of the control regions,  $V^{CR}/(L_x \times L_y)$ .

Relevant simulation	Side	$w$	$k_i$	$Z_F$	$V^{CR}/(L_x \times L_y)$
		(nm)	(kJ.nm <sup>3</sup> /mol)	(nm)	(nm)
<b>Single Permeation of Methane, Ethylene and Ethane</b>	Inlet	0.25	$k_{methane} = 8,000$	4.875	2.5
			$k_{ethylene} = 8,000$		
			$k_{ethane} = 3,000$		
	Outlet	0.25	500,000	23.625	2.5
<b>Mixture Permeation of Ethane/Ethylene</b>	Inlet	0.25	$k_{ethylene} = 25,000$	4.875	2.5
			$k_{ethane} = 50,000$		
	Outlet	0.25	500,000	23.625	2.5

The flux due to concentration difference in the z direction,  $J_z$ , was calculated by counting the number of molecules which passed through a plane at the centre of the membrane and dividing that by the production simulation time, t, and the cross sectional area of the membrane,  $A_{xy}$ , (Frentrup et al., 2012)

$$J_z = \frac{N_i^+ - N_i^-}{tA_{xy}} \quad (3.5)$$

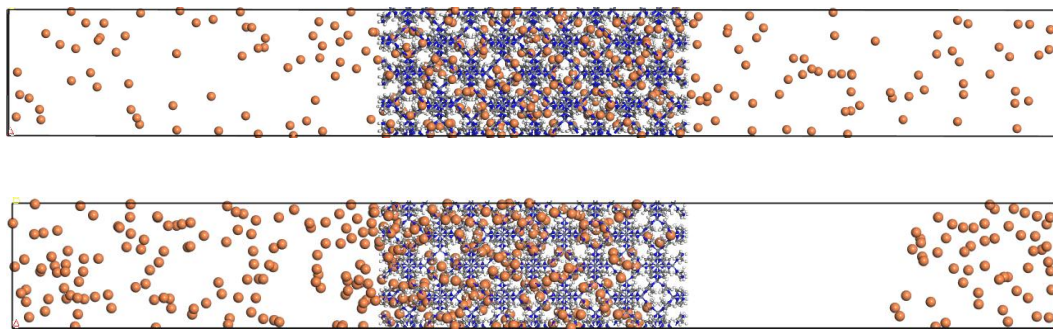
where  $N_i^+$  and  $N_i^-$  denote the number of molecule species i that have passed the plane in positive and negative directions, respectively. Permeability,  $\Pi$ , was calculated according to the following formula:

$$\Pi = \frac{J_z}{\Delta P/l_{mem}} \quad (3.6)$$

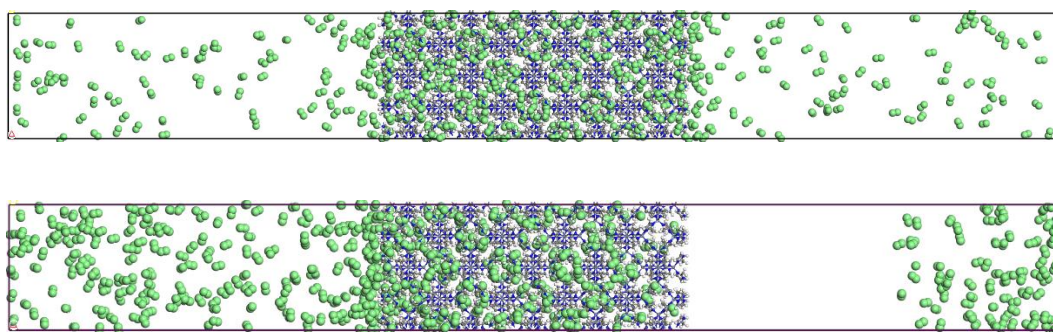
where  $l_{mem}$  is the membrane thickness in the  $z$  direction and  $\Delta P$  is the difference in the pressures of the fluid in ICR and OCR which can be estimated from pressure/density data. (Lemmon et al., 2005)

In order to generate initial configurations of the fluid molecules in the simulation box, prior to an MD run we simulated the adsorption of fluid molecules by performing grand canonical Monte Carlo (GCMC) simulations using RASPA (Dubbeldam et al., 2015) molecular simulation package. In the grand canonical ensemble temperature, volume and chemical potential of the species are fixed. GCMC simulations were performed at 300 K and at a total pressure which is the average of pressures corresponding to the target densities of the fluid in the ICR and OCR of the MD simulation box. For instance, for 40 bar feed pressure and 0 bar permeate pressure GCMC simulation was performed at 20 bar. We found that this provides a good starting configuration for MD simulations to reach steady state quickly (Figure 3-3). GCMC simulations included  $10^5$  cycles for initialization and  $10^5$  cycles for production, where each cycle is  $N$  steps.  $N$  is equal to the number of molecules present in the system. For single component methane GCMC simulations, swap moves (insertion/deletion) between the bulk and adsorbed phases, translation and reinsertion moves were sampled. For ethylene and ethane simulations a rotation move was added to the above list. For the ethylene-ethane mixture simulation an identity exchange move between the species was also sampled. All moves were sampled with equal probability.

a)



b)



c)

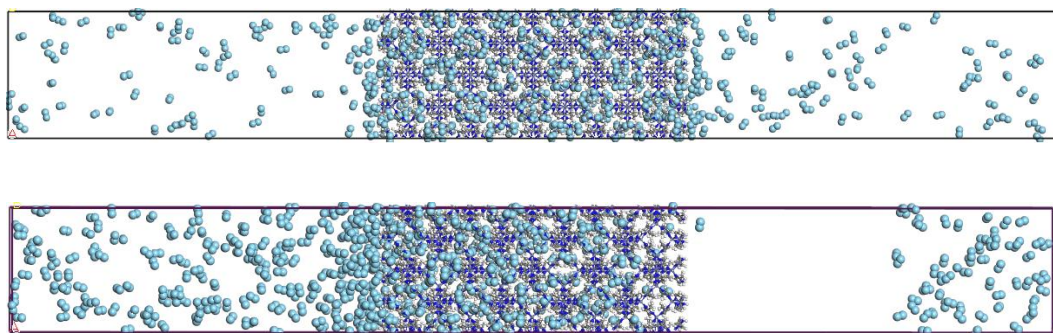


**Figure 3-3** Starting (top) and after 10ns (bottom) configurations for pure (a) methane, (b) ethylene and (c) ethane.

### 3.3: Results and Discussion

#### 3.3.1: Permeation of Pure Methane, Ethylene and Ethane

In Figure 3-4 we report the variation of concentrations in ICR and OCR for pure methane, ethylene and ethane as a function of simulation time. In these simulations the target concentrations in ICR were set to the molecular density of the fluid at 40 bar (feed pressure). In all cases concentration of the species are stable and fluctuate around an average value. The average concentrations calculated for ICR and OCR are given in Table 3-3 for each fluid. For the inlet the standard deviations are very small in comparison to the average concentrations, which demonstrate excellent control of the concentration in ICR. The relatively high fluctuations in OCR with respect to the average values indicates the difficulty of controlling the concentration at very low target values (see Figure 3-5 for OCR concentration data plotted on a smaller scale). However, such fluctuations are actually insignificant because the number of molecules present in the OCR at any time is extremely small due to the vacuum effect. For instance, for methane,  $14.7 \text{ mol/m}^3$  (Table 3-3) corresponds to only 0.26 molecules in the whole ICR volume ( $28.9 \text{ nm}^3$ ).

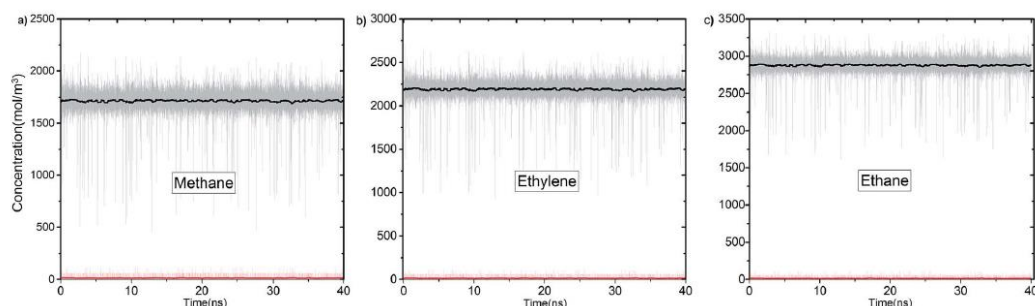
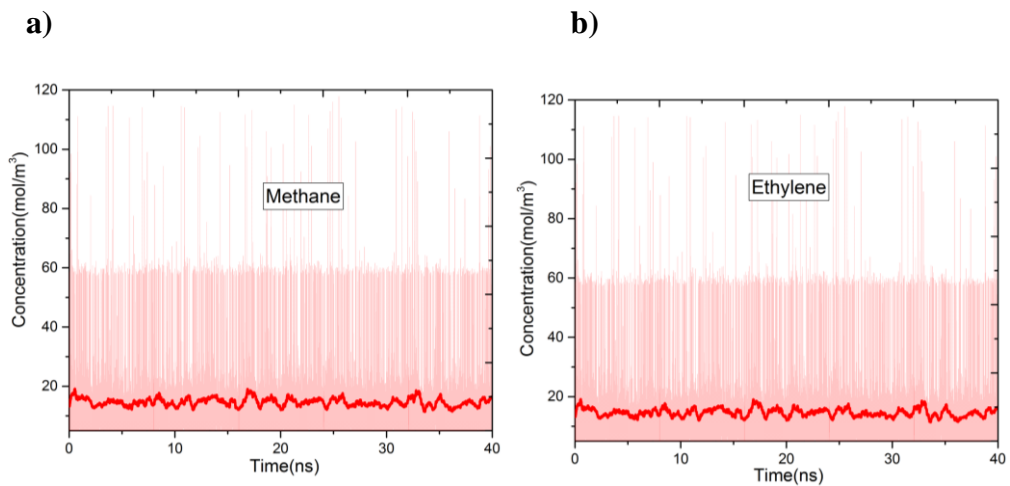


**Figure 3-4** The variation of inlet (black lines) and outlet (red lines) concentrations for (a) methane, (b) ethylene and (c) ethane as a function of simulation time in production runs. The instantaneous values are represented with faded colour, while the full colour curves are moving averages obtained with a characteristic smoothing time of 0.5 ns.

**Table 3-3** The average concentrations in ICR and OCR for methane, ethylene and ethane

	ICR (mol m <sup>-3</sup> )	OCR (mol m <sup>-3</sup> )
Methane	1716 ± 1	14.7 ± 0.3
Ethylene	2202 ± 1	15.2 ± 0.4
Ethane	2810 ± 3	12.2 ± 0.7



c)

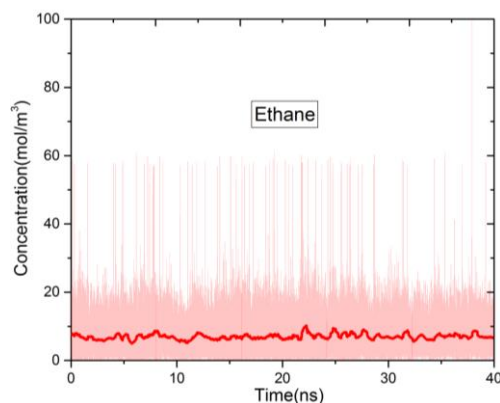


**Figure 3-5** The variation of outlet concentrations for (a) methane, (b) ethylene and (c) ethane as a function of simulation time in production runs. The instantaneous values are represented with faded colour, while the full-colour curves are moving averages obtained with a characteristic smoothing time of 0.5 ns.

The number densities of methane, ethylene and ethane are plotted against the z coordinate of the simulation box in Figure 3-6 and it demonstrates how the concentration gradient works along the membrane. These density profiles were obtained by averaging data over the 40 ns production runs. The density of fluid molecules decreases through membrane in an almost linear fashion. Density is higher at the entrance of the membrane (molecules adsorbed by ZIF-8) and it decreases along the z direction of membrane (molecules inhaled by vacuum).

Overall, data for single component permeation simulations shows that our methodology controls the concentration of fluid molecules around a targeted value in specified regions to remarkable accuracy (Figure 3-6). We highlight that the bias force acts in a localized region out of the membrane. Permeation is purely due to the diffusive transfer of molecules, driven by the steady difference in concentration maintained across the two sides of the membrane (Figure 3.4).

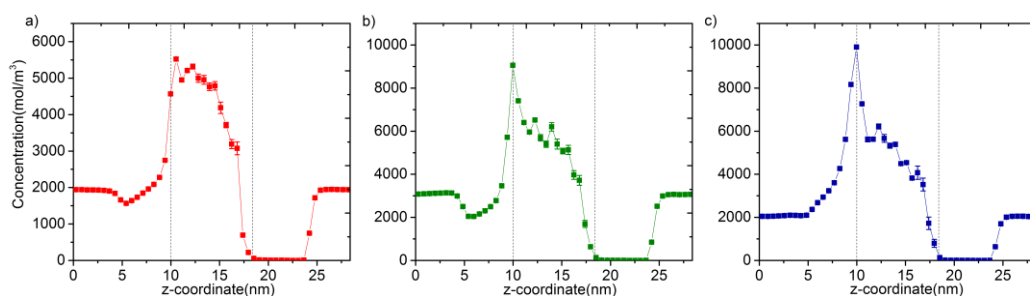


**Figure 3-6** Concentration profiles of (a) methane, (b) ethylene and (c) ethane molecules along the z-coordinate of the simulation box. Dashed lines show membrane entrance and exit.

In Figure 3-7, we show the variation of methane flux ( $J_z$ ) with respect to concentration difference across the membrane. This was obtained by performing additional MD simulations of methane permeation at 300 K where target concentrations in the ICR were set to molecular densities corresponding to 36 bar, 30 bar, 24 bar, 14 bar, 10 bar, 5 bar, 4 bar and 2 bar, and in the OCR was set to 0. Again the initial positions for the methane molecules were obtained from GCMC simulations which were performed at half of the pressure values given above. The flux initially increases rapidly with increasing concentration difference but then starts levelling-off after about  $500 \text{ mol/m}^3$  and then reaches a plateau. The initial part is known as the pressure/concentration difference controlled region and the final part where a plateau is observed is known as the mass transfer controlled region. Such behaviour was reported experimentally for propane and propylene permeation in ZIF-8 based membranes (Fan et al. 2014, Eum et al. 2015)

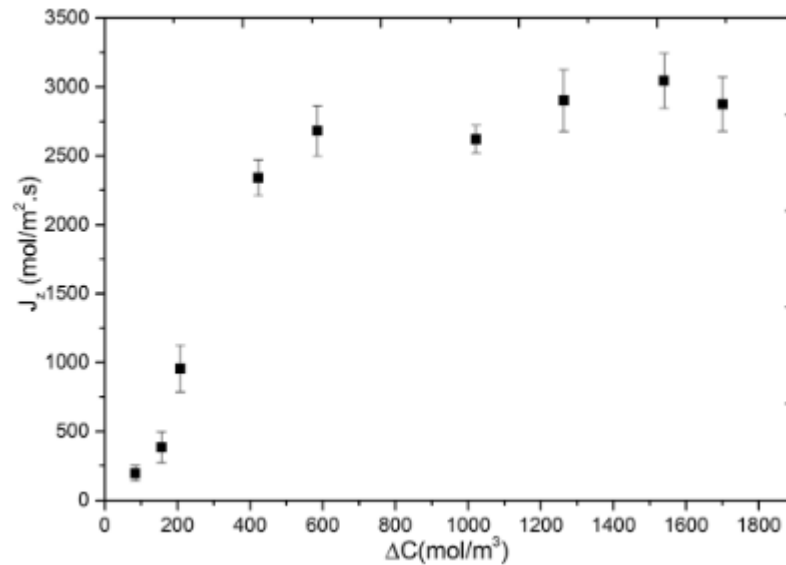


**Figure 3-7** The variation of methane flux ( $J_z$ ) with concentration gradient

In Table 3-4, permeabilities of methane, ethane and ethylene from simulations, in which target concentration in ICR for each fluid was set to a density corresponding to 4 bar, are compared against experimental data. Simulated permeabilities are about one order of magnitude larger than those reported by Pan et al. (Pan et al, 2011) who reported the permeabilities for all three fluids, and those reported by Bux et al. (Bux et al, 2011) in two different studies. But most importantly simulated permeabilities match with the order of experimentally measured permeabilities, that is,  $\Pi_{ethylene} > \Pi_{methane} > \Pi_{ethane}$ , which is the most important outcome in a computational screening study. Given the simulations were conducted in the molecular scale; the agreement with experiments is remarkable.

On the other hand, direct permeability values calculated from simulations contradict with experimental data with 2 orders of magnitude as seen in Table 3-4. This could be due to several reasons. Firstly, the thickness of membrane is at the nanometer scale in these simulations and this is an ultra-short length scale with

respect to a micron scale membrane in lab. Secondly, TRAPPE force field, that we used for permeant molecules, is benchmarked according to vapor-liquid equilibria of bulk fluids but penetrant molecules are at very confined nanopores in our simulations. Force field may not capture well this condition and that could generate a discrepancy between direct experiment and simulated permeation. Additionally, in our simulation we used a perfect crystal of ZIF-8 structure, but some imperfection (e.g. blocked pores by solvent molecules, guest molecule trapping point or line defects etc.) can be highly likely in a real membrane. These imperfections could reduce the total permeation of guest molecules with respect to permeation in a pristine crystal.

**Table 3-4** Permeabilities ( $10^{-13}$  mol.m/m<sup>2</sup>.s.Pa) for methane, ethylene and ethane.

	<b>Simulation<sup>a</sup></b>		<b>Experimental</b>	
<b>Methane</b>	97.5	<sup>b</sup> 1.56	<sup>c</sup> 2.7	-
<b>Ethylene</b>	152.5	<sup>b</sup> 2.8	-	<sup>d</sup> 4.5
<b>Ethane</b>	67.5	<sup>b</sup> 1.38	-	<sup>d</sup> 1.63

<sup>a</sup>Feed pressures corresponding to the average ICR concentrations obtained from simulations are 3.9 bar for methane, 4.8 bar for ethylene and 4.8 bar for ethane.

<sup>b</sup>Feed pressure=1bar, Pan et al.; <sup>c</sup>Feed pressure=1bar, Bux et al.; <sup>d</sup>Feed pressure=6bar, Bux et al.

### 3.3.2: Equimolar ethylene/ethane mixture separation

We studied the separation of an equimolar ethylene/ethane mixture with a ZIF-8 membrane in order to demonstrate the applicability of the new method for mixture simulations. Besides, to the best of our knowledge, present work is the first simulation study reporting the separation of ethylene/ethane mixture in a flexible ZIF-8 membrane. The target concentrations of ethylene and ethane in the ICR were set to molecular densities so that the corresponding total pressure is 2 bar. Figure 3-8 shows the variation of the concentrations of ethylene and ethane in ICR and OCR. Similar to the single component simulations, the concentrations fluctuate around the target values. The average concentrations are given in Table 3-5. For the inlet side, these correspond to ethylene and ethane mole fractions of 0.48 and 0.52, respectively. Despite the difficulty in controlling concentrations at low target values our method successfully keeps the mixture very close to the equimolar target composition. (see Figure3-9 for histogram analyses of instantaneous concentration of ethylene and ethane molecules)

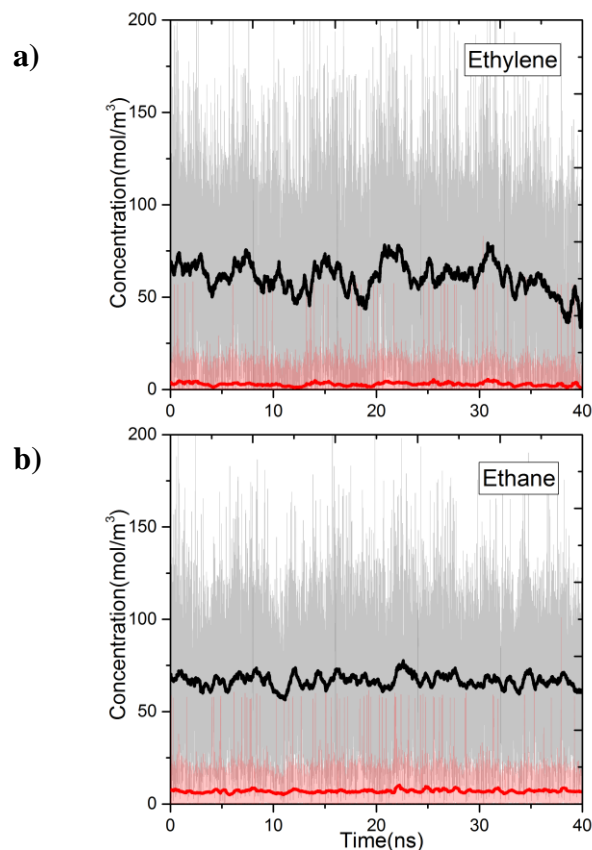


**Figure 3-8** Variation of inlet (black lines) and outlet (red lines) concentrations for a) ethylene and b) ethane for the equimolar mixture as a function of simulation time in the production run. The instantaneous values are represented with faded colour, while the full-colour curves are moving averages obtained with a characteristic smoothing time of 0.5 ns.

Furthermore, we calculated the permeation selectivity,  $S$ , for the equimolar ethylene/ethane separation simulation as follows:

$$S = \frac{\Pi_i}{\Pi_k} \quad (3.6)$$

where  $\Pi_i$  and  $\Pi_k$  are permeability of species  $i$  and  $k$ , and was found to be 2, which compares very well with the experimental selectivity, 2.6, reported by Bux et al.41 at 3.5 bar total feed pressure.

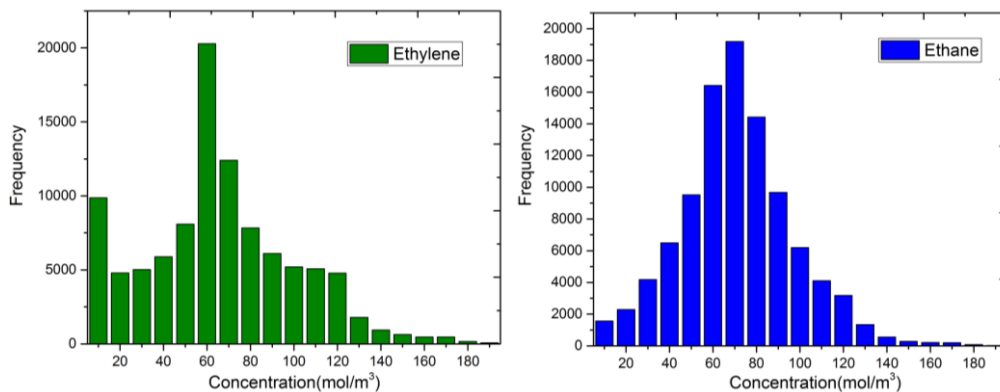


**Figure 3-9** Concentration histograms of ethylene (left) and ethane (right) in ICR during the equimolar mixture simulation.

**Table 3-5** The average concentrations in ICR and OCR for ethylene and ethane in the equimolar mixture simulation

	ICR <sup>a</sup> (mol/m <sup>3</sup> )	OCR (mol/m <sup>3</sup> )
Ethylene	61 ± 4	2.9 ± 0.4
Ethane	66.7 ± 0.8	7.0 ± 0.2

<sup>a</sup>Total feed pressure corresponding to the average ICR concentration of the mixture from simulation is 3.15 bar.

### 3.4: Conclusions

In this study, we presented a new non-equilibrium MD method; concentration gradient driven MD (CGD-MD), in order to simulate the permeation of pure fluids and mixtures through membranes. The new method works by using

bias forces to fix the concentration of fluids at target values at the inlet and outlet of a membrane. This in turn creates a concentration gradient which drives the diffusion of the molecules through the membrane. CGD-MD addresses two main shortcomings of previous NEMD methods used for simulating membrane separation processes in the molecular scale. First, it avoids the feed depletion issue and allows running, in principal, an infinitely long simulation. Second, it maintains the feed composition without the need of any complex MC-MD coupling. We successfully demonstrated our new method for the permeation of pure methane, ethylene and ethane and for the separation of an equimolar ethylene/ethane mixture in a ZIF-8 membrane by predicting the methane, ethylene and ethane permeabilities, and the ethylene/ethane selectivity in very good agreement with the experimental data. Given its predictive success, CGD-MD can be an invaluable tool to computationally screen new and existing materials for membrane separation processes.

In our simulations, pure or mixture, CGD-MD maintained the concentration of species at their target values in the denser feed side to a remarkable accuracy. Based on this, we expect that CGD-MD will perform very well for dense phases. Indeed, a preliminary simulation of pure liquid water permeation through the ZIF-8 membrane clearly demonstrates that our method works for such systems with a great accuracy. Therefore, our future work will include separations in liquid phase where DCV-GCMD method is known to struggle.

### 3.5: References

1. R. W. Baker, Membrane technology, Wiley Online Library, 2000.
2. H. Sakai, T. Ueyama, M. Irie, K. Matsuyama, A. Tanioka, K. Saito and A. Kumano, Desalination, 2016, 389, 52-57.
3. V. G. Gude, Renew. Sus. Ener. Rev., 2016, 57, 1038-1065.
4. E. D. P. Bernardo, and G. Golemme, Ind. Eng. Chem. Res., 2009, 48, 4638–4663.
5. R. P. L. David S. Sholl, Nature, 2016, 532, 435-437.
6. A. Callison and G. Davidson, Oil & Gas J., 2007, 105, 56-56.
7. S. Qiu, M. Xue and G. Zhu, Chem. Soc. Rev., 2014, 43, 6116-6140.
8. N. C. Bruce J. Hinds, Terry Rantell, Rodney Andrews, Vasilis Gavalas, Leonidas G. Bachas, Science, 2004, 303, 62-65.
9. P. C. R. K. Joshi, F. C. Wang, V. G. Kravets, Y. Su, I. V. Grigorieva, H. A. Wu, A. K. Geim, R. R. Nair, Science, 2014, 343, 752-754.
10. M. P. Allen and D. J. Tildesley, Computer simulation of liquids, Oxford university press, 1989.
11. G. S. Heffelfinger and F. v. Swol, J. Chem. Phys., 1994, 100, 7548.
12. R. F. Cracknell, D. Nicholson and N. Quirke, Phys. Rev. Lett., 1995, 74, 2463-2466.
13. G. S. H. Phillip I. Pohl, J. Membr. Sci., 1999, 155, 1-7.
14. M. G. S. Lifang Xu, Muhammad Sahimi, Theodore T. Tsotsis, Phys. Rev. Lett., 80, 3511-3514.
15. Z. Ható, Á. Kaviczki and T. Kristóf, Mol. Simul., 2015, 42, 71-80.

16. L. Wang, R. S. Dumont and J. M. Dickson, *J. Chem. Phys.*, 2013, 138, 124701.
17. L. Wang, R. S. Dumont and J. M. Dickson, *RSC Adv.*, 2016, 6, 63586-63596.
18. M. Shen, S. Keten and R. M. Lueptow, *J. Membr. Sci.*, 2016, 506, 95-108.
19. Z. Hu, Y. Chen and J. Jiang, *J. Chem. Phys.*, 2011, 134, 134705.
20. K. M. Gupta, K. Zhang and J. Jiang, *Langmuir*, 2015, 31, 13230-13237.
21. K. M. Gupta, Z. Qiao, K. Zhang and J. Jiang, *ACS Appl. Mater. Interfaces*, 2016, 8, 13392-13399.
22. F. A. Cabrales-Navarro, J. L. Gómez-Ballesteros and P. B. Balbuena, *J. Membr. Sci.*, 2013, 428, 241-250.
23. E. T. Fangqiang Zhu, Klaus Schulten, *Biophysical Journal*, 2002, 83, 154-160.
24. M. Ding, A. Szymczyk and A. Ghoufi, *Desalination*, 2015, 368, 76-80.
25. H. Frentrup, C. Avendaño, M. Horsch, A. Salih and E. A. Müller, *Mol. Simul.*, 2012, 38, 540-553.
26. H. Frentrup, K. E. Hart, C. M. Colina and E. A. Muller, *Membranes (Basel, Switz.)*, 2015, 5, 99-119.
27. C. Perego, M. Salvalaglio and M. Parrinello, *J. Chem. Phys.*, 2015, 142, 144113.
28. K. S. Park, Z. Ni, A. P. Cote, J. Y. Choi, R. Huang, F. J. Uribe-Romo, H. K. Chae, M. O'Keeffe and O. M. Yaghi, *Proc. Natl. Acad. Sci. U.S.A.*, 2006, 103, 10186-10191.
29. A. Van Miltenburg, W. Zhu, F. Kapteijn and J. A. Moulijn, *Chem. Eng. Res. Des.*, 2006, 84, 350-354.

30. M. Rungta, C. Zhang, W. J. Koros and L. Xu, *AIChE J.*, 2013, 59, 3475-3489.
31. P. Krokidas, M. Castier, S. Moncho, E. Brothers and I. G. Economou, *J. Phys. Chem. C*, 2015, 119, 27028-27037.
32. C. W. Yong Duan, Shibasish Chowdhury, Mathew C. Lee, Guoming Xiong, Wei Zhang, Rong Yang, Piotr Cieplak, Ray Luo, Taisung Lee, James Caldwell, Junmei Wang, Peter Kollman, *J. Comput. Chem.*, 2003, 24, 1999-2012.
33. M. G. M. a. J. I. Siepmann, *J. Phys. Chem. B*, 1998, 2569-2577.
34. M. J. Abraham, T. Murtola, R. Schulz, S. Páll, J. C. Smith, B. Hess and E. Lindahl, *SoftwareX*, 2015, 1-2, 19-25.
35. G. A. Tribello, M. Bonomi, D. Branduardi, C. Camilloni and G. Bussi, *Compt. Phys. Commun.*, 2014, 185, 604-613.
36. E. Lemmon, M. McLinden and D. Friend, *NIST chemistry webbook, NIST standard reference database*, 2005, 69.
37. D. Dubbeldam, S. Calero, D. E. Ellis and R. Q. Snurr, *Mol. Simul.*, 2015, 42, 81-101.
38. M. Fang, C. Wu, Z. Yang, T. Wang, Y. Xia and J. Li, *J. Membr. Sci.*, 2015, 474, 103-113.
39. K. Eum, C. Ma, A. Rownaghi, C. W. Jones and S. Nair, *ACS Appl. Mater. Interfaces*, 2016, 8, 25337-25342.
40. Y. Pan and Z. Lai, *Chem. Commun. (Cambridge, U. K.)*, 2011, 47, 10275-10277.
41. H. Bux, C. Chmelik, R. Krishna and J. Caro, *J. Membr. Sci.*, 2011, 369, 284-289.

42. H. Bux, C. Chmelik, J. M. van Baten, R. Krishna and J. Caro, *Adv. Mater.* (Weinheim, Ger.), 2010, 22, 4741-4743.

## **Chapter 4: MODELLING GAS TRANSPORT THROUGH POLYMER/MOF INTERFACES: A MICROSECOND SCALE CONCENTRATION GRADIENT DRIVEN MOLECULAR DYNAMICS STUDY**

---

### **4.1: Introduction**

There has been substantial progress in the development of membranes for gas separations over the past two decades (Funke, Argo et al. 1997, Merkel, Bondar et al. 2000, Tuan, Li et al. 2001, Li, Falconer et al. 2006, Smith, Hernández et al. 2015, Ogieglo, Ghanem et al. 2018, Zhang, Zhang et al. 2018, Genduso, Litwiller et al. 2019); however, there are still a number of long-standing problems. The main challenge has been to overcome the trade-off between permeability and selectivity, which was illustrated by Robeson's upper bound (Robeson 1991, Robeson 2008). Even though polymeric membranes dominate the majority of current membrane-based applications, they are bounded by this permeability-selectivity trade-off. As a remedy, combining polymers and metal-organic frameworks (MOFs) in the form of a mixed matrix membrane (MMM) has been proposed, and this has shown significant promise (Benzaqui, Pillai et al. 2017, Castarlenas, Téllez et al. 2017, Ghalei, Sakurai et al. 2017, Kusuda, Kitagawa et al. 2017, Xie, Fu et al. 2017, Liu, Chernikova et al. 2018). This approach aims to take advantage of the good processability of polymers and the excellent separation performance of crystalline porous MOFs. On the other hand, gas transport dynamics at the polymer-MOF interface can play a determining role on the separation performance of the composite membrane and understanding the effects of polymer-MOF compatibility

on gas separation is not a trivial task (Semino, Moreton et al. 2018). Molecular simulations can be used to quantify and characterize such interface effects in polymer-MOF composites provided that (i) accurate methods for the computation of the flux of permeants are employed, and (ii) accurate structural atomistic models of the polymer/MOF interface are used.

The earliest molecular simulation of gas separation in a polymer-MOF MMM was reported by Zhang et al. (Zhang, Hu et al. 2012) who studied the H<sub>2</sub>/CO<sub>2</sub> separation performance of polybenzimidazole (PBI)/ZIF-7 MMMs by using equilibrium molecular dynamics simulations. Semino et al. (Semino, Ramsahye et al. 2015) developed an atomistic structural model for PIM-1/ZIF-8 MMM to investigate the surface compatibility between the PIM-1 and ZIF-8. They extended such polymer/MOF surface compatibility studies to Poly(vinyl alcohol)/HKUST-1 (Semino, Dürholt et al. 2017) and 6FDA-DAM/UiO-66 MMMs (Ahmad, Navarro et al. 2018) and further investigated transient concentration of CO<sub>2</sub> in 6FDA-DAM/ZIF-8 MMMs (Hwang, Semino et al. 2018) by molecular modelling and IR microimaging. Velioglu et al. (Velioglu and Keskin 2019) and Altintas et al. (Altintas, Avci et al. 2019) recently studied separations of H<sub>2</sub>/CH<sub>4</sub> and CO<sub>2</sub>/CH<sub>4</sub> mixtures, in polymer/MOF MMMs by carrying out screening calculations based on molecular simulations. However, in most studies, predictions of the separation performance of the polymer/MOF composites were based on the individual constituents of the MMMs by assuming ideal polymer-MOF compatibility and did not consider the impact of interface. Furthermore, there are macroscopic models of permeation widely used to predict the permeability of MMMs based on permeability data available for their constituent materials. Their applicability and

limitations are discussed elaborately in a comprehensive review by (Vinh-Thang and Kaliaguine 2013). These models are usually based on analogies with continuum models that define thermal or electrical conduction in a heterogeneous medium, such as the so-called serial model, but they do not always take into account interface effects. Whereas, it has long been argued that the decrease in the separation of performances of MMMs might be related to issues with the interfaces and our work provides a first proof that indeed this is really the case and that we can quantify the magnitude of this effect.

In this study we report concentration gradient driven molecular dynamics (CGD-MD) simulations of H<sub>2</sub> and CH<sub>4</sub> transport through a polymer/MOF membrane with a specific focus on gas transport properties through the interfaces as well as along the individual components of the MMM. CGD-MD is a non-equilibrium MD method recently developed to study the transport and separation of fluids through membranes (Ozcan, Perego et al. 2017). The advantages of employing the CGD-MD method for separation of gas mixtures over equilibrium MD approaches have been recently demonstrated (Sada et al. 2019). In this work, the PIM-1/ZIF-8 composite was considered as a model membrane. PIM-1 (Polymer of Intrinsic Microporosity-1) is a member of a group of microporous glassy polymers introduced by McKeown, Budd et al. (McKeown, Budd et al. 2005). They are rigid, highly contorted spirobisindane-based ladder polymers, and their backbones have essentially no rotational freedom. This results in relatively large BET areas (BET ~800 m<sup>2</sup>/g (Park, Ni et al. 2006)) and high permanent gas permeabilities. ZIF-8 is one the most studied MOF materials and known to have exceptional thermal and chemical stability (Park, Ni et al. 2006, Pan, Liu et al. 2011, Pan, Li et al. 2012). It

has large cages of 11.6 Å connected by 3.4 Å pore apertures and has been demonstrated for various gas separation applications (Venna and Carreon 2009, Kwon and Jeong 2013, Liu, Ma et al. 2014, Gong, Wang et al. 2017, Wu, Feng et al. 2017). Regarding the investigated gas mixture in this study, H<sub>2</sub>/CH<sub>4</sub> separation by membranes is part of the \$200 million/year hydrogen recovery market which is substantially dominated by polysulfone and polyimide membranes (Galizia, Chi et al. 2017). Due to the relative difference in the size of H<sub>2</sub> and CH<sub>4</sub> molecules (kinetic diameters of 2.8 Å and 3.8 Å, respectively) these molecules are expected to exhibit distinct transport properties in the different regions of the polymer/MOF MMM including the interfaces.

## **4.2: Models & computational details**

### **4.2.1: Construction of the bare PIM-1 and ZIF-8 models, and PIM-1/ZIF-8 mixed matrix membrane model**

The ZIF-8 membrane was derived from previous work (Semino, Ramsahye et al. 2015). It consists of a [011] surface, terminated by –OH and –H groups, as per considering the dissociative adsorption of water, the standard solvent considered in the ZIF-8 synthesis, on the under-coordinated sites. This model optimized at the DFT level by using PBE functional (Hutter, Iannuzzi et al. 2014) with TZVP-MOLOPT (VandeVondele and Hutter 2007) basis set, except metal centres where DZVP-MOLOPT (VandeVondele and Hutter 2007) basis set was employed. GTH pseudopotentials (Goedecker, Teter et al. 1996) were used and DFT-D3 (Grimme 2006) dispersion corrections were added. ZIF-8 model is periodic in x,y direction

and net dipole in z direction is zero. The dimensions of the ZIF-8 model are 5.0, 4.8 and 9.8 nm in the x, y and z directions, respectively.

Different approaches were reported for the generation of polymer models (Harder, Walters et al. 2009, Shen, Keten et al. 2016, Dutta and Bhatia 2018). In this study, the construction of the PIM-1 membrane was performed with the *in silico* polymerization approach developed by Abbot et al. and implemented in the *Polymatic* code (Abbott, Hart et al. 2013). This method was previously employed to build different polymer models, PIM-1 amongst them (Abbott and Colina 2011, Abbott, Hart et al. 2013, Frentrup, Hart et al. 2015). (Semino, Ramsahye et al. 2015). The length of the resulting PIM-1 membrane was 20.8 nm in the z-direction.

Then composite PIM-1/ZIF-8 membrane was constructed by putting together the models of ZIF-8 and PIM-1 in a simulation box and letting the polymer equilibrate in the presence of the MOF. This was achieved by a series of MD simulations, including annealing steps and a rapid compression followed by a slow decompression. The polymer/MOF model was further unwrapped, in the z direction and the polymer slab was duplicated on each side of the MOF in such a way that the MOF was located between two polymer slabs. The resulting MMM of 52.4 nm in the z-direction was further equilibrated using MD simulations. The constructed three membranes (ZIF-8, PIM-1 and composite PIM-1/ZIF-8) are illustrated in Figure 4.1.

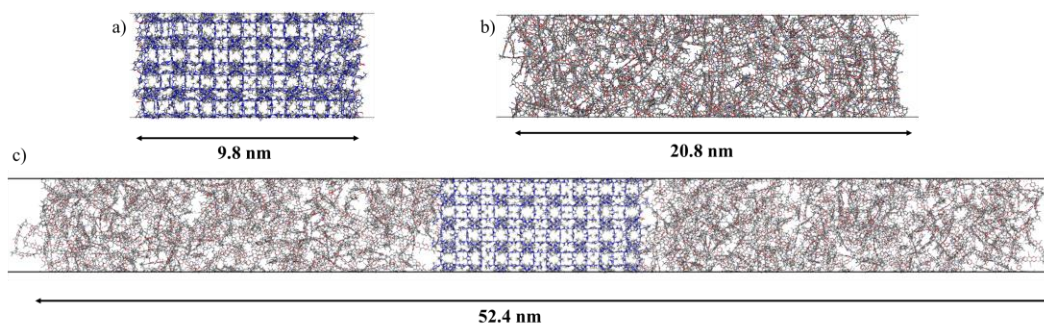


**Figure 4-1.** Illustration of a) ZIF-8 membrane, b) PIM-1 membrane and c) composite PIM-1/ZIF-8 - membrane structural models used in the CGD-MD simulations. Color code is as follows: C (grey), H (white) N (blue), O (red) and Zn (steel blue).

#### 4.2.2: Modelling of the gas transport

Simulations of gas transport through the membranes were performed using GROMACS-5.1.2 simulation package (Abraham, van der Spoel et al. 2015) patched with a modified version of Plumed-2 enhanced sampling plug-in (Tribello, Bonomi et al. 2014) to enable running the CGD-MD simulations (Ozcan, Perego et al. 2017). In CGD-MD simulations, a concentration gradient between the feed and the permeate sides is created which facilitates the transport of molecules across the membrane. The molecular fluxes can then be directly calculated from the CGD-MD simulations. To generate the concentration gradient across the membrane, the density of fluid molecules within designated volumes located at the inlet and outlet of the membrane are taken as collective variables and maintained at a target value with an external biasing scheme. CGD-MD parameters are provided in Table Appendix 1.

In all CGD-MD simulations, the membranes were placed in the middle of the simulation box and void space was added to both sides of the membranes resulting

in simulation box lengths of 40.8 nm for the PIM-1 membrane, 29.8 nm for the ZIF-8 membrane, and 93.6 nm for the PIM-1/ZIF-8 composite membrane in the z direction. Atoms within 1 nm from both ends of the membranes were tethered to their initial z-coordinates to prevent their drifting due to the concentration gradient created. Gas molecules were inserted into the void spaces on both sides of the membranes. Pure H<sub>2</sub> and CH<sub>4</sub> and H<sub>2</sub>/CH<sub>4</sub> mixture simulations were performed. In all simulations the concentration of the gas molecules in the inlet control region (feed) was maintained at their experimentally measured molecular density at 5 bar and 300K (Lemmon, Huber et al. 2007), which were 0.1203 and 0.1217 molecules/nm<sup>3</sup> for H<sub>2</sub> and CH<sub>4</sub>, respectively. The considered mixture corresponds to almost an equimolar feed composition. Outlet gas concentration was set to vacuum. Periodic boundary conditions were applied in all directions. Simulations were run in the NVT ensemble and the temperature of the systems was fixed at 300K by using a Nose-Hoover thermostat. This thermostat was chosen to sample canonical distribution with a deterministic thermostating scheme. The thermostat coupling constant was set to 0.1 ps. Separate thermostats were used for fluid molecules and individual membrane components to prevent asymmetric thermalization in the simulation box due to hot solute-cold solvent effect (Basconi and Shirts 2013). ZIF-8 and PIM-1 were modelled with all-atom flexible force fields. LJ parameters and partial charges for the ZIF-8 and PIM-1 atoms as well as details of intramolecular force field terms can be found in (Semino, Ramsahye et al. 2015). CH<sub>4</sub> and H<sub>2</sub> were modelled with a united atoms force field, both implementing an uncharged single LJ site, with parameters taken from Martin et al (Martin and Siepmann 1998) and Frost et al (Frost, Düren et al. 2006), respectively. Particle Mesh Ewald method was employed to account for long-range electrostatics

interactions. A 1.2 nm cut-off distance was used for the LJ and the real part of the Ewald sum. LJ cross term parameters for the interactions between membrane atoms and gas molecules were tuned in order to capture the magnitude of the available experimental H<sub>2</sub>/CH<sub>4</sub> permselectivity data in literature for the individual PIM-1 and ZIF-8 membranes. These refined parameters given in Table Appendix 2 were also used to study the PIM-1/ZIF-8 composite. The equations of motion were integrated with a 1 fs time step using a Verlet scheme. Pure component permeation simulations of H<sub>2</sub> and CH<sub>4</sub> through the PIM-1 and ZIF-8 membranes and the PIM-1/ZIF-8 composite membrane were run for 1 μs each. In addition, a CH<sub>4</sub>/H<sub>2</sub> mixture separation simulation through the PIM-1/ZIF-8 membrane was also run for 1 μs. For both pure component and mixture simulation results were reported for the last 200 ns. Error bars in relevant graphs were calculated by averaging 5 equal length blocks of these last 200 ns trajectories of simulations. We should emphasize that about 100 ns of simulation is normally sufficient to achieve steady-state diffusion, and the microsecond runs were intended to demonstrate the computational feasibility of the CGD-MD simulations without suffering any feed depletion issue.

The flux of H<sub>2</sub> and CH<sub>4</sub> gases along the z direction ( $J_z$ ) was calculated by counting the net number of molecules which cross an x-y plane located at the centre of the membrane and dividing it by the simulation time (t) and the cross sectional area of the membrane ( $A_{xy}$ ),

$$J_z = \frac{N_i^+ - N_i^-}{t A_{xy}} \quad (4.1)$$

where  $N_i^+$  and  $N_i^-$  represent the number of  $H_2$  or  $CH_4$  molecules that cross the x-y plane in the positive and negative z directions, respectively. The fluxes were then used to calculate gas permeabilities (Table Appendix 3) and  $H_2/CH_4$  permselectivities.

Residence time probability distributions of the  $H_2$  and  $CH_4$  molecules within the membranes were obtained by calculating the time spent by individual molecules within 1 nm-long bins along the z-direction. One important clarification that needs to be made here is that the residence time of a molecule in a bin was determined regardless of the direction (i.e. positive and negative z-directions) it has entered and left the bin. The residence time probability distributions were then used to calculate mean residence times in each bin.

### **4.3: Results and Discussion**

The CGD-MD approach consists of creating a concentration gradient across the membrane, which facilitates the transport of gases. As such, it is essential that the concentrations of molecules are maintained at their target values at the inlet and outlet of the membrane. Figure Appendix 1 shows the concentration of  $H_2$  and  $CH_4$  molecules in the inlet control and outlet control regions of the membrane systems studied. In all systems simulated, CGD-MD method keeps the concentration of the gases very close to the target values.

## Pure H<sub>2</sub> and CH<sub>4</sub> Permeation through PIM-1, ZIF-8 and Mixed Matrix

### Membrane models

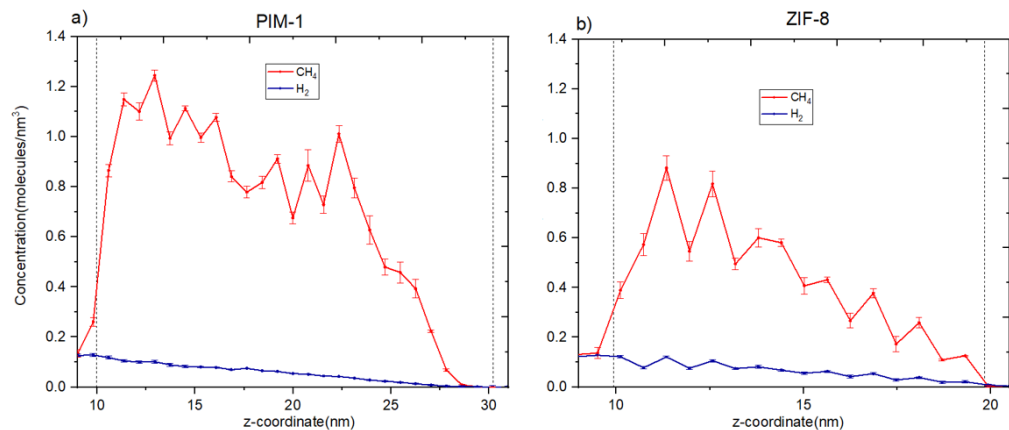
H<sub>2</sub> and CH<sub>4</sub> molecules were simulated as single gas component through PIM-1 and ZIF-8 membrane models initially. Table 4-1 reports the comparison between the simulated ideal H<sub>2</sub>/CH<sub>4</sub> permselectivities in PIM-1 and ZIF-8 membranes and the available experimental ideal permselectivities. The ideal permselectivity is calculated by taking the ratio of pure component permeabilities. The experimental data for both PIM-1 and ZIF-8 vary; however, the simulated ideal permselectivities are in good agreement with several of the reported permselectivity data. Overall, both membranes are H<sub>2</sub> selective, since H<sub>2</sub> permeability is greater than that for CH<sub>4</sub> in both PIM-1 and ZIF-8.

**Table 4-1.** Comparison of experimental and simulated ideal H<sub>2</sub>/CH<sub>4</sub> permselectivities in PIM-1 and ZIF-8 membranes.

PIM-1	10.4 (Budd, Msayib et al. 2005)	6.47 (Staiger, Pas et al. 2008)	5.25 (Bushell, Attfield et al. 2013)	5.42 (Ahn, Chung et al. 2010)	8.37 (Thomas, Pinnau et al. 2009)	6.27 This work
ZIF-8	13.0 (McCarthy, Varela-Guerrero et al. 2010)	4.61 (Pan and Lai 2011)	12.5 (Bux, Liang et al. 2009)	4.86 (Pan, Li et al. 2012)	4.63 (Shekhah, Swaidan et al. 2014)	5.12 This work

Figure 4-2 shows the density profiles of H<sub>2</sub> and CH<sub>4</sub> molecules in the PIM-1 and ZIF-8 membranes along the direction of gas flow (i.e. z direction). Error bars in these graphs calculated by dividing last 200 ns trajectories into 5 equal pieces. H<sub>2</sub>

density values are close to each other in both membranes, that is,  $H_2$  is adsorbed in similar amounts in PIM-1 and ZIF-8. On the other hand,  $CH_4$  adsorption is higher in PIM-1 compared to ZIF-8. The density of  $CH_4$  is higher than that of  $H_2$  in both membranes, and before gradually decreasing due to the concentration gradient there is a sharp increase in the  $CH_4$  density at the entrance of the membranes, whereas,  $H_2$  density almost linearly decreases. These differences are due to the stronger adsorption of  $CH_4$  compared to  $H_2$  in PIM-1 and ZIF-8.  $H_2$  molecules are so weakly adsorbed that they quickly permeate through the membranes and do not exhibit a density increase at the entrance of the membrane compared to its density in the feed. Whereas, strongly adsorbed  $CH_4$  exhibits a much higher density compared to its density in the feed.



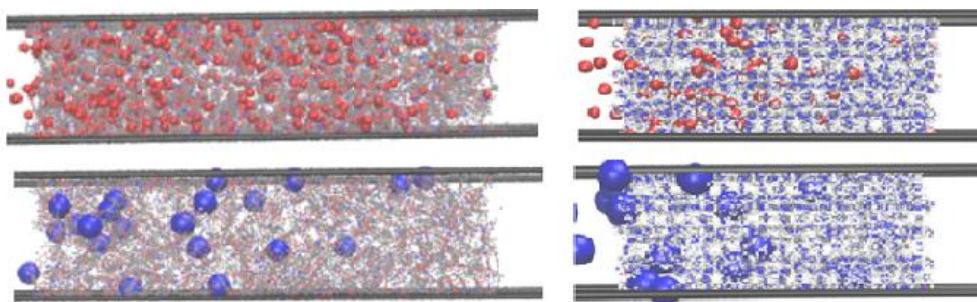


**Figure 4-2.** Density profiles of pure H<sub>2</sub> and CH<sub>4</sub> along the a) PIM-1 and b) ZIF-8 membranes. Dashed lines correspond to the location of membrane surfaces. In lower panel, snapshots are given to visually guide concentration gradient along PIM-1 and ZIF-8 membrane. CH<sub>4</sub> molecules were represented with red, H<sub>2</sub> molecules were represented with blue colours. H<sub>2</sub> molecules were drawn bigger to increase visibility.

Figure 4. 3 shows the residence time analyses of pure H<sub>2</sub> and CH<sub>4</sub> permeation along the PIM-1 and ZIF-8 membranes. To calculate the error bars, last 200 ns was block-averaged with 5 equal length blocks. In the PIM-1 membrane, H<sub>2</sub> exhibits a relatively flat profile, whereas, in the ZIF-8 membrane, thanks to the presence of cages, H<sub>2</sub> molecules exhibit longer residence times. In contrast to H<sub>2</sub>, the residence time profile of CH<sub>4</sub> in PIM-1 exhibits large variations. This is due to the relatively stronger interactions between CH<sub>4</sub> and PIM-1 and local structural fluctuations in the PIM-1 membrane lead to a rather inhomogeneous residence time profile along the membrane. In the ZIF-8 membrane, CH<sub>4</sub> molecules exhibit longer residence times in the cages but overall the residence times of CH<sub>4</sub> molecules in PIM-1 and ZIF-8 are comparable. CH<sub>4</sub> residence times are longer than H<sub>2</sub> residence times in both membranes.

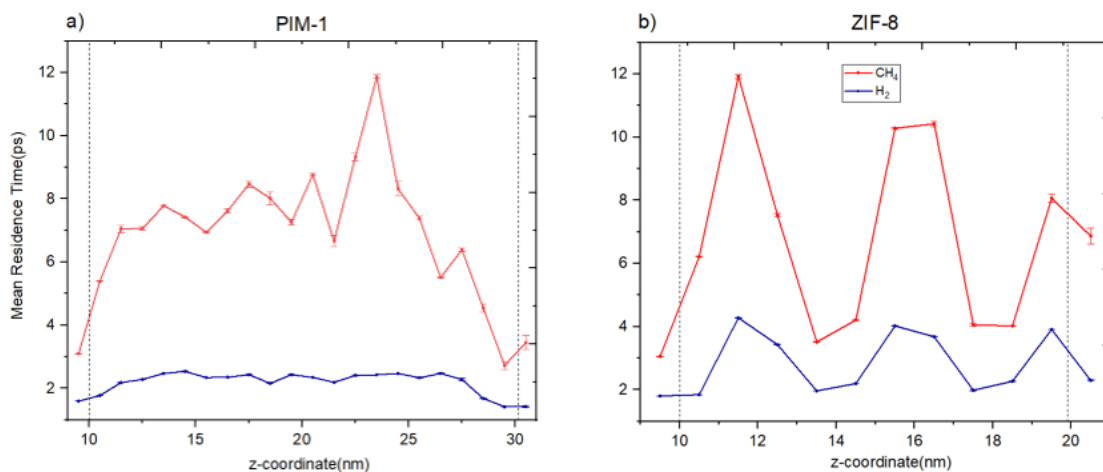


**Figure 4-3.** Mean residence times of H<sub>2</sub> and CH<sub>4</sub> along the z direction of the a) PIM-1 and b) ZIF-8 membranes. Each point corresponds to a mean residence time within a 1 nm wide bin. Dashed lines correspond to the location of membrane surfaces.

After simulating pure component H<sub>2</sub> and CH<sub>4</sub> permeations in PIM-1 and ZIF-8 membranes, we investigated the pure component H<sub>2</sub> and CH<sub>4</sub> permeations and their mixture permeation in the composite PIM-1/ZIF-8 membrane. Figure 4-4 compares the resulting density profiles of H<sub>2</sub> and CH<sub>4</sub>. H<sub>2</sub> density almost linearly decreases along the composite membrane in both cases. The reason for such a linearity along the entire composite structure, despite H<sub>2</sub> permeating through different structures, is because H<sub>2</sub> is adsorbed in similar quantities in PIM-1 and ZIF-8 (Figures 4- 2a and 4.2b). In contrast, CH<sub>4</sub> density decreases along the first PIM-1 slab, then exhibits a drop at the PIM-1/ZIF-8 interface and continues to decrease along ZIF-8 before showing a sharp increase at the interface between ZIF-8 and the second PIM-1 slab. The drop in CH<sub>4</sub> density after the first PIM-1 slab is a consequence of

the fact that ZIF-8 adsorbs less CH<sub>4</sub> compared to PIM-1, and the jump after the onset of the second PIM-1 slab is because PIM-1 adsorbs more CH<sub>4</sub> compared to ZIF-8 (Figures 4-2a and 4-2b).

### **Mixture H<sub>2</sub> and CH<sub>4</sub> Permeation through Mixed Matrix Membrane Model**

Figure 4-4 shows some quantitative differences in the z-density profiles of H<sub>2</sub> and CH<sub>4</sub> for the pure component and mixture simulations. For the mixture, it can be seen that less H<sub>2</sub> is adsorbed through the entire membrane compared to the pure component case. This is because CH<sub>4</sub> molecules occupy some of the space that was previously available for the H<sub>2</sub> molecules in the mixture simulation. On the other hand, the difference between the density profiles of CH<sub>4</sub> for the pure component and mixture simulations is less obvious except for the fact that there is a significant increase in the density of CH<sub>4</sub> near the PIM-1/ZIF-8 interfaces for the mixture case compared to pure component simulation.

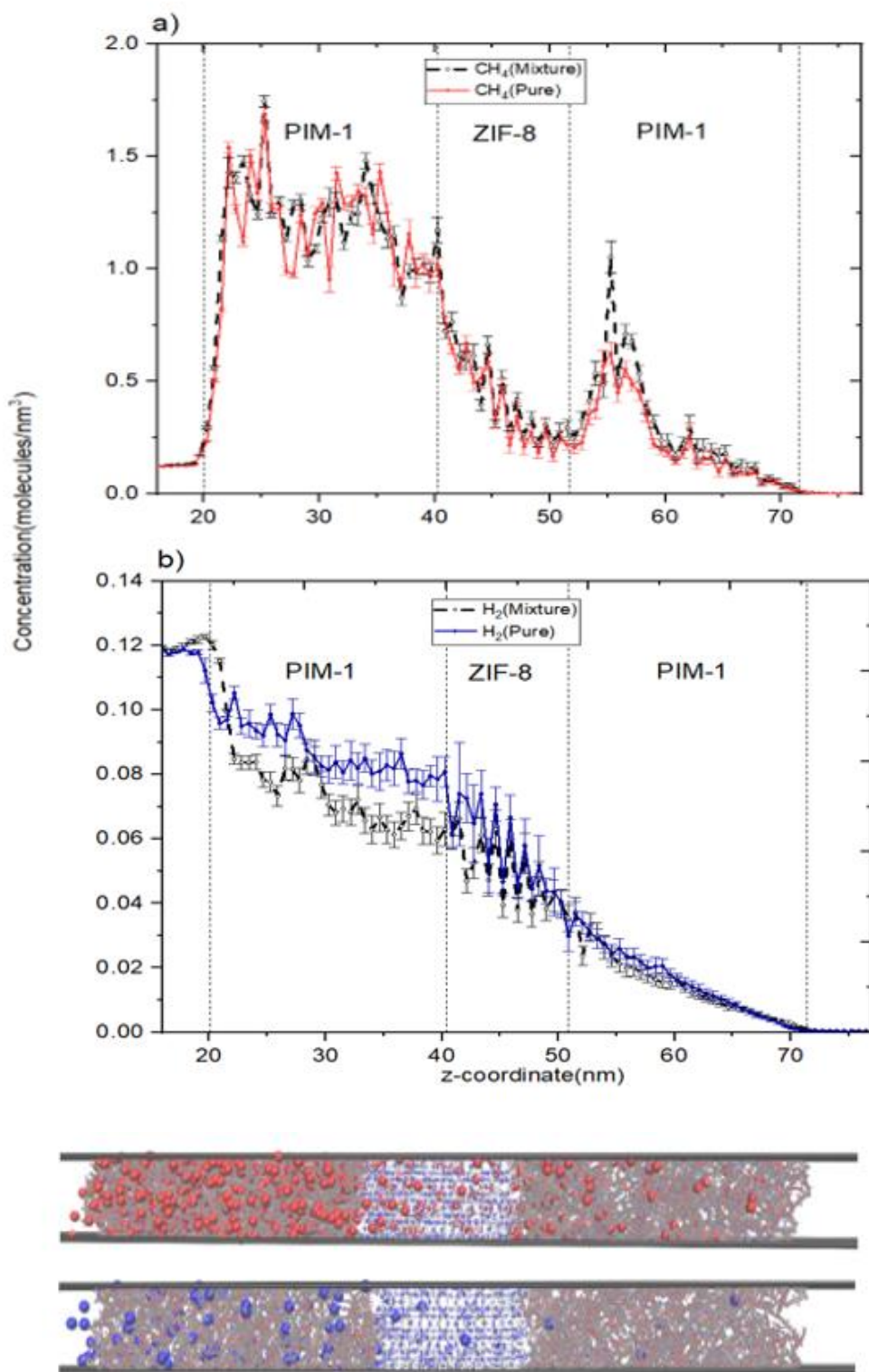


**Figure 4-4.** Density profiles of H<sub>2</sub> and CH<sub>4</sub> in a) pure component and b) mixture simulations along the z direction of the composite PIM-1/ZIF-8 membrane. Dashed lines correspond to the location of membrane surfaces. In lower panel, two

snapshots are given to guide concentration profile visually along composite PIM-1/ZIF-8 membrane. CH<sub>4</sub> molecules were represented with red, H<sub>2</sub> molecules were represented with blue colours. H<sub>2</sub> molecules were drawn bigger to increase visibility.

In principle, the ideal permselectivity of an MMM is expected to be between the permselectivities of its constituent materials. That is, for the PIM-1/ZIF-8 membrane, the expected ideal H<sub>2</sub>/CH<sub>4</sub> permselectivity should be between 6.27 (PIM-1) and 5.12 (ZIF-8). One of the macroscopic permeation models that we can conveniently use to calculate the permselectivity of the composite PIM-1/ZIF-8 membrane is the serial model (Vinh-Thang and Kaliaguine 2013), which is defined as

$$\frac{1}{P_{\text{eff}}} = \frac{\phi_1}{P_1} + \frac{\phi_2}{P_2} \quad (4.2)$$

where  $P_{\text{eff}}$  is the effective permeability of the composite for a given gas, and  $P$  and  $\phi$  are the individual permability and volume fraction of the constituents of the composite membrane. Indeed, when the serial macroscopic model is employed to calculate the ideal H<sub>2</sub>/CH<sub>4</sub> permselectivity of the composite PIM-1/ZIF-8 membrane by using the pure component permeabilities obtained from CGD-MD simulations for the PIM-1 and ZIF-8 membranes (Table 4-1), a permselectivity of 5.51 is obtained (Table 4-2). On the other hand, the ideal H<sub>2</sub>/CH<sub>4</sub> permselectivity calculated based on pure component permeabilities from the CGD-MD simulations in the composite PIM-1/ZIF-8 membrane is 4.61 (Table 4- 2). This value is lower than the permselectivity obtained for the composite PIM-1/ZIF-8 membrane estimated by the serial model. The difference is attributed to the mass transfer

resistances that exist at the PIM-1/ZIF-8 interfaces resulting from the existence of micro-voids (Semino, Ramsahye et al. 2015), phenomenon the serial model does not take into account. In this case the interfacial resistance is relatively significant since the CGD-MD computed ideal H<sub>2</sub>/CH<sub>4</sub> permselectivity of the composite PIM-1/ZIF-8 membrane (4.61) is lower than that of obtained for ZIF-8 as single component (5.12). Furthermore, the H<sub>2</sub>/CH<sub>4</sub> permselectivity obtained by the CGD-MD simulations on the mixture in the composite PIM-1/ZIF-8 membrane (3.92) is even lower than the ideal H<sub>2</sub>/CH<sub>4</sub> permselectivity (Table 4-2). This later value is deemed more accurate since the simulations on the mixture take into account of the presence of micro-voids at the MOF/polymer interfaces as well as the interactions between the H<sub>2</sub> and CH<sub>4</sub> gas molecules.

**Table 4-2.** Comparison of H<sub>2</sub>/CH<sub>4</sub> permselectivities in the composite PIM-1/ZIF-8 membrane obtained from the pure and mixture CGD-MD simulations and that of obtained based on the serial model.

5.51	4.61	3.92
Serial Model (Vinh-Thang and Kaliaguine 2013)	Based on pure component CGD-MD simulations in this study	Based on mixture CGD-MD simulations in this study

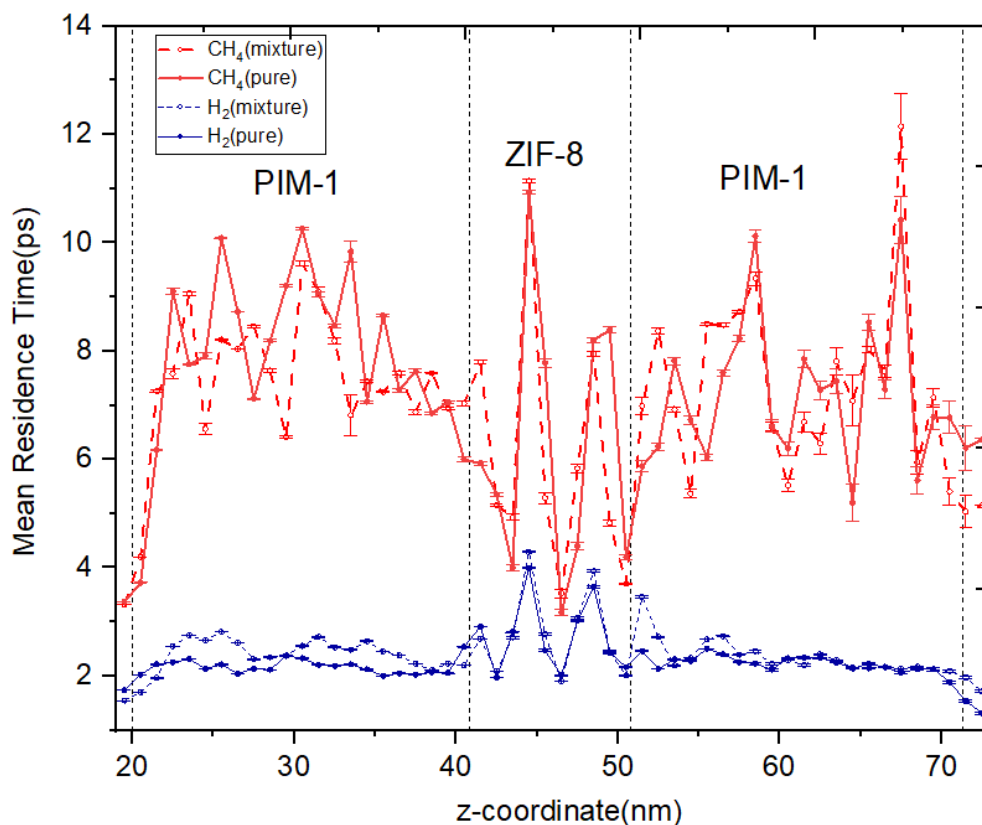


**Figure 4-5.** Mean residence times of H<sub>2</sub> and CH<sub>4</sub> along the composite PIM-1/ZIF-8 membrane in pure component and mixture simulations. Each point corresponds to the mean residence time within a 1 nm wide bin. Dotted lines correspond to the location of membrane surfaces.

Figure 4-5 reports the residence time analyses of H<sub>2</sub> and CH<sub>4</sub> for the pure component and mixture CGD-MD simulations in the composite PIM-1/ZIF-8 membrane. This figure offers insights to the differences in the dynamics of H<sub>2</sub> and CH<sub>4</sub> molecules in the pure component and mixture permeation scenarios. Based on single component permeability data we already know that H<sub>2</sub> is the fast and CH<sub>4</sub> is the slow permeating component in the PIM-1 and ZIF-8 membranes. In mixture permeation, it is expected that the faster gas accelerates the slower gas and the slower gas slows down the faster gas (Skoulidas, Sholl et al. 2003, Liu, Keskin

et al. 2011). Indeed, when we look at Figure 5 we see that the residence times of CH<sub>4</sub> along the first PIM-1 slab decrease, whereas, the residence times of H<sub>2</sub> molecules increase in the mixture simulation, compared to the pure component simulation, due to the interactions between the H<sub>2</sub> and CH<sub>4</sub> molecules. However, the “faster gas accelerates the slower gas and the slower gas slows down the faster gas” formalism does not seem to be valid for the rest of the membrane nor for the entirety of the composite. Because the permeability of CH<sub>4</sub> in mixture is actually lower than its pure component permeability in the composite PIM-1/ZIF-8 membrane (Table Appendix 3), an effect which could be attributed to the existence of micro-voids at the interfaces between the constituents of the MMM. This work demonstrates that the MOF/polymer interface plays a significant role in the permeation dynamics of the guest molecules in the membranes.

#### **4.4: Conclusions**

In this study we report microsecond-long concentration gradient driven molecular dynamics (CGD-MD) simulations of H<sub>2</sub> and CH<sub>4</sub> transport in PIM-1 and ZIF-8 membranes as well as their permselectivity in the composite PIM-1/ZIF-8 membrane. The CGD-MD method allowed us to map the density and mean residence time profiles of the H<sub>2</sub> and CH<sub>4</sub> gases along the membranes while they are diffusing under a concentration gradient. Furthermore, we directly computed the flux of the permeating gases through the membranes from the CGD-MD simulations and characterized the effect of the interfaces on the permselectivity. As we demonstrated for H<sub>2</sub>/CH<sub>4</sub> separation in the composite PIM-1/ZIF-8 membrane, the interface between the constituents of an MMM significantly affects the

permselectivity performance. Typically the presence of non-selective void spaces between PIM-1 and ZIF-8 in the composite PIM-1/ZIF-8 membrane induces a decrease of the H<sub>2</sub>/CH<sub>4</sub> permselectivity compared to the ideal permselectivity obtained by the application of macroscopic model on the data obtained individually for ZIF-8 and PIM-1. The CGD-MD simulations carried out with an accurate description of the MOF/polymer interfaces allow the determination of the magnitude of such a deviation, thus paving the way towards a more critical use of macroscopic models to anticipate the performances of MMMs.

#### 4.5 References:

1. Abbott, L. J. and C. M. Colina (2011). "Atomistic structure generation and gas adsorption simulations of microporous polymer networks." *Macromolecules* 44(11): 4511-4519.
2. Abbott, L. J., et al. (2013). "Polymatic: a generalized simulated polymerization algorithm for amorphous polymers." *Theoretical Chemistry Accounts* 132(3): 1334.
3. Abraham, M., et al. (2015). "the GROMACS development team GROMACS User Manual version 5.1. 2; 2016." MJ Abraham, T. Murtola, R. Schulz, S. Páll, JC Smith, B. Hess, E. Lindahl, *SoftwareX* 1: 19.
4. Ahmad, M. Z., et al. (2018). "Enhanced gas separation performance of 6FDA-DAM based mixed matrix membranes by incorporating MOF UiO-66 and its derivatives." *Journal of Membrane Science* 558: 64-77.

5. Ahn, J., et al. (2010). "Gas transport behavior of mixed-matrix membranes composed of silica nanoparticles in a polymer of intrinsic microporosity (PIM-1)." Journal of Membrane Science **346**(2): 280-287.
6. ALTINTAS, C., et al. (2019). "An Extensive Comparative Analysis of Two MOF Databases: High-Throughput Screening of Computation-Ready MOFs for CH<sub>4</sub> and H<sub>2</sub> Adsorption." Journal of Materials Chemistry A.
7. Basconi, J. E. and M. R. Shirts (2013). "Effects of temperature control algorithms on transport properties and kinetics in molecular dynamics simulations." Journal of chemical theory and computation **9**(7): 2887-2899.
8. Benzaqui, M., et al. (2017). "Revisiting the aluminum trimesate-based MOF (MIL-96): from structure determination to the processing of mixed matrix membranes for CO<sub>2</sub> capture." Chemistry of Materials **29**(24): 10326-10338.
9. Budd, P. M., et al. (2005). "Gas separation membranes from polymers of intrinsic microporosity." Journal of Membrane Science **251**(1-2): 263-269.
10. Bushell, A. F., et al. (2013). "Gas permeation parameters of mixed matrix membranes based on the polymer of intrinsic microporosity PIM-1 and the zeolitic imidazolate framework ZIF-8." Journal of Membrane Science **427**: 48-62.
11. Bux, H., et al. (2009). "Zeolitic imidazolate framework membrane with molecular sieving properties by microwave-assisted solvothermal synthesis." Journal of the American Chemical Society **131**(44): 16000-16001.

12. Castarlenas, S., et al. (2017). "Gas separation with mixed matrix membranes obtained from MOF UiO-66-graphite oxide hybrids." Journal of Membrane Science **526**: 205-211.
13. Cheng, Y., et al. (2018). "Advanced porous materials in mixed matrix membranes." Advanced Materials **30**(47): 1802401.
14. Ding, L., et al. (2018). "MXene molecular sieving membranes for highly efficient gas separation." Nature communications **9**(1): 155.
15. Dutta, R. C. and S. K. Bhatia (2018). "Structure and gas transport at the polymer–zeolite interface: insights from molecular dynamics simulations." ACS applied materials & interfaces **10**(6): 5992-6005.
16. Frentrup, H., et al. (2015). "In silico determination of gas permeabilities by non-equilibrium molecular dynamics: CO<sub>2</sub> and He through PIM-1." Membranes **5**(1): 99-119.
17. Frost, H., et al. (2006). "Effects of surface area, free volume, and heat of adsorption on hydrogen uptake in metal– organic frameworks." The Journal of Physical Chemistry B **110**(19): 9565-9570.
18. Funke, H. H., et al. (1997). "Separations of cyclic, branched, and linear hydrocarbon mixtures through silicalite membranes." Industrial & engineering chemistry research **36**(1): 137-143.
19. Galizia, M., et al. (2017). "50th anniversary perspective: Polymers and mixed matrix membranes for gas and vapor separation: A review and prospective opportunities." Macromolecules **50**(20): 7809-7843.

20. Genduso, G., et al. (2019). "Mixed-gas sorption in polymers via a new barometric test system: Sorption and diffusion of CO<sub>2</sub>-CH<sub>4</sub> mixtures in polydimethylsiloxane (PDMS)." Journal of Membrane Science **577**: 195-204.
21. Ghalei, B., et al. (2017). "Enhanced selectivity in mixed matrix membranes for CO<sub>2</sub> capture through efficient dispersion of amine-functionalized MOF nanoparticles." Nature Energy **2**(7): 17086.
22. Goedecker, S., et al. (1996). "Separable dual-space Gaussian pseudopotentials." Physical Review B **54**(3): 1703.
23. Gong, X., et al. (2017). "ZIF-8-based membranes for carbon dioxide capture and separation." ACS Sustainable Chemistry & Engineering **5**(12): 11204-11214.
24. Grimme, S. (2006). "Semiempirical GGA-type density functional constructed with a long-range dispersion correction." Journal of computational chemistry **27**(15): 1787-1799.
25. Harder, E., et al. (2009). "Molecular dynamics study of a polymeric reverse osmosis membrane." The Journal of Physical Chemistry B **113**(30): 10177-10182.
26. Hutter, J., et al. (2014). "cp2k: atomistic simulations of condensed matter systems." Wiley Interdisciplinary Reviews: Computational Molecular Science **4**(1): 15-25.

27. Hwang, S., et al. (2018). "Revealing the Transient Concentration of CO<sub>2</sub> in a Mixed-Matrix Membrane by IR Microimaging and Molecular Modeling." Angewandte Chemie International Edition **57**(18): 5156-5160.
28. Kusuda, H., et al. (2017). "Enhanced selectivity in mixed matrix membranes for CO<sub>2</sub> capture through efficient dispersion of amine-functionalized MOF nanoparticles."
29. Kwon, H. T. and H.-K. Jeong (2013). "In situ synthesis of thin zeolitic-imidazolate framework ZIF-8 membranes exhibiting exceptionally high propylene/propane separation." Journal of the American Chemical Society **135**(29): 10763-10768.
30. Lemmon, E. W., et al. (2007). NIST standard reference database 23: reference fluid thermodynamic and transport properties-REFPROP, version 8.0.
31. Li, S., et al. (2006). "Improved SAPO-34 membranes for CO<sub>2</sub>/CH<sub>4</sub> separations." Advanced Materials **18**(19): 2601-2603.
32. Liu, D., et al. (2014). "Gas transport properties and propylene/propane separation characteristics of ZIF-8 membranes." Journal of Membrane Science **451**: 85-93.
33. Liu, G., et al. (2018). "Mixed matrix formulations with MOF molecular sieving for key energy-intensive separations." Nature materials **17**(3): 283.
34. Liu, J., et al. (2011). "Molecular simulations and theoretical predictions for adsorption and diffusion of CH<sub>4</sub>/H<sub>2</sub> and CO<sub>2</sub>/CH<sub>4</sub> mixtures in ZIFs." The Journal of Physical Chemistry C **115**(25): 12560-12566.

35. Ma, X., et al. (2018). "Zeolitic imidazolate framework membranes made by ligand-induced permselectivation." Science **361**(6406): 1008-1011.
36. Ma, X., et al. (2018). "Highly compatible hydroxyl-functionalized microporous polyimide-ZIF-8 mixed matrix membranes for energy efficient propylene/propane separation." ACS Applied Nano Materials **1**(7): 3541-3547.
37. Martin, M. G. and J. I. Siepmann (1998). "Transferable potentials for phase equilibria. 1. United-atom description of n-alkanes." The Journal of Physical Chemistry B **102**(14): 2569-2577.
38. McCarthy, M. C., et al. (2010). "Synthesis of zeolitic imidazolate framework films and membranes with controlled microstructures." Langmuir **26**(18): 14636-14641.
39. McKeown, N. B., et al. (2005). "Polymers of intrinsic microporosity (PIMs): bridging the void between microporous and polymeric materials." Chemistry–A European Journal **11**(9): 2610-2620.
40. Merkel, T., et al. (2000). "Gas sorption, diffusion, and permeation in poly (dimethylsiloxane)." Journal of Polymer Science Part B: Polymer Physics **38**(3): 415-434.
41. Ogieglo, W., et al. (2018). "High-pressure CO<sub>2</sub> sorption in polymers of intrinsic microporosity under ultrathin film confinement." ACS applied materials & interfaces **10**(13): 11369-11376.

42. Ozcan, A., et al. (2017). "Concentration gradient driven molecular dynamics: a new method for simulations of membrane permeation and separation." Chemical science **8**(5): 3858-3865.
43. Pan, Y. and Z. Lai (2011). "Sharp separation of C2/C3 hydrocarbon mixtures by zeolitic imidazolate framework-8 (ZIF-8) membranes synthesized in aqueous solutions." Chemical Communications **47**(37): 10275-10277.
44. Pan, Y., et al. (2012). "Effective separation of propylene/propane binary mixtures by ZIF-8 membranes." Journal of Membrane Science **390**: 93-98.
45. Pan, Y., et al. (2011). "Rapid synthesis of zeolitic imidazolate framework-8 (ZIF-8) nanocrystals in an aqueous system." Chemical Communications **47**(7): 2071-2073.
46. Park, K. S., et al. (2006). "Exceptional chemical and thermal stability of zeolitic imidazolate frameworks." Proceedings of the National Academy of Sciences **103**(27): 10186-10191.
47. Perego, C., et al. (2015). "Molecular dynamics simulations of solutions at constant chemical potential." The Journal of chemical physics **142**(14): 144113.
48. Robeson, L. M. (1991). "Correlation of separation factor versus permeability for polymeric membranes." Journal of Membrane Science **62**(2): 165-185.
49. Robeson, L. M. (2008). "The upper bound revisited." Journal of Membrane Science **320**(1-2): 390-400.

50. Semino, R., et al. (2017). "Multiscale Modeling of the HKUST-1/Poly (vinyl alcohol) Interface: From an Atomistic to a Coarse Graining Approach." The Journal of Physical Chemistry C **121**(39): 21491-21496.
51. Semino, R., et al. (2018). "Understanding the origins of metal–organic framework/polymer compatibility." Chemical science **9**(2): 315-324.
52. Semino, R., et al. (2015). "Microscopic model of the metal–organic framework/polymer interface: a first step toward understanding the compatibility in mixed matrix membranes." ACS applied materials & interfaces **8**(1): 809-819.
53. Shekhah, O., et al. (2014). "The liquid phase epitaxy approach for the successful construction of ultra-thin and defect-free ZIF-8 membranes: pure and mixed gas transport study." Chemical Communications **50**(17): 2089-2092.
54. Shen, M., et al. (2016). "Dynamics of water and solute transport in polymeric reverse osmosis membranes via molecular dynamics simulations." Journal of Membrane Science **506**: 95-108.
55. Sholl, D. S. and R. P. Lively (2016). "Seven chemical separations to change the world." Nature News **532**(7600): 435.
56. Skoulidas, A. I., et al. (2003). "Correlation effects in diffusion of CH<sub>4</sub>/CF<sub>4</sub> mixtures in MFI zeolite. A study linking MD simulations with the Maxwell– Stefan formulation." Langmuir **19**(19): 7977-7988.

57. Smith, Z. P., et al. (2015). "Effect of polymer structure on gas transport properties of selected aromatic polyimides, polyamides and TR polymers." Journal of Membrane Science **493**: 766-781.
58. Staiger, C. L., et al. (2008). "Gas separation, free volume distribution, and physical aging of a highly microporous spirobisindane polymer." Chemistry of Materials **20**(8): 2606-2608.
59. Thomas, S., et al. (2009). "Pure-and mixed-gas permeation properties of a microporous spirobisindane-based ladder polymer (PIM-1)." Journal of Membrane Science **333**(1-2): 125-131.
60. Tribello, G. A., et al. (2014). "PLUMED 2: New feathers for an old bird." Computer Physics Communications **185**(2): 604-613.
61. Tuan, V. A., et al. (2001). "Preparation and pervaporation properties of a MEL-type zeolite membrane." Chemical Communications(6): 583-584.
62. VandeVondele, J. and J. Hutter (2007). "Gaussian basis sets for accurate calculations on molecular systems in gas and condensed phases." The Journal of chemical physics **127**(11): 114105.
63. Velioglu, S. and S. Keskin (2019). "Simulation of H<sub>2</sub>/CH<sub>4</sub> mixture permeation through MOF membranes using non-equilibrium molecular dynamics." Journal of Materials Chemistry A **7**(5): 2301-2314.
64. Venna, S. R. and M. A. Carreon (2009). "Highly permeable zeolite imidazolate framework-8 membranes for CO<sub>2</sub>/CH<sub>4</sub> separation." Journal of the American Chemical Society **132**(1): 76-78.

65. Vinh-Thang, H. and S. Kaliaguine (2013). "Predictive models for mixed-matrix membrane performance: a review." Chemical reviews **113**(7): 4980-5028.
66. Wu, T., et al. (2017). "Zeolitic imidazolate Framework-8 (ZIF-8) membranes for Kr/Xe separation." Industrial & Engineering Chemistry Research **56**(6): 1682-1686.
67. Xie, K., et al. (2017). "Increasing both selectivity and permeability of mixed-matrix membranes: Sealing the external surface of porous MOF nanoparticles." Journal of Membrane Science **535**: 350-356.
68. Yampolskii, Y. and B. Freeman (2010). Membrane gas separation, John Wiley and Sons.
69. Zhang, L., et al. (2012). "Metal-organic framework/polymer mixed-matrix membranes for H<sub>2</sub>/CO<sub>2</sub> separation: a fully atomistic simulation study." The Journal of Physical Chemistry C **116**(36): 19268-19277.
70. Zhang, Y., et al. (2018). "Ultrahigh Metal-Organic Framework Loading and Flexible Nanofibrous Membranes for Efficient CO<sub>2</sub> Capture with Long-Term, Ultrastable Recyclability." ACS applied materials & interfaces **10**(40): 34802-34810.
71. Zhou, S., et al. (2018). "Paralyzed membrane: Current-driven synthesis of a metal-organic framework with sharpened propene/propane separation." Science advances **4**(10): eaau1393.

## **Chapter 5: ATOMISTIC SIMULATIONS OF CO<sub>2</sub> PERMEATION THROUGH ASSEMBLED MOF STRUCTURES: A NON-EQUILIRIUM MOLECULAR DYNAMICS (NEMD) STUDY**

---

### **5.1: Introduction**

A successful application of a membrane-based separation process is strongly dependent to chemical, mechanical and mixture separation performance of membrane materials. Initially, polymeric materials have gained a significant attention, but recent development demonstrated that they seemingly reached their limit in trade-off between selectivity and permeability. To overcome permeability-selectivity trade-off of polymeric membranes, a new class of structures have emerged as membrane materials: Zeolites and Metal Organic Frameworks (MOFs). In the context of separation technology, zeolites and MOFs have demonstrated superior performance due to their size-selective molecular sieve under various separation conditions (Baker, 2012).

A novel development for membrane separation requires a fundamental understanding of penetrants' molecular transport. On the other hand, that molecular transport combines a subtle interplay between kinetic (diffusion) and equilibrium (adsorption) phenomena. Many models were proposed to illustrate that complex transport behaviour such as irreversible thermodynamics based models or solution-diffusion model. In this sense, atomistic simulations provide a valuable tool to understand molecular transport through membrane materials and check the validity of the many assumptions of previously develop models in nano scale (Mulder 2012).

Metal-organic frameworks are new class of nanoporous crystalline materials with high porosity, designable topology and chemical functionality. Therefore, they have vast array of applications from gas storage and separation to catalysis. MOFs are crystalline structures however, like many other crystalline materials, they contain local structural features such as point defects, disorders, coherent interfaces and inner surfaces. For application purposes, these local features are as significant as crystallographic structures and can dominate the overall properties of molecular transport, sorption and catalytic activity. Even though their tremendous significance for applications, surface and interface considering MOF studies are rare. In a recent study, Zhu et al. (Zhu, Ciston et al. 2017) have emphasised the importance of inner interfaces for assembled ZIF-8 crystal and have suggested a pioneering experimental methodology for imaging them.

Economic success of membrane-based separations significantly relies on reducing membrane thickness and thereby reducing the driving force requirement thorough membrane for a given flux. Recently, an important amount of effort was dedicated to reduce thickness of nanoporous membranes for specific gas and liquid separation applications with a great success (Jiang, Karan et al. 2018, Zhang, Cheng et al. 2019). But within that fact, it should be kept in mind that, both interfacial barriers and intra-crystalline resistance become equally important at ultra-thin limit of membrane thickness. For a long time, intra-crystalline resistance has been investigated extensively but interfacial barrier has been started to study rather recently. New imaging techniques paved the way to quantify interfacial barriers (Saint Remi, Lauerer et al. 2016, Zhu, Ciston et al. 2017) and these techniques have applied to ZIF-8 and SAPO-34. From the simulation perspective, both equilibrium

molecular dynamics (EMD) and non-equilibrium molecular dynamics (NEMD) methods were utilised successfully to investigate interfacial transport mechanism through nanoporous membranes. Newsome et al.(Newsome and Sholl 2006) and Ahunbay et al.(Heffelfinger and Swol 1994, Ahunbay, Elliott et al. 2004) were both used dual control volume grand canonical MD (DCV-GCMD) method to investigate interface permeation and showed their relative importance in gas transport for ultra-thin membranes. Sestre et al.(Sastre, Kärger et al. 2018) used EMD simulation to study controllable release of benzene from a zeolite structure and pointed out the significance of surface barriers. Dutta et al. (Dutta and Bhatia, 2018) investigated the importance of external barriers on gas transport through a zeolite membranes by using EMD simulation. These simulation studies were concentrated on fluid-solid interface effect on molecular transport and concluded that interface resistance becomes important for comparatively higher surface-volume ratio membranes. In this study, we have concentrated on the solid-solid interface effect on gas transport and to our knowledge, this the first NEMD study that stress the effect of “internal interfaces” on molecular transport.

Here, we apply a newly developed NEMD method called CGD-MD (Ozcan, Perego et al. 2017) to assess the importance of internal interfaces to permeation of CO<sub>2</sub> molecules through a ZIF-8 membrane. Furthermore, we investigated the effect of relative permeability difference of two adjacent ZIF-8 slabs on interfacial transport. Additionally, we compared our atomistic simulations results with continuum models of effective permeability estimations for mixed matrix membranes.

## 5.2: Models and Methods

In our simulations, we used atomistic model of ZIF-8 slabs which was constructed in a recent study (Semino, Ramsahye et al. 2015). The interaction between ZIF-8 slab model atoms included bonded (stretching, bending, proper and improper dihedrals) and nonbonded potentials (Lennard-Jones (LJ) and electrostatics potentials). The force field parameters of ZIF-8 slab was taken from the following reference (Zheng, Sant et al. 2012). Lorenz-Berthelot mixing rules was applied to estimate cross interaction between different LJ units. Non-equilibrium Molecular Dynamics (NEMD) simulations were run to estimate CO<sub>2</sub> permeability through ZIF-8 membrane with a recently developed Concentrations Gradient Driven Molecular Dynamics (CGD-MD) (Ozcan, Perego et al. 2017) method. CO<sub>2</sub> was described as three-point flexible model and parameters were taken from following reference. This flexible model was chosen due to previously reported limitations of rigid description of CO<sub>2</sub> (Cygan, Romanov et al. 2012). The initial velocities of atoms were assigned due to Maxwell-Boltzmann distribution at 300 K. The long-range corrections were set up for the electrostatic interactions through the particle mesh Ewald (PME) method and LJ interactions truncated at 12 Angstroms. Isothermal and constant volume (NVT) simulations were performed by using velocity-rescaling thermostat (Bussi, Donadio et al. 2007) with relaxation time of 1 ps for temperature control. This thermostat is natural selection for Well-Tempered Metadynamics simulations to have better sampling and reliable trajectory. The time step employed was 1 fs in all simulations. All simulation were performed with PLUMED-2.1.0 (Tribello,

Bonomi et al. 2014) patched version of GROMACS 5.1.2(Abraham, van der Spoel et al. 2015).

### **Series Model Membrane Generation**

Well-tempered metadynamics (WTMetaD) method is used to assemble two ZIF-8 slabs and generate an assembled membrane model. (Barducci, Bussi et al. 2008). This enhanced sampling method is used to estimate minimum energy configuration of two slabs when they assembled and to use this structure as Series Mixed Matrix Model. WTMetaD depends on the introducing of a history-dependent bias potential along a low-dimensional set of collective variables (CVs) (Laio and Gervasio 2008, Barducci, Bonomi et al. 2011, Abrams and Bussi 2014). This biasing potential allows for an efficient sampling of phase space by penalising the states that already visited. This bias potential not only makes sampling efficient but also provides an estimation of free energy surface (FES) along the collective variables.

Two CVs selected for assembling ZIF-8 slabs: First one was the distances between centers of masses (COMs) of two ZIF-8 slabs; second collective variable was the distance between center of masses (COMs) of the atoms with 5 Angstroms regions of ZIF-8 slabs that were touching each other at the interface. For WTMetaD, the initial heights of the Gaussians were 0.5 kJ/mol and with width of 0.3 Angstroms for both CVs. The bias factor is either 10 for both. More detailed description of WTMetaD, can be found in a recent review article of Valsson et al. (Valsson, Tiwary et al. 2016).

### 5.3: Results and Discussion

Initially, we performed CO<sub>2</sub> permeation through a single ZIF-8 slab model and calculate CO<sub>2</sub> permeability. Then, we intentionally tuned ZIF-8/CO<sub>2</sub> cross interaction LJ parameters to generate a “less permeable” ZIF-8 slab and called it as CO<sub>2</sub>-phobic ZIF-8. Later, two ZIF-8 slabs were interfaced by using WT-metaD simulations. We generated C-phobic ZIF-8 slab to simulate permeation through a simple mixed matrix model which has two interfacing constituents with different (low and high) gas permeabilites. In the last part, our atomistic simulation results were compared with well-known models to predict mixed matrix membrane permeability from permeabilites of its components.

#### 5.3.1: CO<sub>2</sub> permeation through ZIF-8 Membrane

To calculate permeability of CO<sub>2</sub> through our ultra-thin ZIF-8 membrane model, we performed CGD-MD simulations. In these simulations, 9.8 nm length ZIF-8 membrane model was located in the middle of simulation box and 10 nm empty spaces were left both sides of the membrane. Concentration of CO<sub>2</sub> were controlled within 2.5 nm length control region which was set to 2.5 nm far from membrane surfaces of both sides. In simulations, feed side concentration was fixed to 10 bar density of CO<sub>2</sub> which was read from NIST database (Lemmon, Huber et al. 2007) and outlet set was fixed to vacuum. By using mass transport equation,  $J = K \frac{\Delta P}{L}$ , (where J is to molecular flux,  $\Delta P$  pressure difference between both sides of the membrane, L is the membrane thickness and K is permeability of penetrant molecule), we can calculate CO<sub>2</sub> permeability. CO<sub>2</sub> permeability was calculated  $186.2 \times 10^{-13}$  mol.m/m<sup>2</sup>.s.Pa from our CGD-MD simulations.

Later, a hypothetical CO<sub>2</sub>-phobic ZIF-8 membrane was created by tuning CO<sub>2</sub>/ZIF-8 cross interaction parameters. This different permeability membrane model is needed to test mixed matrix membrane equations to estimate effective permeability for composite membranes. We run CGD-MD simulations for this hypothetical CO<sub>2</sub>-phobic ZIF-8 and CO<sub>2</sub> permeability is calculated as 106.4x10<sup>-13</sup> mol.m/m<sup>2</sup>.s.Pa.

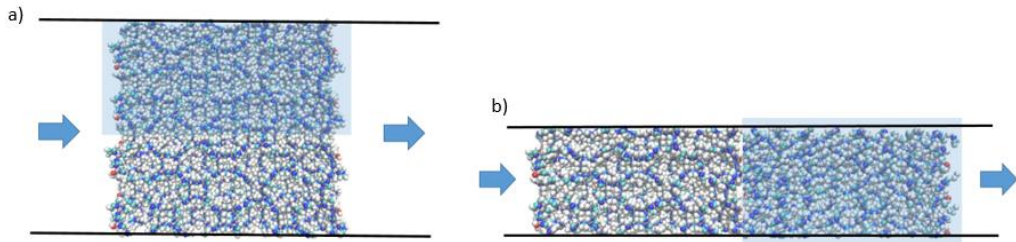


**Figure 5-1.** Parallel and series configurations with two ZIF-8 slabs with Figure a) and b), respectively. Transparent regions stand for high permeability component of the composite structure. Color code is as follows: C (cyan), H (white) N (blue), O (red) and Zn (steel blue).

In MMM literature, effective permeability for two parallel and series layer membrane models estimates effective permeabilities by the following straightforward equations, respectively:

$$P_{eff} = (1 - \phi)P_1 + \phi P_2 \quad (5.1)$$

$$\frac{1}{P_{eff}} = \frac{(1-\phi)}{P_1} + \frac{\phi}{P_2} \quad (5.2)$$

Where  $P_1$  accounts of permeability of first component,  $P_2$  for permeability of second component and  $\phi$  for volume fraction of the second component.

**Table 5-1** CO<sub>2</sub> permeability for experimental and simulations of different ZIF-8 models.

	Simulated ZIF-8	ZIF-8 (exp.) (Zhu et al., 2017)	Simulated CO <sub>2</sub> -phobic ZIF-8	Parallel Model (Vinh-Thang and Kaliaguine 2013)	Atomistic Simulations for Parallel Slabs
CO <sub>2</sub> permeability (x10 <sup>13</sup> mol.m/m <sup>2</sup> .s.Pa)	186.2	74.2	106.4	146.3	139.6

We located ZIF-8 and CO<sub>2</sub>-phobic ZIF-8 in two parallel slabs and performed CGD-MD simulation to calculate effective permeability. The inlet pressure set to 10 bar and outlet pressure set to vacuum. The effective permeability, which is calculated from our CGD-MD simulations, is 139.6x10<sup>-13</sup> mol.m/m<sup>2</sup>.s.Pa. In these parallel mode simulations, permeability of high permeation region is 161.936x10<sup>-13</sup> mol.m/m<sup>2</sup>.s.Pa and 117.214x10<sup>-13</sup> mol.m/m<sup>2</sup>.s.Pa for low permeation region. According to Equation 5.1, effective permeability equals to 146.3x10<sup>-13</sup> mol.m/m<sup>2</sup>.s.Pa for 0.5 volume fraction which is reasonably close with the result coming from our CGD-MD simulations. These results were summarised in Table 5-1.

### 5.3.2: Interfacing two thin ZIF-8 slabs

To perform permeation simulation for series configuration, an interfaced ZIF-8/ZIF-8 composite is needed. We performed Well-Tempered Metadynamics (WTmetaD) simulations to interface two thin ZIF-8 slabs. In our WTmetaD simulations, two collective variables were used simultaneously. These collective variables were distance between center of masses (COMs) of two membrane slabs

and distance between center of masses (COMs) between atoms at the interfacing surfaces of each ZIF-8 slabs. The atoms within 5 Angstroms from surface were defined as “surface atoms” and distance between their COMs was taken as a collective variable. In WTmetaD simulations, two ZIF-8 slabs were located with 20 Angstroms separation and 100 Angstroms empty regions both sides. These empty regions were taken considerably larger to prevent interaction between atoms through periodic images through z-direction.

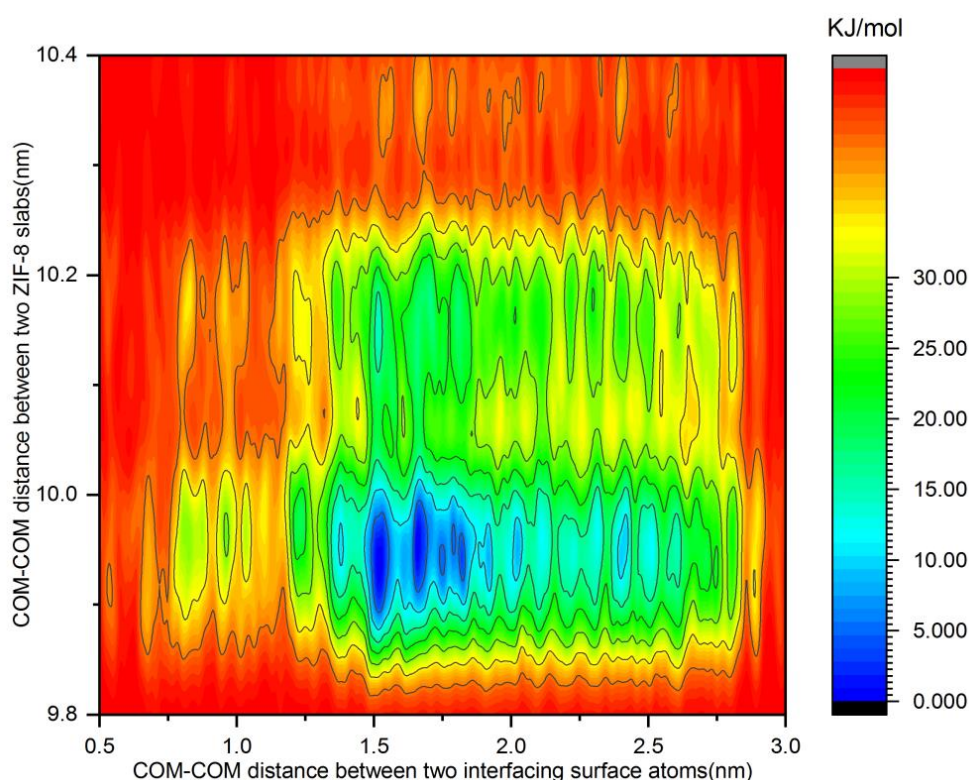


**Figure 5-2.** Free Energy Surface (FES) for assembling two ZIF-8 slab models

We employed this methodology to interface two components of a composite structure to bring insight to well-known “surface compatibility” issue of composite membrane structures from free energy calculation perspective. For mixed matrix membranes, surface compatibility problem is a long-standing problem. Most common surface compatibility issues are well-known in the relevant literature: One

of them is penetration of one component into the other and pore blockage at the surface (Duan, Moreton et al. 2019) and the other one is surface rigidification due to molecular interactions at the interface (Semino, Moreton et al. 2018). By keeping these two problems in mind, we infer a possible definition for surface compatibility between components of a composite membrane: If two structure are surface compatible, COM-COM distance between two structure should have one stable free energy minimum (implies these two structure do not intrude each other) and COM-COM distance between interfacing surface atoms should have multiple free energy minima which separated by low free energy barriers (implies interfacing surfaces are not got rigidified and “locked” on the top of each other). Obviously, this definition is not the “ultimate definition” of surface compatibility but gives a clue on surface compatibility problem from free energy perspective. Due to this definition, surfaces of our ZIF-8 models are “compatible”. In Figure 5-2, we gave 2-D free energy plot of two ZIF-8 slabs assembling simulations which fits to our compatibility definition well. COM-COM distance between two ZIF-8 slabs has one stable minimum around 9.9-9.95 nm distance between each other and this can be interpreted as these two structures have not infiltrate each other which is a requirement for good surface compatibility. Additionally, COM-COM distance between two interfacing surfaces have multiple minima between 1.5-2 nm distance and this can be interpreted as another indicator of good surface compatibility. Because, these two interfacing surfaces are flexible enough to “touch” each other in different conformations and this can be taken as a sign of not suffering interface-induced rigidification for this specific system. To sum up, ZIF-8 slabs have compatible surfaces according to our definition which do not infiltrate through each other and do not rigidify at interfacing surfaces.

### 5.3.3: CGD-MD simulations for Interfaced ZIF-8 Slabs:

After two ZIF-8 slabs were interfaced, we performed a CGD-MD simulation with this interfaced structure. These simulations provide a suitable setup to perform a multilayer composite structure in series morphology. To investigate the effect of physical interface between low permeability-high permeability regions of a MMM, we performed a CGD-MD simulation with an assembled multilayer membrane. By this way, we had an opportunity to model gas permeation through a “mixed matrix” ZIF-8 membrane and physical interface.

We calculated permeability is  $111 \times 10^{13}$  mol.m/m<sup>2</sup>.s.Pa of CO<sub>2</sub> through multilayer ZIF-8 mixed matrix membrane model. These direct simulations’ results were compared with three different macroscopic mixed matrix membrane models in Table 5-2.

**Table 5-2** Comparison of direct atomistic simulation results with three different macroscopic MMM permeability prediction models.

	Series Model (Vinh-Thang and Kaliaguine 2013)	Maxwell Model (Vinh-Thang and Kaliaguine 2013)	Te Hanepe Model (Hennepe, Smolders et al. 1991)	Atomistic Simulations
CO <sub>2</sub> permeability (x10 <sup>13</sup> mol.m/m <sup>2</sup> .s.Pa)	135.0	140.1	135.8	111.0

Table 5-2 shows that macroscopic models remain short to capture the direct simulations results. That can be attributed to no consideration of the effect of inner interfaces on overall mass transport in these macroscopic models. To investigate the effect of inner interfaces on mass transport, we performed residence time

distribution (RTD) analysis in CGD-MD simulations. In figure 5-3, RTD plot was given for assembled low and high permeability ZIF-8 models.

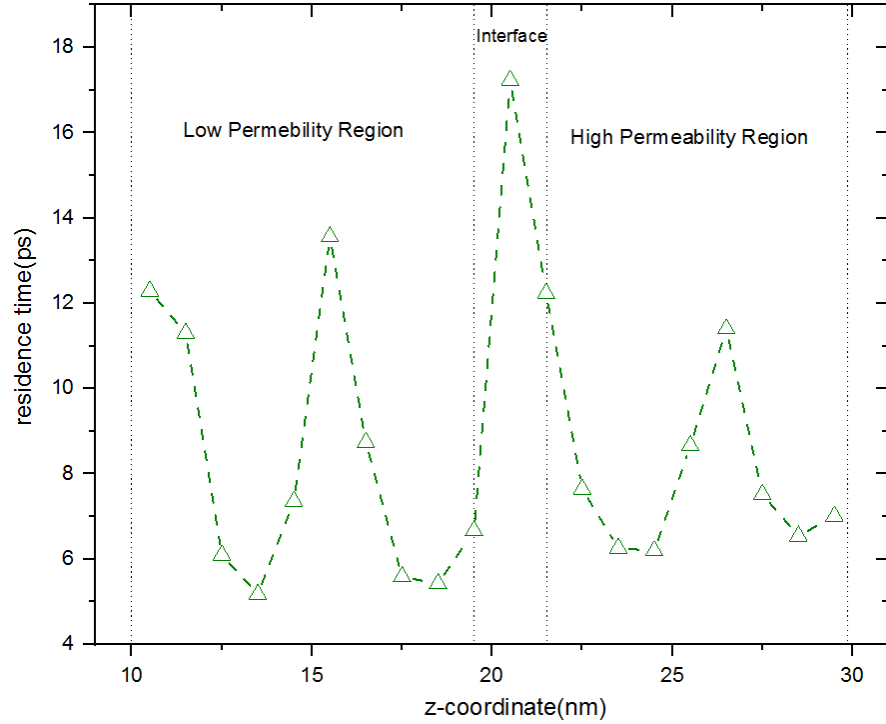


**Figure 5-3** RTD for assembled low and high permeability ZIF-8 slabs.

Residence time distributions unveil an interesting effect of interfaces on transport of CO<sub>2</sub> molecules. According to our RTD analysis, CO<sub>2</sub> molecules spend more time at the low permeability/high permeability regions separating interface than each “bulk” regions. By standing upon this observation, we assigned a new permeability to term to inner interface and intended to calculate interface permeability directly for CGD-MD simulations.

$$\frac{1}{P_{eff}} = \frac{\phi_1}{P_1} + \frac{\phi_{int.}}{P_{int.}} + \frac{\phi_2}{P_2} \quad (5.3)$$

$\phi_1$ ,  $\phi_{int.}$ ,  $\phi_2$  were ratio of first component, interface and second component of MMM structures and  $P_1$ ,  $P_{int.}$ ,  $P_2$  stand for corresponding

permeability of each regions and  $P_{eff}$  stands for effective permeability of composite system. From RTD analysis given in Figure 5-3, the ratio first component, second component and interface could be decided and we have plugged these values to equation. Interface permeability,  $P_{int.}$ , was be calculated as  $30 \times 10^{13} \text{mol.m/m}^2.\text{s.Pa}$  according to these calculations This lower permeability was expected due to RTD analysis, which shows the inner interface as rate limiting region along the molecular transport axis.

#### **5.4: Conclusions**

In this study, we proposed a simulation methodology to include interfacial surface effects on gas permeation through a nanoporous membrane. To achieve this goal, we performed a newly developed non-equilibrium molecular dynamics method called Concentration Gradient Driven Molecular Dynamics (CGD-MD) to calculate  $\text{CO}_2$  permeability and an enhanced sampling methodology called Well-Tempered Metadynamics (WT-MetaD) to interface two ZIF-8 slabs. At the end, a  $\text{CO}_2$ -phobic ZIF-8 membrane was generated by tuning cross interaction parameter between  $\text{CO}_2$  and ZIF-8 interaction and simple “mixed matrix membrane” model was created by assembling standard and  $\text{CO}_2$ -phobic slabs. In these simulations, an important effect of physical interface was observed on  $\text{CO}_2$  transport. This effect was quantified and interface permeability was calculated directly from atomistic simulations.

## 5.5: References

1. Abraham, M., et al. (2015). "the GROMACS development team GROMACS User Manual version 5.1. 2; 2016." MJ Abraham, T. Murtola, R. Schulz, S. Páll, JC Smith, B. Hess, E. Lindahl, SoftwareX **1**: 19.
2. Abrams, C. and G. Bussi (2014). "Enhanced sampling in molecular dynamics using metadynamics, replica-exchange, and temperature-acceleration." Entropy **16**(1): 163-199.
3. Ahunbay, M. G., et al. (2004). "Surface resistance to permeation through the silicalite single crystal membrane: Variation with permeant." The Journal of Physical Chemistry B **108**(23): 7801-7808.
4. Baker, R. W. (2012). Membrane technology and applications, John Wiley & Sons.
5. Barducci, A., et al. (2011). "Metadynamics." Wiley Interdisciplinary Reviews: Computational Molecular Science **1**(5): 826-843.
6. Barducci, A., et al. (2008). "Well-tempered metadynamics: a smoothly converging and tunable free-energy method." Physical review letters **100**(2): 020603.
7. Bussi, G., et al. (2007). "Canonical sampling through velocity rescaling." The Journal of chemical physics **126**(1): 014101.
8. Cygan, R. T., et al. (2012). "Molecular simulation of carbon dioxide capture by montmorillonite using an accurate and flexible force field." The Journal of Physical Chemistry C **116**(24): 13079-13091.

9. Duan, P., et al. (2019). "Polymer Infiltration into Metal-organic Frameworks in Mixed-Matrix Membranes Detected In Situ by NMR." Journal of the American Chemical Society.
10. Dutta, R. C. and S. K. Bhatia (2018). "Interfacial barriers to gas transport in zeolites: distinguishing internal and external resistances." Physical Chemistry Chemical Physics **20**(41): 26386-26395.
11. Heffelfinger, G. S. and F. v. Swol (1994). "Diffusion in Lennard-Jones fluids using dual control volume grand canonical molecular dynamics simulation (DCV-GCMD)." The Journal of chemical physics **100**(10): 7548-7552.
12. Hennepe, H. t., et al. (1991). "Exclusion and tortuosity effects for alcohol/water separation by zeolite-filled PDMS membranes." Separation science and technology **26**(4): 585-596.
13. Jiang, Z., et al. (2018). "Water transport through ultrathin polyamide nanofilms used for reverse osmosis." Advanced Materials **30**(15): 1705973.
14. Laio, A. and F. L. Gervasio (2008). "Metadynamics: a method to simulate rare events and reconstruct the free energy in biophysics, chemistry and material science." Reports on Progress in Physics **71**(12): 126601.
15. Lemmon, E. W., et al. (2007). NIST standard reference database 23: reference fluid thermodynamic and transport properties-REFPROP, version 8.0.
16. Monsalve-Bravo, G. and S. Bhatia (2018). "Modeling permeation through mixed-matrix membranes: a review." Processes **6**(9): 172.

17. Mulder, J. (2012). Basic principles of membrane technology, Springer Science & Business Media.
18. Newsome, D. A. and D. S. Sholl (2006). "Influences of interfacial resistances on gas transport through carbon nanotube membranes." Nano letters **6**(9): 2150-2153.
19. Ozcan, A., et al. (2017). "Concentration gradient driven molecular dynamics: a new method for simulations of membrane permeation and separation." Chemical science **8**(5): 3858-3865.
20. Saint Remi, J. C., et al. (2016). "The role of crystal diversity in understanding mass transfer in nanoporous materials." Nature materials **15**(4): 401.
21. Sastre, G., et al. (2018). "Molecular Dynamics Study of Diffusion and Surface Permeation of Benzene in Silicalite." The Journal of Physical Chemistry C **122**(13): 7217-7225.
22. Semino, R., et al. (2018). "Understanding the origins of metal–organic framework/polymer compatibility." Chemical science **9**(2): 315-324.
23. Semino, R., et al. (2015). "Microscopic model of the metal–organic framework/polymer interface: a first step toward understanding the compatibility in mixed matrix membranes." ACS applied materials & interfaces **8**(1): 809-819.
24. Tribello, G. A., et al. (2014). "PLUMED 2: New feathers for an old bird." Computer Physics Communications **185**(2): 604-613.

25. Valsson, O., et al. (2016). "Enhancing important fluctuations: Rare events and metadynamics from a conceptual viewpoint." Annual review of physical chemistry **67**: 159-184.
26. Vinh-Thang, H. and S. Kaliaguine (2013). "Predictive models for mixed-matrix membrane performance: a review." Chemical reviews **113**(7): 4980-5028.
27. Zhang, W., et al. (2019). "Ultrathin nanoporous membrane fabrication based on block copolymer micelles." Journal of Membrane Science **570**: 427-435.
28. Zheng, B., et al. (2012). "Force field for molecular dynamics computations in flexible ZIF-8 framework." The Journal of Physical Chemistry C **116**(1): 933-938.
29. Zhu, Y., et al. (2017). "Unravelling surface and interfacial structures of a metal–organic framework by transmission electron microscopy." Nature materials **16**(5): 532.

## Chapter 6: GENERAL CONCLUSIONS AND DISCUSSIONS

---

In this part, a general conclusion and comments are given on the works developed in this study. For each of the points, perspectives are drawn with possible implications in MOF membranes for gas separation applications and some further applications.

Metal organic frameworks (MOFs) have been proposed exciting developments in nanoporous materials with promising applications for adsorption and membrane-based separations. The number of known MOFs exceed 70 000 (Widmer, Lampronti et al. 2019) currently and the efforts to predict the performance of MOF based adsorbents and/or membranes using molecular simulations have a significant role in identifying right materials for right applications and understanding physical mechanism to achieve desired engineering application. Molecular simulations provide an atomistic understanding of the system under investigation which is not very easily accessible from experimental point of view in many times. That's why, molecular simulations are important to develop design principles for membrane materials by unveiling the effect of molecular level properties such as pore, gate and window size, pore volume, accessible pore surfaces and molecular interfaces. In this chapter, we first summarize our membrane simulation results then review the challenges and opportunities of current simulation techniques for further studies.

In this thesis, we investigated first to propose a simulation methodology to fix some well-known problems of recent MD methods to simulate membrane-based gas separation. The first results examining the applicability of our proposed

methodology (namely CGD-MD) on a membrane of ZIF-8 (one of the prominent example of MOF structure which has wide variety of applications) to methane, ethane and ethylene separation. Single permeation simulations were performed for methane, ethane and ethylene and binary mixture separation for ethane/ethylene mixture. The predictions for single methane, ethane and ethylene permeation demonstrated a quantitative consistency with experimental data available in literature. Mixture separation simulation were confirmed ethane/ethylene separation of ZIF-8 even for ultrathin ZIF-8 membranes. The data available in the literature for considerably thicker membranes (in the order of micron length), but in our study we have demonstrated that even ultra-thin ZIF-8 membranes could separate ethane and ethylene. If we keep mind the importance of ethane/ethylene separation, this could be count as an important contribution to show that ZIF-8 is a promising candidate material for this separation even in the ultra-thin (lower than 10 nm) limit.

MOFs are promising materials for some specific gas separations but fabrication of a MOF membrane is process that is very far away from being trivial and straightforward. Due to well-known difficulties of scaling up MOF membrane fabrication, Mixed Matrix Membranes (MMMs) were proposed as a possible solution. Polymer membranes have a long tradition for gas separation applications and mixing them with some MOF with superior gas separation properties seems a promising direction to suppress scaling up problem. That's why, we perform a Nonequilibrium Molecular Dynamics (NEMD) study for a MMM structure to gain some understanding about gas transport through such composite system. We choose PIM-1 as polymer matrix and ZIF-8 as filler and investigated CH<sub>4</sub>/H<sub>2</sub>

separation due to industrial significance of hydrogen purification. We performed first microsecond long simulations for MOF and MOF/Polymer mixed matrix membranes available in the literature (more than 6 microseconds in total). Long simulations were suggested for polymeric systems one of the recent publications of Neyertz et al. (Neyertz and Brown 2018) and they performed 300 ns simulations for air separation study. In our study, we investigated the effect of Polymer/MOF interface on gas transport. This study showed the importance of interfacial defects and micro-voids between polymer and MOF structure on gas permeation properties for the first time directly. This could be taken as a first direct simulations to evaluate relation of surface compatibility and gas transport for MOF-polymer composite systems.

For MMM structures, surface compatibility is one the most significant aspects for high performance gas separation. Under light of our atomistic simulations, we have tried to approach the problem of surface compatibility from a free energy calculation perspective. In recent years, free energy calculation methodologies have been expanded extensively. These promising methodologies and computational tool gives an opportunity to bring a free energy calculation perspective to this challenging problem. In our case, we performed Well-Tempered Metadynamics simulations to map out a “surface compatibility” free energy landscape. Additionally, some of the well-known morphologies with high-low permeability pairs were directly simulated in atomistic level and results compared with continuum models. Up to date, simulation studies on MOF membranes have not been considered effect of inner interfaces on gas transport and we investigated this inner interface effect on CO<sub>2</sub> transport.

On the other hand, atomistic molecular simulations for membranes has many challenges. First and arguably biggest challenge is length and time scale problem of atomistic simulations. Despite the rapid increase of computational power of computer along last decades, atomistic simulations are still restricted to nm ( $10^{-9}$  m) and microsecond ( $10^{-6}$  s) length-time scales. Current developments on experimental techniques open the way for ultrathin membranes and some studies have been reported around 100 nm membrane thickness (Ogieglo, Ghanem et al. 2018). It seems that the gap between experimental accessible range and MD length scale getting closer. However, the gap with respect to time still problematic and the order of nanosecond is far from time scales of membrane separation processes. Another big challenge is to develop more realistic membrane models to capture physical picture of membrane separation better. It is nearly impossible to fabricate defect-free, continuous membranes, therefore membrane should have different defects (point, line, dislocation etc.). Realistic membrane models should consider these defects and their effect on penetrant molecule transport. Other than the recently published (Zhang, Han et al. 2016, Han, Verploegh et al. 2018, Han, Tyminska et al. 2019) studies, there is no detailed literature data which includes the defects in the model and their influence on gas transport. There are some opportunities in the direction of developing defective membrane structures and investigating the effect of defects on gas separation. Another important challenge is to develop accurate force field parameter sets for MOF structures. Many MOFs exhibit structural flexibility, therefore reliable modelling of MOFs requires well-defined intermolecular and intramolecular force field parameters. There are some improvements in this direction (Krokidas, Castier et al. 2015, Vanduyfhuys, Vandenbrande et al. 2018, Dürholt, Fraux et al. 2019, Jawahery, Rampal et al.

2019) but there is still some room for improvement for developing better flexible force fields.

Other than challenges, there is also some significant opportunities for possible future research directions. Generating more realistic MOF/Polymer morphologies (such as embedding a MOF nanoparticle into polymer matrix) can provide better understanding on mass transport through MOF/Polymer interfaces in a composite MMM structure.

The subject of this thesis proposes a new methodology to perform membrane separation simulations in full atomistic details, but there is still some room for improvement from method perspective. For example, the parameter sets that we used in our CGD-MD simulations are optimised by trial and error generally. Even though, we had some heuristic about how to optimise them, an “on-fly” parameter optimisation could be nice improvement for this method. Additionally, we mainly dealt with gas molecules’ permeation in this thesis which is a simpler phenomenon with respect to more complex molecules such drug molecules and their permeation. For example, this drug permeation application could be important to bring molecular insight to water remediation problem. Amount of pesticides such as atrazine, carbamazepine, triclosan etc. have an increasing trend in rural water supplies and remediating that contaminated water content is an important problem. CGD-MD method could be design to simulate this pesticide molecules permeation through membranes and separation from the water. By applying this NEMD methodology, transport properties of pesticide molecules could be investigated in detail and this information could be supplemented (or replaced) expertise-need experimental efforts such High Pressure Liquid Chromatography (HPLC)

techniques. From sampling point of view, transport of simple gas molecules such  $H_2$  is not a rare event and timescales of standard MD simulations is enough to generate adequate number of samples to make reliable statistics. But, this will obviously not be case for sizable and complex drug molecules. For this kind of simulations, a further investigation is needed to develop an understanding on how to combine the method that we proposed in this thesis and enhanced sampling methods to simulate rare events.

More direct impact of the method presented in this thesis could be on the liquid membrane separation set-ups such water desalination and pervaporation. To our understanding, this method could be directly applied to these simulations without needing an extensive amount of effort.

Another interesting application could be investigating on simulation responsive membranes. Many MOF materials show different stimuli responsive behaviours and transform their physical phases under different external effects such as electric field (Ghoufi, Benhamed et al. 2017, Knebel, Geppert et al. 2017, Boulé, Roland et al. 2018). By applying different external fields, performance of MOF membrane can be enhanced. For example, an open pore-closed pore transition due to external electric field can increase separation factor for a mixture by sharply closing the “door” to one of the components in permeating mixture through the membrane structure.

Another possible direction could be an investigation of polarizability of molecules and membrane framework on separation performance.  $H_2/H_2S$  separation has industrial significance to protect pipeline form corrosion and it is well-known that  $H_2S$  is a highly polarisable molecule. It could be an interesting

direction to unveil the effect of molecule and membrane framework polarizability on mixture separation.

Last but not least, an investigation of “impurity” effects on membrane separation could bring some contribution to current literature. For zeolite membranes (Funke, Frender et al. 1997, Li, Falconer et al. 2006, Wu, Diaz et al. 2015, Luo, Funke et al. 2016, Chisholm 2017), it was experimentally shown that small amount of H<sub>2</sub>O impurity in mixture could change CO<sub>2</sub>/CH<sub>4</sub> separation performance of the membrane. But, a mechanistic understanding on this performance loss is missing. Does similar situation also happen for MOF or Polymer membranes also? Does it happen due to water and mixture components cross interactions in the inlet? Or water binds strongly to membrane surface and blocks the gates? The detailed answers of these questions are missing.

## 6.1: References

1. Boulé, R., et al. (2018). "Thermal and guest-assisted structural transition in the NH<sub>2</sub>-MIL-53 (Al) Metal Organic Framework: A molecular dynamics simulation investigation." *Nanomaterials* 8(7): 531.
2. Chisholm, N. O. (2017). "The Effect of Impurities on Permeance through Chabazite Zeolite Membranes."
3. Dürholt, J. P., et al. (2019). "Ab initio derived force fields for Zeolitic Imidazolate Frameworks: MOF-FF for ZIFs." *Journal of chemical theory and computation*.

4. Funke, H. H., et al. (1997). "Influence of adsorbed molecules on the permeation properties of silicalite membranes." *Journal of Membrane Science* 129(1): 77-82.
5. Ghoufi, A., et al. (2017). "Electrically induced breathing of the MIL-53 (Cr) metal–organic framework." *ACS central science* 3(5): 394-398.
6. Han, C., et al. (2018). "Assessing the impact of point defects on molecular diffusion in ZIF-8 using molecular simulations." *The journal of physical chemistry letters* 9(14): 4037-4044.
7. Han, R., et al. (2019). "Propagation of Degradation-Induced Defects in Zeolitic Imidazolate Frameworks." *The Journal of Physical Chemistry C*.
8. Jawahery, S., et al. (2019). "Ab Initio Flexible Force Field for Metal-Organic Frameworks Using Dummy Model Coordination Bonds." *Journal of chemical theory and computation*.
9. Knebel, A., et al. (2017). "Defibrillation of soft porous metal-organic frameworks with electric fields." *Science* 358(6361): 347-351.
10. Krokidas, P., et al. (2015). "Molecular simulation studies of the diffusion of methane, ethane, propane, and propylene in ZIF-8." *The Journal of Physical Chemistry C* 119(48): 27028-27037.
11. Li, S., et al. (2006). "Improved SAPO-34 membranes for CO<sub>2</sub>/CH<sub>4</sub> separations." *Advanced Materials* 18(19): 2601-2603.
12. Luo, Y., et al. (2016). "Adsorption of CO<sub>2</sub>, CH<sub>4</sub>, C<sub>3</sub>H<sub>8</sub>, and H<sub>2</sub>O in SSZ-13, SAPO-34, and T-type zeolites." *Industrial & engineering chemistry research* 55(36): 9749-9757.
13. Neyertz, S. and D. Brown (2018). "Air Sorption and Separation by Polymer Films at the Molecular Level." *Macromolecules* 51(18): 7077-7092.

14. Ogieglo, W., et al. (2018). "High-pressure CO<sub>2</sub> sorption in polymers of intrinsic microporosity under ultrathin film confinement." *ACS applied materials & interfaces* 10(13): 11369-11376.
15. Vanduyfhuys, L., et al. (2018). "Extension of the quickff force field protocol for an improved accuracy of structural, vibrational, mechanical and thermal properties of metal–organic frameworks." *Journal of computational chemistry* 39(16): 999-1011.
16. Widmer, R. N., et al. (2019). "Pressure promoted low-temperature melting of metal–organic frameworks." *Nature materials*: 1.
17. Wu, T., et al. (2015). "Influence of propane on CO<sub>2</sub>/CH<sub>4</sub> and N<sub>2</sub>/CH<sub>4</sub> separations in CHA zeolite membranes." *Journal of Membrane Science* 473: 201-209.
18. Zhang, C., et al. (2016). "Computational characterization of defects in metal–organic frameworks: Spontaneous and water-induced point defects in ZIF-8." *The journal of physical chemistry letters* 7(3): 459-464.

## Chapter 7: APPENDICES

**Table Appendix 1** CGD-MD specific parameters used in simulations.  $Z_F$  is the position where the centre of a bell shaped bias function is placed with respect to the  $z=0$  (i.e. these correspond to the centre of the IFR and OFR shown in Figure S1),  $w$  is the width of the bias force function (i.e. width of IFR and OFR), and  $k_i$  is the bias force constant.

Relevant simulations	Simulation Length	Side	$w$ (nm)	$k_i$ (kJ.nm <sup>3</sup> /mol)	$Z_F$ (nm)	VCR/(Lx x Ly) (nm)
PIM-1 (Single Permeation)	1 microsecond	Inlet	0.25	$k_{\text{methane}} = 5,000$ $k_{\text{hydrogen}} = 5,000$	4.875	2.5
		Outlet	0.25	500,000	35.925	2.5
ZIF-8 (Single Permeation)	1 microsecond	Inlet	0.25	$k_{\text{methane}} = 5,000$ $k_{\text{hydrogen}} = 8,000$	4.875	2.5
		Outlet	0.25	500,000	24.925	2.5
MMM (Single Permeation)	1 microsecond	Inlet	0.25	$k_{\text{methane}} = 5,000$ $k_{\text{hydrogen}} = 5,000$	14.875	2.5
		Outlet	0.25	500,000	76.525	2.5

MMM (Mixture Permeation)	1 microsecond	Inlet	0.25	k <sub>methane</sub> =5,000 k <sub>hydrogen</sub> =5,000	14.875	2.5
		Outlet	0.25	500,000	76.525	2.5

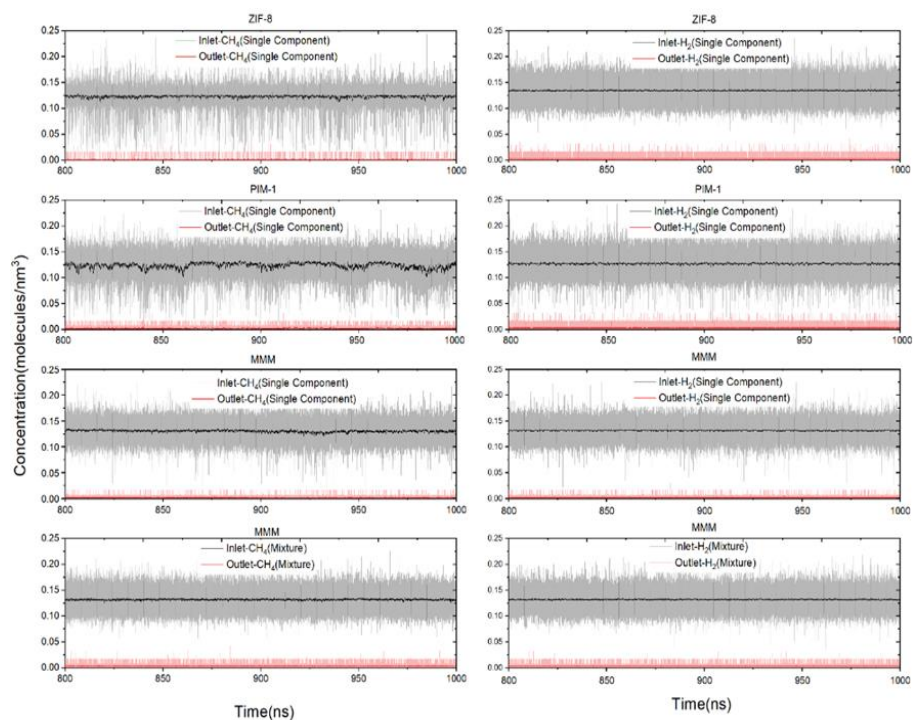
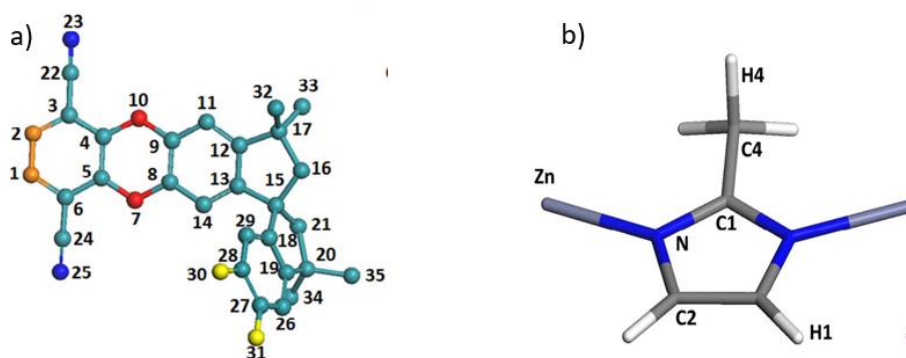


**Figure Appendix 1:** Variation of a) CH<sub>4</sub> and b) H<sub>2</sub> concentrations as a function of simulation time in the inlet (black lines) and outlet (red lines) control regions (ICR and OCR, respectively), for (from top to bottom), pure component ZIF-8, PIM-1 and PIM-1/ZIF-8 and mixture PIM-1/ZIF-8 CGD-MD simulations. Dark lines are moving averages of the gas concentrations whereas transparent colours are instantaneous concentrations in the control regions.

**Table Appendix 2:** Tuned Lennard-Jones cross parameters between gas molecules and the atoms of a) PIM-1 and b) ZIF-8.



[nonbond\_params]

;	i	j	sigma(nm)	epsilon(KJ/mole)
H <sub>2</sub>	H1[ZIF-8 gate hydrogen]		0.20508	0.141483900
H <sub>2</sub>	OS[7,10]		0.19453	0.430446008
H <sub>2</sub>	CA1[4,5]		0.22953	0.284900364
H <sub>2</sub>	CA2[3,6]		0.23933	0.235649165
H <sub>2</sub>	CA3[11,14,26,29]		0.232848	0.366100728
H <sub>2</sub>	CA4[12,13,18,19]		0.23933	0.235649165
H <sub>2</sub>	CA5[27,28](terminal)		0.22953	0.284900364
H <sub>2</sub>	C31[15,17,20]		0.32753	0.036426312
H <sub>2</sub>	C32[16,21]		0.23968	0.367564207
H <sub>2</sub>	C33[33,33,34,35]		0.23478	0.509420772
H <sub>2</sub>	C[22,24]		0.22778	0.398226791
H <sub>2</sub>	N1[23,25]		0.20678	0.398226791
H <sub>2</sub>	CO[8,9,27,28]		0.22953	0.284900364
H <sub>2</sub>	LCA[1,2](terminal)		0.22953	0.284900364
H <sub>2</sub>	LOS[30,31](terminal)		0.20993	1.118952898
H <sub>2</sub>	F(terminal)		0.20328	0.540185055
CH <sub>4</sub>	H1[ZIF-8 gate hydrogen]		0.35390	0.299106000
CH <sub>4</sub>	OS[7,10]		0.35540	0.864266552
CH <sub>4</sub>	CA1[4,5]		0.41154	0.572034239
CH <sub>4</sub>	CA2[3,6]		0.42726	0.473145735
CH <sub>4</sub>	CA3[11,14,26,29]		0.41688	0.735071548
CH <sub>4</sub>	CA4[12,13,18,19]		0.427269	0.473145735
CH <sub>4</sub>	CA5[27,28](terminal)		0.411548	0.572034239
CH <sub>4</sub>	C31[15,17,20]		0.568757	0.073138192
CH <sub>4</sub>	C32[16,21]		0.427831	0.738009976
CH <sub>4</sub>	C33[33,33,34,35]		0.419970	1.022835212
CH <sub>4</sub>	C[22,24]		0.408741	0.799575532
CH <sub>4</sub>	N1[23,25]		0.375054	0.799575532
CH <sub>4</sub>	CO[8,9,27,28]		0.411548	0.572034239

CH <sub>4</sub>	LCA[1,2](terminal)	0.411548	0.572034239
CH <sub>4</sub>	LOS[30,31](terminal)	0.380107	2.246677968
CH <sub>4</sub>	F(terminal)	0.369439	1.084604956

**Table Appendix 3:** Permeabilities of H<sub>2</sub> and CH<sub>4</sub> obtained from CGD-MD simulations.

Membrane	Permeability (x10 <sup>13</sup> mol.m/m <sup>2</sup> sPa)	
	CH <sub>4</sub>	H <sub>2</sub>
ZIF-8	62.5	320.2
PIM-1	128.0	803.2
PIM-1/ZIF-8 (pure)	136.4	628.4
PIM-1/ZIF-8 (mixture)	120.2	470.8